

NASA-CR-54039



N64-19224
CODE-1

LOW VISCOSITY BEARING STABILITY INVESTIGATION

TC FINAL REPORT,

Period: October 10, 1961 thru December 31, 1963

BY J. D. McHUGH

1 Apr. 1964

154p

ref

prepared for
NATIONAL AERONAUTICS AND SPACE ADMINISTRATION
(NASA CONTRACT NAS-3-2111)

ADVANCED TECHNOLOGY LABORATORY
SPACE POWER AND PROPULSION SECTION
MISSILE AND SPACE DIVISION

1038512

GENERAL ELECTRIC Co.

CINCINNATI 15, OHIO

OTS:PRICE

XEROX

MICROFILM

\$ 11.50 ph
\$ 4.82 ref

NOTICE

This report was prepared as an account of Government sponsored work. Neither the United States, nor the National Aeronautics and Space Administration (NASA), nor any person acting on behalf of NASA:

- A.) Makes any warranty or representation, expressed or implied, with respect to the accuracy, completeness, or usefulness of the information contained in this report, or that the use of any information, apparatus, method, or process disclosed in this report may not infringe privately owned rights; or
- B.) Assumes any liabilities with respect to the use of, or for damages resulting from the use of any information, apparatus, method or process disclosed in this report.

As used above, "person acting on behalf of NASA" includes any employee or contractor of NASA, or employee of such contractor, to the extent that such employee or contractor of NASA, or employee of such contractor prepares, disseminates, or provides access to, any information pursuant to his employment or contract with NASA, or his employment with such contractor.

Requests for copies of this report
should be referred to:

National Aeronautics and Space Administration
Office of Scientific and Technical Information
Washington 25, D.C.
Attention: AFSS-A

CASE FILE COPY

LOW VISCOSITY BEARING STABILITY INVESTIGATION

FINAL REPORT

Prepared by:-

J. D. McHugh

for

NATIONAL AERONAUTICS AND SPACE ADMINISTRATION

Contract: NAS 3-2111

APRIL 1, 1964 ✓

Technical Management

NASA-Lewis Research Center
SPACE ELECTRIC POWER OFFICE
J. P. JOYCE - Technical Manager

ADVANCED TECHNOLOGY LABORATORY
and
SPACE POWER AND PROPULSION SECTION
MISSILE AND SPACE DIVISION
CINCINNATI 15, OHIO 45215

FOREWARD

This program was administered under the direction of Mr. J. P. Joyce of the Space Electrical Power Office at the Lewis Research Center, National Aeronautics and Space Administration during the period of October 10, 1961 to December 31, 1963.

The work was jointly carried out by personnel of the Space Power and Propulsion Section, Missile and Space Division, Cincinnati, Ohio, and by personnel of the Bearing and Lubrication Center, Advanced Technology Laboratory, Schenectady, New York.

The responsible personnel engaged in this investigation were:

E. Schnetzer	SPPS - Evendale	Project Manager
H. Ernst	SPPS - Evendale	Project Engineer Test Rig Design and Fabrication
G. Fox	ATL - Schenectady	Manager-Analysis and Test
J. P. McHugh	ATL - Schenectady	Project Engineer Bearing Analysis Test and Test Evaluation

TABLE OF CONTENTS

	<u>Page</u>
I. Summary	1
II. Conclusions and Recommendations	5
III. Discussion	6
A. Rotor-Bearing System Considerations for Liquid Metal Bearings	6
B. Evaluation of Bearings for Liquid Metal Operation	7
C. Selection of Test Bearings	10
D. Test Bearings and Rotor Description	12
E. Test Rig Description	15
F. Test Procedure and Whirl Determination	17
G. Range of Bearing Variables Tested	19
H. Tests on Two Axial Groove Bearings, $L/D = 1$	20
I. Tests on Two Axial Groove Bearings, $L/D = 1-1/2$	23
J. Tests on Tilting-Pad Bearing, $L/D = 1$	26
K. Tests on Three Lobe Bearing, $L/D = 1$	27
L. Tests on Displaced Elliptical Bearing, $L/D = 1$	28
M. Tests on Compound Cylindrical Bearing, $L/D = 1$	28
N. Comparison of Bearing Performance	29
IV. References	34
Tables	
Figures	

LIST OF FIGURES

1. Close-up View of Test Rig Assembly
2. Two Axial Groove Bearing, $L/D = 1$
3. " " " " $L/D = 1-1/2$
4. Tilting Pad Bearing, $L/D = 1$
5. Three-Lobe Bearing, $L/D = 1$
6. Compound Cylindrical Bearing, $L/D = 1$
7. Orthogonally Displaced Elliptical Bearing, $L/D = 1$
8. Water Viscosity vs Temperature
9. Clearance Ratio Between Potassium and Water-Lubricated Bearings for Equal Sommerfeld Numbers.
10. Clearance Ratio Between Potassium and Water-Lubricated Bearings for Equal Taylor Numbers
11. Comparison of Bearing Radial Stiffness at No Load
12. Test Shaft
13. Effect of Temperature on Shaft-Bearing Clearance
14. Tilting Pad Bearing-Pad Details
15. Compound Cylindrical and Three Lobe Bearing Geometry
16. Three Lobe Bearing Measurements
17. " " " "
18. Three Lobe Bearing Contour
19. Compound Cylindrical Bearing Measurements
20. " " " "
21. " " " Contour
22. Orthogonally Displaced Elliptical Bearing Geometry
23. " " " " Measurements
24. " " " " "
25. " " " " Contour
26. Rotor End Flywheel
27. High Inertia Shaft
28. View of Three Test Shafts
29. Bearing Stability Test Rig Assembly
30. Pneumatic Load Piston Calibration
31. Eccenters for Dynamic Load Application

(List of Figures, Con't)

32. Eccenter Unbalance Ratio at Different Angular Settings
33. Torque Read-Out System Calibration
34. Diagram of Lubricant Loop
35. Oscilloscope Traces of Half-Frequency and Synchronous Whirl
36. Threshold Speed of Half-Frequency Whirl vs Sommerfeld Number
37. " " " " " " " "
38. Oscilloscope Traces of Shaft Orbit in Tilting-Pad Bearings
39. Gage Zero Shift with Speed
40. Eccentricity Ratio vs Sommerfeld Number - 2 Axial Groove L/D = 1
Lower Bearing, Test No. 3
41. Attitude Angle vs Eccentricity Ratio - 2 Axial Groove L/D = 1
Lower Bearing, Test No. 3
42. Eccentricity Ratio vs Sommerfeld Number - 2 Axial Groove L/D = 1
Lower Bearing, Test No. 4
43. Attitude Angle vs Eccentricity Ratio - 2 Axial Groove L/D = 1
Lower Bearing, Test No. 4
44. Eccentricity Ratio vs Sommerfeld Number - 2 Axial Groove L/D = 1
Upper Bearing, Test No. 3, 60 cps
45. Eccentricity Ratio vs Sommerfeld Number - Tilting Pad
Upper Bearing, Test No. 9
46. Coefficient of Friction vs Sommerfeld Number - Test No. 3
47. " " " " " " - Test No. 300
48. " " " " " " - Test No. 301
49. " " " " " " - Test No. 302
50. " " " " " " - Test No. 4
51. " " " " " " - Test No. 5
52. " " " " " " - Test No. 501
53. " " " " " " - Test No. 6
54. " " " " " " - Test No. 600
55. " " " " " " - Test No. 7
56. " " " " " " - Test No. 701
57. " " " " " " - Test No. 12
58. " " " " " " - Test No. 13
59. " " " " " " - Test No. 18

(List of Figures, Con't)

60.	Torque Coefficient vs Reynolds Number	- Test No. 1
61.	" " " " "	- Test No. 2
62.	" " " " "	- Test No. 3
63.	" " " " "	- Test No. 300
64.	" " " " "	- Test No. 4
65.	" " " " "	- Test No. 5
66.	" " " " "	- Test No. 501
67.	" " " " "	- Test No. 6
68.	" " " " "	- Test No. 600
69.	" " " " "	- Test No. 7
70.	" " " " "	- Test No. 701
71.	" " " " "	- Test No. 8
72.	Torque Coefficient vs Reynolds Number	- Test No. 9
73.	" " " " "	- Test No. 10
74.	" " " " "	- Test No. 11
75.	" " " " "	- Test No. 12
76.	" " " " "	- Test No. 13
77.	" " " " "	- Test No. 14
78.	" " " " "	- Test No. 15
79.	" " " " "	- Test No. 16
80.	" " " " "	- Test No. 17
81.	" " " " "	- Test No. 18
82.	" " " " "	- Test No. 19
83.	Torque Coefficient vs Reynolds Number Ratio	- Test No. 3
84.	" " " " " "	- Test No. 300
85.	" " " " " "	- Test No. 301
86.	" " " " " "	- Test No. 302
87.	" " " " " "	- Test No. 4
88.	" " " " " "	- Test No. 5
89.	" " " " " "	- Test No. 501
90.	" " " " " "	- Test No. 6
91.	" " " " " "	- Test No. 600
92.	" " " " " "	- Test No. 7
93.	" " " " " "	- Test No. 701

(List of Figures, Con't)

- 94. Torque Coefficient vs Reynolds Number Ratio - Test No. 12
- 95. " " " " " " - Test No. 13
- 96. " " " " " " - Test No. 18

TABLES

1. Comparison of Physical Properties of Test Fluids to Potassium
2. Comparison of Dimensionless Load Capacities
3. Journal Measurement of Test Shafts
4. Test Rotors - Masses and Inertias
5. Calculated Critical Speeds of Test Shaft
6. Calibration of Bently Gauges
7. Sensitivity of Torque Drive Shafts
8. Summary of Bearing Variable Test Range
9. Overall Bearing Test Summary
10. Threshold Speed of Half-Frequency Whirl
2 axial groove bearing, $L/D = 1$, 3 mil nominal diam. clearance
11. Threshold Speed of Half-Frequency Whirl
2 axial groove bearing, $L/D = 1-1/2$, 3 mil nominal diam. clearance
12. Threshold Speed of Half-Frequency Whirl
2 axial groove bearing, $L/D = 1-1/2$, 2 mil nominal diam. clearance
13. Threshold Speed of Half-Frequency Whirl
2 axial groove bearing, $L/D = 1-1/2$, 2 mil nominal diam. clearance

I. SUMMARY

Bearing stability is one of the basic problems associated with high speed turbomachinery. Experience has shown that rotors with lightly loaded, high speed fluid film bearings often exhibit destructive shaft whirling which can limit speed or bearing life. The problem is therefore one of particular importance in space power systems currently under development, where high speeds and reliable unattended operation are required in a system which may operate in a zero gravity environment. The program described in this report was conducted in answer to NASA PRGS 3526 of May 22, 1961, to investigate rotor bearing stability.

The objectives of this program were to:

1. Analyze a number of bearing types which experience or theoretical considerations pointed to as promising candidates for stable rotor operation.
2. Select and design specific bearings from among those analyzed for testing under conditions partially simulating those of the actual, liquid metal bearing application.
3. Design and build a test stand capable of evaluating the selected bearings under a wide range of rotor speeds, static and dynamic loads and other significant bearing and rotor parameters.
4. Conduct tests for evaluating the stability performance of the various bearing types with a low viscosity lubricant and over a range of bearing parameters.

The previous objectives were achieved. Figure 1 is a view of the test device. The bearings selected and tested included the following: the two axial groove bearing of length/diameter ratio one and also one and one-half; the three-lobe bearing; tilting pad bearing; the orthogonally displaced elliptical

bearing; and the compound cylindrical bearing. These bearing types are shown in Figures 2 to 7. Tests were conducted over a large span of variables, including:

1. Shaft speed: 60 to 570 rps on a test shaft 1-1/4 inch nominal diameter.
2. Shaft clearance: 3 different shaft sizes employed to vary clearance.
3. Static loads: 0 to 77.4 lbs. external load per bearing.
4. Unbalance: 0 to 6.25 gram-inch per bearing.
5. Mass distribution: 3 different rotor mass distributions.
6. Lubricant: distilled water at temperatures between 75°F and 150°F, and at typical supply pressures between 5 psig and 70 psig.

During the tests, the primary objective was to observe the effect of the bearing and rotor variables upon the stability of rotor motion; a second objective was the measurement of power loss for the bearings in turbulent operation. Accordingly, the test device was equipped with non-contacting displacement gages to measure shaft center position. Drive torque to the test rotor was measured with the aid of a special non-contacting instrumentation system sensing the twist in a long, thin drive shaft.

While the displacement gages permitted quantitative measurement of the shaft center vibration and observation of the shaft orbit, they were found inadequate for accurate film thickness and attitude angle measurements. This is attributed to erratic shift in the gage zero which occurs when the shaft rotates at speeds above 100 cps. Measurements indicate that the sensitivity of the gages (volts change per unit displacement change) is unaffected by the zero shift. Hence, the ability to observe the onset and severity of shaft whirling was not hampered.

All bearing-rotor combinations were found to permit shaft whirl at some test speed. The type of whirl was either half-frequency, synchronous,

or a combined type. The mode of whirling was frequently complex despite the symmetry of the shaft, bearings, and the applied static and dynamic loads. That is, when the mode of whirl was observed, a simple cylindrical or conical type motion was unusual.

The bearing types which exhibited half-frequency whirl under some test conditions were the two-axial groove, the displaced elliptical and the compound cylindrical. The tilting pad and the three-lobe bearing permitted only a synchronous shaft orbiting for any of the test conditions.

The occurrence of half-frequency whirl was found to be a complex but reproducible phenomenon. With the two axial groove bearing, for example, the threshold speed at which it occurred was found to depend upon bearing length/diameter ratio, clearance, static load and unbalance and rotor mass. For a given rotor mass and clearance, the threshold speed for half-frequency whirl correlated with bearing Sommerfeld number (Fig. 36, 37)

In contrast to synchronous whirl, in which the shaft orbit size increased relatively slowly with speed, half-frequency whirl usually appeared with incremental changes in the test conditions; the shaft center position when viewed on an oscilloscope changed suddenly from a steady point to an orbit of amplitude equal to that of the bearing clearance. Half-frequency whirl is judged to be potentially the most destructive form of instability for liquid metal operation. The large amplitude of shaft orbit implies nearly zero film thickness in the bearings. Furthermore, even if the shaft is perfectly balanced about the journal axis, when the journal axis itself orbits at a large amplitude, large dynamic forces occur. The combination of large forces together with boundary lubrication at high speeds is a condition conducive to short bearing life. The materials chosen for the test shaft and bearing for operation in water, however, exhibited sufficient compatibility

to avoid seizures under momentary contact. Thus, it was found possible to observe shaft instabilities without damage to the test rig.

Although the two axial groove bearing type was not free from half-frequency whirl over all the test conditions, the highest test speed (570 rps) was achieved with this bearing type for an acceptable amplitude. Half-frequency whirl could be suppressed through static or dynamic loading. Furthermore, with an $L/D = 1-1/2$ and a 2 mil diametrical clearance shaft, it was demonstrated that the instability region had an upper (but relatively low) speed limit. Higher speeds eliminated the half-frequency whirl instability and permitted maximum test speeds to be attained.

The compound cylindrical bearing and the orthogonally displaced elliptical bearings both permitted half-frequency shaft whirl at zero load, the former at 60 rps and the latter at 270 rps. The compound cylindrical bearing exhibited a reduced load-carrying capacity compared to the other bearing types. Synchronous whirl amplitudes limited the test speed with the displaced elliptical bearing.

Tests with the rotor supported on the three lobe and the tilting pad bearing revealed no half-frequency whirl. Speeds, however, were limited to 350 cps because of synchronous shaft amplitudes.

Among the bearings tested, none allowed the rotor speed to be increased to more than 350 cps with an unloaded bearing (Test 18, 2 axial groove $L/D = 1-1/2$). Speeds were limited either by half-frequency or synchronous type whirl. Increased static loads permitted higher rotational speeds to be achieved with a two axial-groove bearing, $L/D = 1-1/2$, (Test No. 18) under a static bearing load of 34.4 lbs. The maximum test speed for a lightly loaded bearing (8.6 lbs.) was 400 cps, (Test No. 6), also with a 2 axial groove bearing of $L/D = 1-1/2$.

II. CONCLUSIONS AND RECOMMENDATIONS

It is concluded that the long, 2 axial groove bearing, the tilting pad bearing and the three lobe bearing merit continued consideration for liquid metal turbomachinery operation in view of their demonstrated ability to operate at high speeds and moderate loads without destructive half-frequency whirl.

It is recommended that tests on these bearing types be continued to establish the non-whirling, steady-state characteristics, including: film thickness (eccentricity ratio), attitude angle and more accurate power loss measurements. This data should be obtained both in the laminar region and at several values of high Reynolds' number sufficient to establish the effect of turbulence. The Taylor criterion for vortex formation marking the transition to turbulence with concentric, ungrooved cylindrical bearings is inadequate for complex bearings such as tested in the present program. It is also recommended that the dynamic spring and damping coefficients of these bearing types be evaluated experimentally. This information is necessary to permit the performance of other rotor configurations to be predicted.

III. DISCUSSION

A. Rotor-Bearing System Considerations for Liquid-Metal Operation

The operation of a high speed rotor on fluid-film bearings presents problems similar in kind but more severe in degree to those existing in more conventional oil-lubricated bearing-rotor systems. The problem of material compatibility with the liquid metal lubricant is an important one, but belongs to a separate category and will not be discussed further. Three of the most important considerations are the stability of shaft motion; load-carrying capacity of the bearings for an arbitrary load direction; and the presence of turbulence.

Different definitions of shaft instability can be given; for the present purpose, however, we will define shaft instability as any motion of the geometric center of the journal which does not disappear with time. Two types of instability can then be distinguished, i.e.,

1. Synchronous whirl - is a forced vibration of the journal caused by a rotating load. Its frequency is equal to that of the shaft rotating speed. Synchronous whirl can occur with an unbalanced rotor or with a well-balanced rotor operating at the critical (resonant) speed of the bearing-rotor system. It may be difficult to distinguish between rotor vibration due to unbalance or resonance. The amplitude of vibration may prevent increasing the rotor speed to pass through a possible resonant condition.
2. Half-frequency whirl - is an instability of the fluid film of the bearing which is characterized by a whirl of the journal centers at a speed approximately one-half that of the shaft rotational frequency. For such a condition, bearing theory predicts a complete loss of the load-carrying capacity of the fluid film. Experience has shown that

lightly loaded journal bearings operating at high speeds are especially prone to half-frequency whirl instability. The absence of gravity loads for space-power turbomachinery plant therefore points to half-frequency whirl as a very important consideration.

A rotor operating on fluid-film bearings is analagous to a distributed mass on non-linear springs. Consequently, the system is theoretically capable of exhibiting resonances either of the flexible or rigid body type. With low viscosity lubricants and high shaft stiffness of space power plants, rigid-body resonances are the phenomenon most likely to occur in achieving the desired speed. Therefore, the effect of bearing stiffness upon the rotor resonances and the ability of the bearing to damp out rotor vibrations form a further consideration in the selection of bearings.

The low viscosity of the liquid metals such as potassium and sodium together with the high rotational speeds leads to turbulent conditions in the bearing fluid film. The classical bearing theory has been developed on the basis of laminar bearing operation which is adequate for most conventional oil-film applications. There has been little experimental data available on bearings in turbulent flow, and a special lack of information on the complex bearings which experience has shown to inhibit half-frequency whirl. It is known, however, that turbulence increases the load-carrying capacity and also the power loss by a large but poorly-defined factor. In order to predict the rotor-bearing system resonances, the effect of turbulence on fluid film stiffness and damping requires careful consideration.

B. Evaluation of Bearings for Liquid Metal Operation

A direct evaluation of bearing hydrodynamic performance using liquid metals presents severe experimental difficulty. An alternative approach is to simulate the performance of liquid metals with a fluid having similar properties

at much reduced temperatures. An ideal fluid for simulation at room temperature would possess an identical absolute viscosity, density, specific heat, thermal conductivity and vapor pressure as the liquid metal at an elevated temperature. Shaft sizes, speeds, clearances, loads, etc., can then be the same size in the simulated test as in the actual application. No such ideal test fluid is known. Hence, with a real test fluid it is possible only to approach some of the physical properties of the test fluid. Similarity of the flow conditions must be achieved partly by adjusting geometrical similarity, as will be shown.

Table 1 compares the properties of potassium with three possible test fluids, i.e., water, silicone oils and N heptane. In the present program, distilled water was selected as the lubricant to simulate liquid metal operation in order to simplify handling and eliminate any explosion hazard. Two of the fluid properties which are of particular importance are the absolute viscosity and the kinematic viscosity. From Table 1 it is seen that the viscosities of potassium and water are similar but not identical. Figure 8 is a plot of the variation of water absolute viscosity with temperature.

Absolute viscosity is the fluid property of significance in establishing identical Sommerfeld numbers with the test and liquid metal fluids. Sommerfeld number determines the film thickness, coefficient of friction and required lubricant flow for a bearing in laminar flow. It is defined as:

$$S = \frac{\mu N}{P} \left(\frac{R}{C} \right)^2$$

If we wish to maintain frequency, shaft size and unit load the same between the two fluids, for equal Sommerfeld numbers:

$$\frac{\mu_1}{C_1^2} = \frac{\mu_2}{C_2^2}$$

or,

$$\frac{C_1}{C_2} = \left(\frac{\mu_1}{\mu_2} \right)^{1/2}$$

That is, the clearance ratio may be chosen for the tests using distilled water so as to simulate the application fluid Sommerfeld number. Speeds and unit loads can then be identical between the two.

Figure 9 illustrates the clearance ratio required to produce identical Sommerfeld numbers for the two fluids, assuming equal speeds and loads. With a test lubricant temperature of 120°F, for example, the Sommerfeld number of a potassium-lubricated bearing can be simulated for any speed and load over a potassium temperature range of 800°F to 1300°F. The comparable clearance of the potassium-lubricated bearing must be approximately one-half that of the water-lubricated bearing. A test on a bearing lubricated with water at 120°F, with a clearance of 0.0025 inches produces the same Sommerfeld number (at the same speed and unit load) as a potassium-lubricated bearing with a clearance of 0.00125 inches at a temperature of 1200°F.

Kinematic viscosity is the fluid property of significance in establishing identical Reynolds' and Taylor numbers between the two fluids. Taylor number is a measure of the degree of turbulence existing in the bearing. For concentric cylinders, a Taylor number of 41.1 indicates the formation of vortices which precede turbulence. Taylor number is defined as:

$$N_{Ta} = \frac{2\pi N(C^3R)^{1/2}}{\nu}$$

If we wish to maintain equal Taylor numbers between the two fluids at a given speed and shaft size:

$$\frac{C_1^{3/2}}{\nu_1} = \frac{C_2^{3/2}}{\nu_2}$$

or,

$$\frac{c_1}{c_2} = \left(\frac{\nu_1}{\nu_2} \right)^{2/3}$$

That is, adjustment of the clearance ratio between the test and application fluid can produce identical Taylor numbers. Figure 10 is a plot indicating how clearance with a water-lubricated bearing can be adjusted to simulate Taylor number for potassium between 800°F and 1300°F. With a water lubricant temperature of 120°F, for example, tests on a water-lubricated bearing with a given clearance produce the same Taylor number as would be obtained with a potassium-lubricated bearing having about one-half the clearance.

Tests were carried out at different temperature levels between 70°F and 150°F and no-load radial clearances ranging from approximately 1/2 to 2.5 mils. From Figures 9 and 10 therefore, at the test speeds and loads, equivalent Sommerfeld and Taylor numbers were obtained as for potassium-lubricated bearings between 800 and 1300°F and with clearances between 0.4 and 0.7 those of the water tests.

C. Selection of Test Bearings

Prior to testing, a number of bearing configurations were analyzed to provide a guide as to load-carrying capacity and probable stability ranking. The test bearing types and specific designs were chosen from among those studied, which also included the Rayleigh step bearing, the pressure dam and the plain (ungrooved) cylindrical bearing.

At present there does not exist a generalized theory for predicting the onset of half-frequency whirl with complex bearings (i.e., bearings which do not exhibit an axisymmetric response to load.) Even for simple cylindrical bearings operating in laminar flow, the effect of bearing variables upon the threshold speed is difficult to predict beforehand. However, in most analyses,

such as Ref. [1], the fluid-film stiffness of the bearing fluid film enters as an important parameter. According to the criterion of Poritsky, [2], a shaft is unstable when the operating speed is equal to or twice the critical frequency of the rotor-bearing system. Since the stiffness of the bearing is likely to be a significant factor in the system critical speed, a high fluid-film stiffness is therefore desirable to remove instability from the operating region. One criterion for bearing selection, therefore is the radial fluid-film stiffness of the different bearing types.

As described in detail in Ref. [3], a comparison of fluid-film stiffness among several bearing types can be misleading if the basis for comparison is dissimilar. In the analysis of different bearing types, the radial stiffness of the bearings were compared on the basis of zero load and an equal, no load maximum film thickness. Figure 11 presents the results of the analysis. It will be seen that the radial stiffness depends upon bearing type and length/diameter ratio even for the criteria specified.

A further criterion for bearing selection and design is the load-carrying capacity. Table 2 from Ref. [3] presents a comparison of the dimensionless load carrying capacity among several different bearing types and designs. To establish a fair method of comparison between the different bearing types, it is assumed that (1) the bearings have the same no-load minimum clearance between shaft and bearing and (2) that load capacities at equal film thickness under load are being compared. Table 2 compares the capacities of the bearings for an assumed minimum film thickness under load of 0.0005 inches and at different values of length/diameter ratio, and no-load clearance.

With such a basis of comparison among the bearings studied, it was found that the four pad, tilting-pad bearing studied has the highest static

stiffness at zero load, at a bearing length/diameter ratio of one-half. The calculated value, in fact, is greater than the stiffness for the other bearing types at twice the L/D studied for the four-pad bearing. Moreover, as shown in the load comparison, the load capacity is comparable to that of the three-lobe bearing, and at least one-half that of the two axial groove bearing. Thus, on the basis of these two criteria, the tilting-pad bearing is the most attractive.

It must be remembered, however, that other criteria are possible and may even be of greater significance. For example, static stiffness may be compared on the basis of an assumed load. Different bearings will exhibit different eccentricity ratios for the same load. Hence, the ranking of radial stiffness at a given load may be different from the relative ranking at zero load. Attitude angle and inherent damping ability are two further bearing characteristics which may be significant in improving the range of stable operation.

From among the bearings analyzed, therefore, the following bearings were selected for testing: the two axial groove of $L/D = 1$ and $1-1/2$; the three-lobe bearing $L/D = 1$; the compound cylindrical bearing, $L/D = 1$; the orthogonally displaced elliptical bearing $L/D = 1$ and the four pad, tilting pad bearing $L/D = 1$, as shown in Figures 2 to 7.

D. Test Bearings and Rotor Description

The bodies of the test bearings were manufactured from stainless steel to match the temperature coefficient of expansion of the shaft. To prevent seizure or galling at start up, a thin cylindrical liner of SAE 660 bronze was pressed into the body and glued or soldered in place.

For the cylindrical bearings, the static load is applied midway between the two axial feed-grooves. The water lubricant was introduced at the midpoint

of each groove.

Clearances were varied by substituting shafts of different diameters rather than substituting bearings. Figure 12 is a drawing of the plain test shaft used in most tests. Diametral clearances of 0.002, 0.003, and 0.005 inches were obtained by substituting the three shafts into the cylindrical test bearings of Figures 2 and 3. Figure 13 shows the effect of lubricant temperature upon the shaft-bearing clearance with the two-groove bearings in place. It will be seen that a 50°F rise in temperature reduces clearance about 0.2 mil.

The four pad, tilting-pad bearing ($L/D = 1$) selected for testing is shown in Figure 4. A four-pad bearing was chosen to provide a more nearly symmetric response to a rotating load. Figure 14 is a detailed drawing showing pad dimensions for the 1-1/4 inch wide pad. Static load was applied during test in the pivot direction. Therefore, the effective area carrying static load is taken as the product of the pad chord (0.80 inch) and the pad axial length (1.25 inch). Each of the tilting pads was individually supplied with lubricant through a drilled hole in the cylindrical pivot which connected with a feed hole in each pad. The cylindrical pivot and pad rotate as an integral unit in the retainer.

With a four-pad bearing of the type shown, it can be demonstrated that the maximum locus of the shaft center approximates a square, with the distances between sides representing the pivot-to-pivot clearances. The pivot-to-pivot of this bearing type were chosen to correspond to the diametral clearance of the test shafts in the two axial groove, cylindrical type bearings.

In the displaced arc bearing types shown in Figures 5, 6, and 7, the center of the bearing arc does not coincide with the journal center when the shaft is unloaded and theoretically centered. For the three lobe bearing shown schematically in Figure 15, for example, when the shaft is centered at point o,

the minimum clearance between shaft and bearing is given by:

$$h_o = (R_L - R_S) - \epsilon = \frac{C}{2} - \epsilon$$

where the terms are defined in Figure 15.

In the present program the lobe radius of the 3 lobe and compound cylindrical bearing is fixed and the bearing clearance is varied by substituting shafts. With a lobe radius of 0.6285 inch and the medium diameter test shaft (1.2520 inch) of Figure 12, the minimum, calculated no-load clearance between shaft and bearing is 0.5 mil. The smallest diameter test shaft (1.2500 inch) produces a theoretical minimum film thickness at no-load of 1.5 mils. Thus, with the three-lobe and compound cylindrical bearings, the minimum calculated clearances obtained with the small and medium test shafts are the same as those obtained with the medium and large diameter shafts, respectively, in cylindrical bearings. Some measurements taken on the three-lobe and compound cylindrical bearings are shown in Figures 16-21.

A schematic diagram of the displaced elliptical bearing is shown in Figure 22. The minimum, no-load clearance h_o can be related to the displacement of the lobe centers by the expression:

$$h_o = (R_L - R_S) - [\lambda^2 + \delta^2]^{1/2}$$

For the smallest diameter shaft, the calculated minimum clearance between shaft and bearing at no-load is 1.06 mils. With the medium diameter shaft, the calculated clearance is only 0.06 mils. Actual displacement measurements of the medium diameter shaft in this test bearing, however, indicated a larger clearance than the previously calculated value. Measurements of the bore of the displaced elliptical bearings are shown in Figures 23-27.

Three variations of rotor mass distribution were employed during the tests. The majority of tests were conducted with the plain shaft of Figure 12

together with eccentric or unbalance discs outboard of each test bearing. A variation in the mass distribution was obtained by substituting the cylindrical concentric flywheels of Figure 26 for the eccenters. A further variation in the mass was tested by substituting the high inertia shaft of Figure 27 for the plain shaft. Figure 28 is a photograph of the test shafts. Table 4 summarizes the calculated values of polar and transverse moments of inertia.

Calculations were made using an IBM computer to estimate the effect of shaft diameter, mass distribution and fluid film stiffness on the critical speed of the test rotors. These calculations are summarized in Table 5. For the plain shaft with eccenters, calculations assuming rigid bearing supports predict a critical speed of 24,845 rpm. With fluid film bearings having a stiffness of 0.5×10^5 lb/inch, the critical speed is reduced to 20,770 rpm.

Thus, the fluid-film stiffness has a pronounced effect on the system resonant frequency. Since the stiffness can only be estimated even for laminar bearing flow, the system resonant speed range can only be approximated.

E. Test Rig Description

A cross-section of the test rig is shown in Figure 29. A test shaft with a journal diameter of 1.250 inches is driven by a 15 hp variable frequency induction motor through a flexible drive shaft. The two water-lubricated bearings are separated by a 12.5 inch centerline span. Partial arc water-lubricated loader bearings apply the desired static load through a pneumatic piston arrangement. Both pneumatic pistons are coupled to the same adjustable air-supply line to produce a symmetrical loading on the shaft. The loader bearings are mounted on spherical pivots so as to be self-aligning. Figure 30 shows the calibration data for the static load pistons.

Dynamic loads are applied by eccenters located outboard of each test bearing. Each eccentric consists of a pair of cylindrical discs bored off center

(Fig. 31). The discs can be rotated relative to one another on the shaft to produce a deliberate unbalance of known magnitude and position. Eccenter calibration is discussed in Reference 4. It can be shown that the ratio of unbalance at any angular setting $\bar{W}y_{\theta}$ to the maximum unbalance $\bar{W}y_M$ is given by the expression:

$$\frac{\bar{W}y_{\theta}}{\bar{W}y_M} = \frac{\sqrt{2}}{2} [1 - \cos \theta]^{1/2}$$

where θ is the angular displacement of the discs from the position of zero unbalance. The calculated maximum unbalance of 36.3 gram-inches agreed well with the measured value of 35.9 gram-inches. A plot of the unbalance ratio as a function of angle is given in Figure 32.

Four non-contacting displacement probes of the eddy-current inductance type located outboard of the best bearings measured the shaft position relative to the gage. Two gages are located at each test bearing in radial position 90° with respect to one another and at 45° to the load line imposed by the pneumatic loader pistons. Gage calibration is described in References 4 and 5. Table 6 summarizes the calibration data obtained with air only in the clearance gap.

Shaft speed is measured by means of an electronic counter sensing the once-per-revolution pulse from an electromagnetic pickup mounted adjacent to one eccenter.

Torque input to the test shaft is measured with a special non-contacting instrumentation system detecting the twist in the long, thin drive shaft. Table 7 from Reference 4 lists the calibration values of torque to twist for the phosphor bronze drive shafts. To calibrate the torque readout system, the two discs whose angular displacement is measured were mounted on a rigid shaft extension of the motor. The discs were rotated relative to one another preset amounts and the torque output meter readings taken at various speeds. Results shown in Figure 33

indicate satisfactory correlation between input angular twist and meter readings.

Lubricant inlet pressure and temperature are measured in the annular feeding groove surrounding the bearing shell. Lubricant exit temperature is measured by thermocouples adjacent to each test bearing. All thermocouple temperatures are recorded on a multi-point recorder.

A schematic diagram of the test loop is shown in Figure 34. Heated lubricant is drawn from a hot water tank by a positive displacement rotary pump and fed to the test and loader bearings. Pressure is maintained through a pressure regulator by-passing part of the pump output back to the hot water reservoir. A sump pump returns lubricant to the reservoir through a heat exchanger. To prevent sump pump cavitation, a by-pass on the sump pump automatically maintains a pre-set level of lubricant. Lubricant inlet feed pressure can be further regulated through needle valves as shown on the diagram. An emergency water supply to the rotor has also been provided to automatically supply city tap water to the rotor in the event of pump failure. No difficulties were encountered, however, in several months of testing and the test loop has proved to be satisfactory for supplying lubricant under the widely varying test conditions.

F. Test Procedure and Whirl Determination

In the usual testing procedure, the test rig is first brought to temperature by circulating the water lubricant at the desired temperature level. The non-contacting gages for shaft motion measurements are adjusted so that the variation in the gap as the shaft displaces is within the calibration range. Usually the gages are adjusted so that a voltage signal nearly zero represents the position of the shaft mid-way in its clearance along the particular gage axis. Those values are recorded and are referenced to as the gage zero's, i.e., the gage output signal corresponding to the zero eccentricity position.

With the test rig at the desired temperature, a series of static loads are imposed on the shaft through the partial arc loader bearings. For each of the static loads (beginning with zero load) the shaft speed is raised in increments until either half-frequency whirl occurs, or a synchronous orbiting occurs of an amplitude judged to produce near-rubbing conditions. For each of the speed increments, data is recorded on shaft speed, displacement gage d.c. voltage level, flow to test and loader bearings, static load, torque meter readings, etc. The stability of shaft motion is monitored on an oscilloscope. For such monitoring the biased output of the Bently probes is fed directly (without amplification) to the x and y axes of an oscilloscope. A calibration established for this voltage-gap relationship using the oscilloscope permits a realistic picture of relative shaft amplitude to be obtained with the shaft orbiting.

Plotting the x vs. y coordinates of the shaft axis as previously described eliminates time as a parameter on the oscilloscope picture. Hence, without further information, it would not be known whether an orbit of the shaft was occurring at the shaft rotational frequency or at some other sub-harmonic value.

To provide this further information, therefore, the oscilloscope beam is intensified in brightness once each revolution of the shaft. This is accomplished by taking the signal generated by the magnetic speed pick-up, amplifying it and feeding it into the "Z" axis of the oscilloscope. The result is that a stable synchronous whirl appears as an orbit with one dot or intensification on the trace. (Fig. 35). A sub-harmonic orbiting of exactly half-frequency appears as a stationary orbit with two such dots (Fig. 35B). If the orbiting is slightly less than one-half frequency, the dots appear to rotate on the otherwise stationary trace.

When the shaft is exhibiting such an instability, the output signal of the unamplified probes is fed into a wave analyzer and the frequencies and

amplitude of the generated voltage wave is measured and recorded. From the unamplified voltage-gap calibration of the displacement gages, the wave analyzer r.m.s. voltage readings can be converted to vibrational amplitudes.

G. Range of Bearing Variables Tested

Table 8 summarizes the range of bearing test variables covered in the present program. Table 9 summarizes the conditions under which tests were conducted. As was discussed earlier in Section III-B, if the test fluid (water) and the application fluid (potassium) possess identical absolute and kinematic viscosities, tests on the water-lubricated bearing would then produce flow conditions identical to those which would exist on a geometrically similar potassium lubricated bearing. Since the viscosities of the two fluids are similar, but not identical, tests on the water-lubricated bearing produce flow conditions similar to those of a smaller-clearance potassium-lubricated bearing of the same diameter and running at the same speed and load as the test bearing. For example, tests on a water-lubricated, 2 axial groove bearing at 30,000 rpm and with a 2 mil diametral clearance produce an identical Taylor number to a similar bearing of 1 mil diametral clearance lubricated with potassium at 1200°F. The Sommerfeld number of the test bearing likewise will be close to that of the potassium lubricated bearing at one-half the clearance.

From Table 8 and Figures 9 and 10, the potassium bearing conditions comparable to the water-tests can be determined quickly. Since a majority of the tests were carried out with 120°F water lubricant inlet temperature, it can be seen that the test Sommerfeld and Taylor numbers correspond to those of a potassium bearing at approximately one-half the test bearing clearance.

For an unloaded, plain cylindrical bearing, a Taylor number of 41.1 marks the formation of vortices which precede turbulence. Taylor numbers of 244 were obtained with the two axial groove bearing; even higher values (400)

were produced with the tilting pad bearing. Thus, tests were carried on well into the turbulent region by the previous criterion. It must be recalled, however, that the critical Taylor number of 41.1 is based on concentric cylinders (i.e., unloaded plain bearings). There exists no comparable turbulence criterion for the complex geometries as tested in the present program.

Sommerfeld number was varied over a wide range for each test bearing by varying both speed and load. The overall Sommerfeld number ranged from approximately 0.01 to ∞ (zero load). For comparison, with the above Sommerfeld number range the theoretical laminar flow solution predicts an eccentricity ratio for a two axial groove bearing ($L/D = 1$) between 0 and 0.95.

Selected tests were carried out with the eccenters of Figure 31 deliberately unbalanced to produce a symmetrical unbalance force on the test bearings. The maximum unbalance setting was 20° . Based on the measured maximum unbalance at 180° and from the equation given in the previous section, III-E, the unbalance force is calculated as 14.1 lbs. at 100 r.p.s. For a non-orbiting journal axis, the unbalance force increases as the square of the speed. The maximum deliberate unbalance force attained (disregarding orbiting of the journal axis) is calculated to be approximately 66 lbs. Most tests were carried out with only residual unbalance in the system. It is quite possible and perhaps even likely that the actual dynamic loads due to residual unbalance and synchronous shaft whirling exceeded the deliberate unbalance forces.

H. Tests on Two Axial Groove Bearings, $L/D = 1$

The tests conducted on this bearing type can be grouped into two categories according to clearance and whether or not the shaft was deliberately unbalanced. All tests were carried out with the shaft vertical. The table below summarizes the tests with the medium diameter balanced shaft of Figure 12 having a nominal diametral clearance of 3 mils. These tests were No. 1, 100,

2, 3, 300, 4, and 12. In Tests 1, 2, and 3, the primary condition changed was the lubricant temperature. Tests 100 and 300 were essentially partial repeats of Tests 1 and 3, respectively. Test 12 was a repeat of Test 3 with a new bearing set. In Test 4, the eccenters of Figure 31 were replaced by the circular flywheel discs of Figure 26.

1. Tests with 3 mil diametral clearance, zero deliberate unbalance

TWO AXIAL GROOVE BEARING, $L/D = 1$

Test No.	Lube Inlet Temp. °F	Static Load Range Per Bearing, Lbs.	Shaft Speed Range, cps	Rotor Description
1 } 100 }	90°	0-43	60-421	Plain Shaft with Eccenters
2	150°	8.6-43	60-350	"
3 } 300 } 12 }	120°	0-43	60-321	"
4	120°	0.68.8	60-420	Plain Shaft with End Flywheels

In these tests, half-frequency whirl was usually observed at the lowest test speed with no static load. Increased radial static load increased the threshold speed of half-frequency whirl. Table 10 lists the conditions prevailing at the onset of half-frequency whirl. A good correlation was found between the half-frequency whirl threshold and Sommerfeld number, as shown in Figure 36. At Sommerfeld numbers less than approximately 0.25, the data show that speed can be substantially raised for the test shaft without the limitation imposed by half-frequency whirl. A further observation is that the increased lubricant temperature of Test 2 and presumably the greater turbulence level did not affect the threshold speed significantly. When the static load was sufficient to suppress half-frequency whirl, synchronous whirl limited the test speed.

One test was conducted under conditions similar to the previous Test 3, but with a tighter clearance, i.e., the large diameter shaft with a nominal diametral clearance of 2 mils was used. The data is summarized below.

2. Test with 2 mil diametral clearance, zero deliberate unbalance

TWO AXIAL GROOVE BEARING L/D = 1

plain shaft with eccenters

(*HFW = Half-Frequency Whirl)

(SW = Synchronous Whirl)

<u>Test No.</u>	<u>Lube Temp.</u>	<u>Bearing Load-Lbs.</u>	<u>Speed Range cps</u>	<u>Type of Shaft Orbit*</u>
13	120°F	0	60	HFW
		8.6	60-350	HFW
		17.2	60-114	HFW
		"	114-265	Stable (Slight SW)
		"	265-350	HFW + SW
		25.8	60-250	Stable + (Slight SW)
		"	250-350	HFW + SW
		34.4-77.4	60-350	SW at 250 No HFW

In contrast with the tests using a larger clearance bearing, in Test 13, half-frequency whirl disappeared under certain conditions. At a low load (8.6 lbs), half-frequency whirl, (HFW), occurred over the full speed range. At a higher load, (17.2 lbs), the HFW which occurred at 60 cps start-up speed disappeared at 114 cps.

It reappeared again at 265 cps and in combination with synchronous whirl, (SW), at still higher speeds. At and above a bearing load of 34.4 lbs., however, only synchronous whirl was found to occur over the 60 to 350 cps speed range tested.

Tests at two levels of unbalance were carried out with the two axial groove bearing, L/D = 1 and a 3 mil nominal diametral clearance shaft. The conditions for Test 301 were:

- a) plain shaft with eccenters set for 10° unbalance (3.26 gram-inch)
- b) lubricant nominal inlet temperature: 120°F
- c) lubricant inlet pressure: 10 psig
- d) loader bearing nominal flow rate: 0.4 gpm

For Test 302, the unbalance level was increased to 20° (6.25 gram-inches) and other conditions kept similar to Test 301.

3. Tests with 3 mil diametral clearance and deliberate unbalance

TWO AXIAL GROOVE $L/D = 1$

Test No.	L/D	C_D (Mils)	Unbalance at 100 rps lbs.	Static Load Range lbs.	Speed Range	Shaft Stability
301	1	3	7.37	0-51.6	60-300	Half-Frequency Whirl only below 8.6 lbs., 60 cps
302	1	3	14.1	0-43	60-183	Half-Frequency Whirl at 0 load, 60 cps

I. Tests on Two Axial Groove Bearing, $L/D = 1-1/2$

This bearing geometry was tested with three different rotor mass distributions and three journal sizes at a zero unbalance level; in addition, for two of the tests, the shaft was deliberately unbalanced a predetermined amount and data collected on performance.

1. Test with 5 mils nominal diametral clearance, zero unbalance, 2 axial groove, $L/D = 1-1/2$

One test, (No. 5), was run with the above combination.

The testing conditions were:

- a) plain shaft with eccenters set for zero unbalance
- b) lubricant nominal inlet temperature : 120°F
- c) lubricant inlet pressure: 10 psig

d) loader bearing flow rate: 0.4 gpm

The static load on the shaft was varied between 0 and 43 lbs. per bearing in 6 steps; the speed range was 60 to 350 cps, limited by HFW amplitudes. A behavior was observed similar to that obtained with the 3 mil nominal clearance shaft. That is, the HFW threshold was delayed by the application of static load. Table 11 summarizes the conditions prevailing at the threshold speed. Figure 36 is a plot of the threshold speed versus Sommerfeld number, which can be seen to be similar to that obtained with the shorter L/D and tighter clearance shaft (Fig. 35).

2. Test with 3 mil nominal diametral clearance shaft, zero unbalance, 2 axial groove, L/D = 1-1/2

Conditions a, c, and d were kept the same for this test, (No. 7), as for Test 5 above. The lubricant inlet temperature, however, was permitted to be at room ambient to ascertain whether eccentricity ratio and attitude angles could be determined more precisely. In this test the load was varied between 0 and 43.0 lbs. per bearing. The speed range was 60 to 350 cps, with the upper limit imposed by a combination of synchronous and half-frequency whirl. Data is summarized in Table 11 and plotted in Figure 36.

3. Tests with 2 mils nominal diametral clearance, zero unbalance, 2 axial groove, L/D = 1-1/2

Several tests were conducted with this configuration and are summarized in the table below.

TWO AXIAL GROOVE BEARING L/D = 1-1/2

(HFW = Half-Frequency Whirl)

(SW = Synchronous Whirl)

Test No.	Temp.	Static Load Lbs.	Speed Range	Mass Distr.	Stability Behavior
6	75° (15 psig)	0-51.6	60-400	Eccenters	HFW disappears with speed, load increases
600	75° (70 psig)	0-43.6	60-400	Eccenters	" "
18	120°F	0-77.4	60-570	End Flywheels	HFW at low speeds, loads. None at loads > 34.4 lbs. up to 570 cps
19	120°F	0-0	60-250	Central Mass	HFW
		8.6	60-400	"	HFW or HFW + SW over range
		17.2-77.4	60-330	"	" "

Table 12 summarizes the test conditions at which HFW disappeared for Test 6 and 600. Table 13 summarizes the threshold speeds for the data of Tests 18 and 19.

4. Test with 5 mil nominal diametral clearance, and deliberate unbalance, 2 axial groove bearing, L/D = 1-1/2

Test No. 501 conditions were as follows:

- a) plain shaft with eccenters set for 5° unbalance (1.63 gram-inch)
- b) lubricant nominal inlet temperature: 120°F
- c) lubricant inlet pressure: 10 psig
- d) loader bearing nominal flow rate: 0.4 gpm

Bearing static load was varied between 0 and 43.0 lbs. in 6 steps; maximum test speed was 300 cps at the highest load, at which HFW occurred. The general behavior observed was a synchronous shaft orbiting for a given load until the speed was raised sufficiently to produce the combination type instability. Higher static loads delayed the onset from 150 cps at 8.6 lbs.

bearing load to 202 cps at 34.4 lbs. load.

5. Test with 3 mil nominal diametral clearance, and deliberate unbalance, 2 axial groove, $L/D = 1-1/2$

One test, (No. 701), was conducted on this configuration. The test conditions were:

- a) plain shaft with eccenters set for 10° unbalance (3.26 gram-inches)
- b) lubricant nominal inlet temperature: 75°F
- c) lubricant inlet pressure: 10 psig
- d) loader bearing flow rate: 0.4 gpm

The load was varied between 0 and 43.0 lbs. per bearing and the speed between 60 and 300 cps. Half-frequency whirl was observed only at low speeds, (60 cps), and at loads of 25.8 and below. Higher speeds and loads produced synchronous shaft orbiting, limiting the maximum test speed.

J. Tests on Tilting-Pad Bearing, $L/D = 1$

The four pad bearing shown in Figure 4 was tested with three shafts to provide varying clearances. The test conditions imposed were:

- 1. Test No. 8 - largest shaft (1.253 inch diameter)
 - a) plain shaft with eccenters set for zero unbalance
 - b) lubricant nominal inlet temperature: 120°F
 - c) lubricant pressure adjusted to maintain flow of 0.4 gpm to test and loader bearing

For this test the load was varied from zero to 77.4 lbs. per bearing in 7 steps. The speed range covered was 60 to 350 cps and was limited by a predominantly synchronous shaft orbiting. Half-frequency whirl was not observed; however, tests at all levels of static load showed synchronous whirl beginning at 150 to 200 cps. At speeds in the vicinity of 300 to 350 cps, the shaft orbit pattern observed on the oscilloscope became non-repetitive, i.e., the orbit appeared to "flutter." Typical oscilloscope traces showing this fluttering

are given in Figures 38A and B.

2. Test No. 9 - smallest shaft (1.2500 inch diameter)

Test conditions a, b, and c were kept the same as for Test No. 8. The load was varied between 0 and 77.4 lbs. and the speed between 60 and 350 cps. The behavior was substantially the same as for Test 8. Speed was limited by synchronous orbiting, with a "fluttering" of the shaft orbit observed at the higher test speeds.

3. Test No. 10 - medium shaft (1.2520 inch diameter)

Test conditions were kept the same as in Tests 8 and 9. Load and speed ranges were also identical. The shaft behavior was similar to that occurring with Tests 8 and 9, with an unstable, predominantly synchronous orbiting of the shaft limiting the test speed.

K. Tests on Three-Lobe Bearing, $L/D = 1$

One test, (No. 11), was carried out on this bearing configuration with the medium clearance shaft size, (diameter 1.252 inches). The other test conditions imposed were:

- a) plain shaft with eccenters set for zero unbalance
- b) lubricant nominal inlet temperature: 120°F
- c) lubricant nominal inlet pressure: 20 psig

The load was varied between 0 and 51.6 lbs. per bearing in 6 steps for this test, and the speed range covered was 0 to 350 cps. An attempt to raise the bearing load to 77.4 lbs. resulted in a scoring of the lower bearing. HFW was not observed with this bearing type. The bearing, however, exhibited synchronous whirl for all static loadings at speeds beginning at 200 to 250 cps. No further deliberate unbalance was imposed since testing was already limited by synchronous whirl.

L. Tests on Displaced Elliptical Bearing, L/D = 1

Three tests were carried out on this bearing configuration shown in Figure 7. The test conditions common to all three tests were:

- a) plain cylindrical shaft (Fig. 12) with eccenters (Fig. 31)
- b) lubricant nominal inlet temperature: 120°F
- c) flow rate to test bearing maintained at 0.14 gpm

The range of test variables and the observations on stability are summarized below:

DISPLACED ELLIPTICAL BEARINGS				
		L/D = 1	120°F	
Test No.	Shaft Size	Load Range Lbs.	Speed Range cps	Shaft Motion
15	Medium	0-51.6	60-400	HFW at 0 load, 270 cps. SW + HFW at 0 load, 400 cps
16	Medium + Unbalance (7.1b/100 cps)	0-25.8	60-200	SW, entire range
17	Small	0-51.6	60-392	HFW at 0 load HFW + SW with load ≥ 8.6 lb, speeds > 260 cps

M. Tests on Compound Cylindrical Bearing, L/D = 1

One test, (No. 14), was carried out on this bearing type shown in Figure 6. The essential test conditions were:

- a) plain test shaft (Fig. 12) of smallest diameter with eccenters (Fig. 31)
set for zero unbalance
- b) lubricant nominal inlet temperature 120°F
- c) lubricant inlet pressure: 5 psig

Half-frequency whirl was observed with no radial load at a test

speed of 60 cps. With a light load of 8.6 lbs., only synchronous whirl existed until a speed of 350 cps was attained. A combination of half-frequency and synchronous whirl was then observed. Heavier static loads produced only synchronous whirl up to the maximum test speed of 350 cps. Loads were limited to 34.4 lbs.

N. Comparison of Bearing Performance

Two of the test bearing types - the three-lobe and tilting pad bearings - did not exhibit half-frequency whirl under any of the imposed test conditions. The three-lobe bearing was tested at zero static load at speeds up to 350 rps, (Test No. 11). Speed was arbitrarily restricted to 350 cps because of an increasing amplitude of synchronous orbiting. A static load of 77.4 lbs. on the bearing stalled the test shaft. A similar test speed (350 cps) was attained with the tilting pad bearing under a light load, (8.6 lbs), and for each of the three test clearances (Tests 8, 9, 10). A static load of 77.4 lbs. applied even at the lowest test speed of 60 cps produced no difficulty.

With the compound cylindrical bearing, a speed of 350 cps was attained under a static load of 8.6 lbs, (Test No. 14). A combination of half-frequency and synchronous whirl prevented further speed increases. It was found necessary to limit the static load to 34.4 lbs. The displaced elliptical bearing was operated at zero load and speeds up to 350 cps; half-frequency whirl and synchronous whirl were both observed over this frequency range (Tests 15, 16, 17). The maximum applied load was 51.6 lbs.

With a two axial groove bearing, $L/D \approx 1-1/2$, a test speed of 400 cps was attained without failure under a light static load of 8.6 lbs. (Test No. 600) and a 2 mil shaft diametral clearance. Half-frequency whirl which had occurred at low speeds disappeared with the higher test speed values. A similar test (No. 18) in which the eccenters were replaced by end flywheels permitted a

speed of 350 cps to be reached with no static load. A combination type whirl had appeared at 293 cps. With a load greater than 34.4 lbs., however, no half-frequency whirl instability was observed. The maximum test speed of 570 cps was reached with this bearing type which also was found capable of sustaining 77.4 lbs. static load at a shaft speed of only 60 cps.

In Test No. 3 on the 2 axial groove bearing $L/D = 1$ with a light load (8.6 lbs.) and a 3 mil diametral clearance, half-frequency whirl limited the test speed to 195 cps.

Several tests were conducted in which a deliberate unbalance was superimposed on the system. A similar amount of unbalance (3.26 gram-inch) was imposed on the two axial groove bearing ($L/D = 1$, and $1-1/2$) and the orthogonally displaced elliptical bearing in Tests No. 301, 701, and 16 respectively. This deliberate unbalance corresponds to a rotating load of approximately 7.4 lbs. at 100 rps.

For both two axial groove bearings ($L/D = 1$, $1-1/2$) a speed of 300 cps was attained with a light static load (8.6 lbs.) and the above deliberate unbalance on each test bearing. A previous test (No. 3, $L/D = 1$) with no unbalance produced a half-frequency orbiting at 195 cps; a static load of 25.8 lbs. with no deliberate unbalance was required to delay the onset of half-frequency whirl to 300 cps. For the longer two axial groove bearing with no deliberate unbalance, a smaller static load (17.2 lbs.) was sufficient to suppress half-frequency whirl to a speed of 307 cps.

The data on film thickness and attitude angle is not accurate enough to permit a detailed comparison among the different bearing types. As is explained more fully in Reference 6, an apparent shifting of the gage zero occurs when the shaft is rotating. The magnitude of the shift appears to be speed dependent. The displacement gage calibration sensitivity, however, does

not appear to be affected by the zero shift, as is shown by Figure 39. Hence the item of primary interest - the observation of shaft stability - was not hampered.

When a different gage zero position is assumed for the high and lower speed test runs, a reasonable trend of eccentricity ratio (or film thickness) with Sommerfeld number exists. Typical data is shown in Figures 40-44, for the two axial groove bearing. Figure 44 illustrates the fact that small variations in film thickness due to varying load at a constant shaft speed can be detected. An attitude angle and eccentricity ratio for one of the test points are assumed and the data referred to this test point. Figure 45 shows the variation in eccentricity ratio with Sommerfeld number for one test with the tilting pad bearing. In Figure 45, the gage zero position assumed for the data reduction was the "static" zero, i.e., the zero eccentricity position measured by back-and-forth shaft displacement. Although the data trend at a given speed is in the direction predicted by theory, the variation in absolute level precludes a detailed comparison of film thickness and attitude angles.

A substantial amount of data on friction torque was accumulated in the course of testing. Figures 46-59 presents the data in the form of plots of friction factor (coefficient of friction) vs Sommerfeld number. Figures 60-82 presents plots of torque coefficient vs Reynolds number, where torque coefficient is the dimensionless ratio of unit shear stress to velocity head.

$$T_C = \frac{t}{4RA_s} \div \frac{1}{2} \frac{\rho V^2}{g}$$

$$\frac{t}{4R} = \text{friction force at test bearing surface}$$

R = shaft radius

A_s = test bearing area exposed to viscous shear

$\frac{\rho}{g}$ = mass density of water lubricant

V = journal surface velocity

Figures 83-96 present friction torque data in the form of plots of torque coefficient versus Reynold's number ratio. Reynold's number ratio is the value of the test run Reynold's number to the critical value according to the Taylor criterion marking the transition to turbulence. The test run Reynold's number is based on the radial clearance for the cylindrical bearings and on the minimum measured clearance for the displaced arc bearing types.

The maximum power measured in the tests occurred in Test No. 18 with the two axial groove bearing, $L/D = 1-1/2$ and a nominal 2 mil diametral clearance. The power absorbed was 3.14 hp at a test speed of 500 cps. The calculated torque coefficient was 0.00299 at a Reynold's number of 2277, or about 2.15 times the critical Reynold's number based on the Taylor criterion. By comparison, for an unloaded cylindrical bearing in laminar flow the torque coefficient is given by $2/Re$. The measured torque coefficient therefore is about 3.4 times greater than that for laminar flow.

A comparison of power loss and torque coefficient for several different bearing types at 350 cps shaft speed is given below. In all tests, a light static load of 8.6 lbs. was applied to the bearing. Lubricant temperature was 120°F . Power is the total delivered to the shaft.

<u>Bearing Type</u>	<u>L/D</u>	<u>Journal Diam.*</u>	<u>Horsepower</u>	<u>Torque Coefficient</u>
2 axial groove	1	L	0.991	0.00274
	1-1/2	L	1.28	0.00354
Tilting pad	1	L	0.772	0.00240
		S	0.899	0.00277
Displaced ellipt.	1	L	0.807	0.00223
		M	.991	0.00274
Three lobe	1	M	1.055	0.00292
Compound Cylindrical	1	L	0.945	0.00262

*L = 1.253 inch

M = 1.252 inch

S = 1.250 inch

From the previous table it will be seen that the difference among the bearing types is not great. The highest power was consumed by the long, 2-axial groove bearing, which was also experiencing a combined synchronous and half-frequency whirl under the test condition imposed. The tilting-pad bearing with the special feed arrangement absorbed the least power.

REFERENCES

1. A. C. Hagg, "The Influence of Oil Film Journal Bearings on the Stability of Rotating Machines," Journal of Applied Mechanics, Sept., 1946, pp. A-211-220.
2. H. Poritsky, "Contribution to the Theory of Oil Whip," Trans. ASME Vol. 75, 1953, pp. 1153-1161.
3. "Low Viscosity Bearing Stability Investigation," General Electric Company Quarterly Progress Report No. 3, Under Contract NAS 3-2111 for N.A.S.A.
4. "Low Viscosity Bearing Stability Investigation," General Electric Company Quarterly Progress Report No. 6, Under Contract NAS 3-2111 for N.A.S.A.
5. "Low Viscosity Bearing Stability Investigation," General Electric Company Progress Report for July, 1963, Under Contract NAS 3-2111 for N.A.S.A.
6. "Low Viscosity Bearing Stability Investigation," General Electric Company Quarterly Progress Report No. 8, Under Contract NAS 3-2111 for N.A.S.A.

Table I

COMPARISON OF PHYSICAL PROPERTIES

of

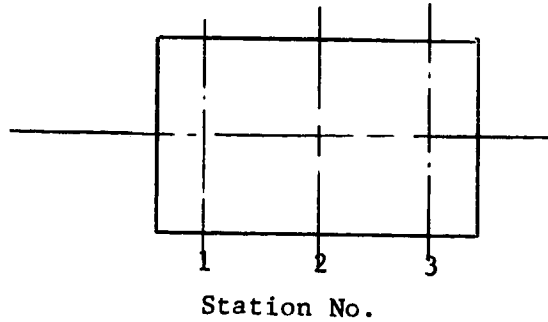
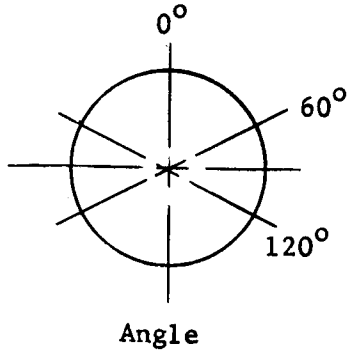
TEST FLUIDS TO POTASSIUM

Physical Properties	Potassium		Water		Silicones				N-Heptane	
	Prop.	Temp. °F	Prop.	Temp. °F	.65cs Fluid Prop.	Temp. °F	1.0cs Fluid Prop.	Temp. °F	Prop.	Temp. °F
Absolute Viscosity #/Ft-Hr.	.45	800	1.66	100	1.07	100	1.77	100	.83	100
	.38	1000	1.04	150	.88	150	1.39	150	.68	150
	.33	1300	.74	200	.80	200	1.15	200	.61	200
Density #/Ft ³	44.6	1000	61.2	150	47.5	120	51	120	42.5	150
Kinematic Viscosity Ft ² /Hr.	.0085	1000	.0170	150	.0185	150	.0270	150	.0160	150
Specific Heat BTU/#-°F	.19	1000	1.00	150	.34	150	.34	150	.52	150
Conductivity BTU/Hr.-Ft-°F	21	1000	.38	150	.06	120	.06	120	.09	150
Vapor Pressure PSIA	.16	800	.95	100	1.35	100	.15	100	.97	80
	.95	1000	3.72	150	4.6	150	.58	150	3.9	134
	8.0	1300	11.5	200	12.6	200	2.0	200	14.5	200

Table 2 - COMPARISON OF DIMENSIONLESS LOAD CAPACITIES

BEARING TYPE & DESCRIPTION		$\frac{L}{D}$	LOAD CAPACITY $10^{-6} \frac{W}{\mu N D^2}$ FOR 0.0005 IN. MIN. FILM, CENTRAL LOAD, 1-1/4 IN. DIA. SHAFT			
			NO LOAD MIN. FILM h_o , IN.			
			0.001	0.00175	0.0020	0.0025
2 AXIAL GROOVE CYLINDRICAL		1/2	0.39	.42		.38
		1	2.1	1.83		1.53
		1-1/2	4.4	3.2		2.53
DIS- PLACED ARC BRGS.	THREE LOBE (FIG. 15) = 0.002 IN. $m = \frac{\epsilon}{h_o + \epsilon}$	1/4	.055		.067	
		1/2	.272		.25	
		1	.81		.82	
	COMPOUND CYL. (FIG. 15) = 0.002 $m = \frac{\epsilon}{h_o + \epsilon}$	1-1/2	0.30		0.31	
		1	0.11		0.12	
	ORTHOG. DISP. (FIG. 22) $q=s=0.5 \quad \lambda=0.002$ IN.	1/2	0.1		0.045	
RAYLEIGH STEP, 16 PAD $B_1/B_2 = 7/3, \Delta/D = 0.00025$		1/2	.00393		0.0045	
		1	.00785		0.0099	
TILTING PAD (FIG. 4) $d/B = 0.5588$ PIVOT LOCATION		1/2	$\frac{0.212}{.048}$ Max./Min.	$\frac{.289}{.209}$		$\frac{.298}{.208}$

Table 3
Journal Measurement of Test Shaft



Drawing & Part No.	STA. No.	Journal 1			Journal 2		
		0°	60°	120°	0°	60°	120°
4012000- 782-P1	1	1.25295	1.25297	1.25299	1.25296	1.25297	1.25296
	2	1.25298	1.25297	1.25298	1.25300	1.25301	1.25300
	3	1.25297	1.25299	1.25300	1.25298	1.25299	1.25299
4012000- 782-P2	1	1.25210	1.25208	1.25208	1.25204	1.25204	1.25203
	2	1.25208	1.25208	1.25208	1.25206	1.25206	1.25205
	3	1.25202	1.25201	1.25202	1.25207	1.25207	1.25204
4012000- 782-P3	1	1.24998	1.24999	1.24996	1.24997	1.24996	1.24996
	2	1.25000	1.25000	1.24997	1.25002	1.25001	1.25001
	3	1.24996	1.24996	1.24995	1.25001	1.25000	1.24998
<u>LARGE SHAFT</u>							
4012000- 765-P1	1	1.25300	1.25297	1.25300	1.25299	1.25298	1.25297
	2	1.25298	1.25297	1.25296	1.25291	1.25294	1.25291
	3	1.25300	1.25301	1.25296	1.25292	1.25295	1.25294

Table 4

TEST ROTOR MASSES & INERTIAS

Test Rotor Description	Weight of Assembly	Polar Moment of Inertia About Shaft Axis I_P $10^3 \times \text{lb. in. sec.}^{-2}$	Transverse Moment of Inertia About Rotor c.g. I_T $10^3 \times \text{lb. in. sec.}^{-2}$	Ratio of Polar to Transverse Inertias I_P/I_T
Lbs.				
Plain shaft (Fig. 12) with eccenters (Fig. 31)	7.13	5.57	746	0.00746
Plain shaft (Fig. 12) with flywheels (Fig. 26)	8.77	21.8	1100	0.01975
Large shaft (Fig. 27) with eccenters (Fig. 31)	29.4	194	940	0.204

Table 5

CALCULATED CRITICAL SPEEDS [RPM]

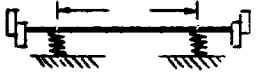




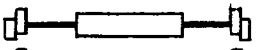
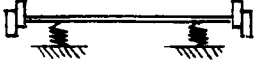
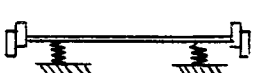
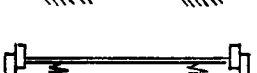


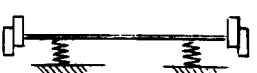

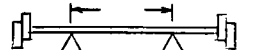
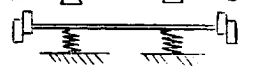
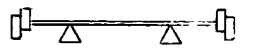


CRITICAL SPEED			HINGED - HINGED	RIGID SHAFT ON SPRINGS	CONFIGURATION
SHAFT DIAMETER [inch]	SHAFT SPAN [inch]	FILM STIFFNESS [lb/inch]			
1.0	12	1×10^5	-----	1. Critical = 16,314 2. Critical = 25,482 3. Critical = 32,469	
1.0	12	-----	1. Critical = 17,565 2. Critical = 34,971	-----	
1.0	12	-----	1. Critical = 14,721 2. Critical = 30,240	-----	
1.25	12.5	-----	1. Critical = 27,147	-----	
1.25	12.5	-----	1. Critical = 24,845	-----	
1.25	12.5	-----	1. Critical = 33,889	-----	
1.25	12.5	$.5 \times 10^5$	-----	1. Critical = 15,697 2. Critical = 20,770 3. Critical = 26,719	
1.25	12.5	1×10^5	-----	1. Critical = 19,665 2. Critical = 27,574 3. Critical = 29,541	
1.25	12.5	5×10^5	-----	1. Critical = 23,522 2. Critical = 39,492	
1.5	12.5	-----	1. Critical = 34,713	-----	
1.5	12.5	0.5×10^5	-----	1. Critical = 16,664 2. Critical = 18,853 3. Critical = 35,622	
1.5	12.5	1.0×10^5	-----	1. Critical = 23,226 2. Critical = 26,004 3. Critical = 36,120	
1.5	12.5	5×10^5	-----	1. Critical = 34,370	
1.25	7.5	-----	1. Critical = 33,159	-----	
1.25	7.5	1.0×10^5	-----	1. Critical = 19,170 2. Critical = 30,032	
1.25	7.5	-----	1. Critical = 29,919	-----	
1.5	7.5	-----	1. Critical = 55,964	-----	
1.5	7.5	1×10^5	-----	1. Critical = 21,436 2. Critical = 28,939	

Table 6 below summarizes the results of the calibration with the sensing tips recessed in the holders. Group A shows the results with air alone; group B in distilled water, no air.

Table 6

CALIBRATION OF BENTLY GAUGES, 6/21 - 6/25/63

Group No.	Gauge No.	Voltage Change for 0.006 inch nominal displacement (± 2.955 mils)	Gauge Sensitivity volts/mil - increasing gap + decreasing gap	Mean Deviation Micro-inches
A	1B*	61.864	10.386	29
	2	62.392	10.425	27
	3	61.776	10.302	32
	4	62.555	10.815	18
	Avg.		10.482	
B	1B*	45.382	7.473	28
	2	46.991	7.743	18
	3	46.163	7.838	72
	4	47.621	7.501	34
	Avg.		7.639	

* Different sensing tip in No. 1 gauge holder than in original calibration

Table 7

SENSITIVITY OF TORQUE DRIVE SHAFTS

Shaft No.	Shaft Dia, inch	Expt. Sensitivity 1b inch/degree twist	Sensitivity Ratio (compared to largest shaft)	
			Experimental	Theoretical
1	0.1865	0.705	1	1
2	0.1558	0.346	.491	.487
3	0.1238	0.139	.197	.194
4	0.092	0.0414	.0587	.0592

Table 8

SUMMARY OF BEARING VARIABLE TEST RANGE

Bearing Type	$\frac{\text{Length}}{\text{Diameter}}$ Ratio	Lube Temp. (°F)	Lube Abs. Viscosity $\frac{\text{lb. sec.} \times 10^7}{\text{in}^2}$	Nom. Diametral Clearance (in.) ($\times 10^{-3}$)	Speed Range (RPM)	Film Reynolds No. Range	Taylor* No.	Bearing Static Radial Load (lbs.)	Bearing Deliberate Unbalance Load (lbs. at 100 cps)
2-Axial Groove	1	90°F 120°F 150°F	1.1 0.82 0.64	2, 3, 5	3,600 34,200	216 3,713	9 to 222	0 to 77.4	Residual, 7.4 14.1
2-Axial Groove	$1\frac{1}{2}$	75°F 120°F	1.4 to 0.82	2 3 5	3,600 to 34,200	190 4,000	7.4 to 244	0 to 77.4	Residual to 7.4
Tilting Pad (4-Pads)	1	120°F	0.82	3.2 4.3 6	3,600 to 21,000	388 to 5,500	18 to 400	0 to 77.4	Residual
3-Lobe	1	120°F	0.82	1 mil nom.	3,600 to 21,000	78 756	3.2 to 20	0 to 51.6	Residual
Compound Cylindrical	1	120°F	0.82	3 mils nom.	3,600 to 21,000	408 2,530	20 to 126	0 to 34.4	Residual
Displaced Elliptical	1	120°F	0.82	3 mils 5.4	3,600 to 23,500	414 4,580	20 to 310	0 to 51.6	Residual to 7.4

* Based on minimum nominal clearance for bearing type.

Bearing Description	Type	L/D	Fig. No.	Test No.	Rotor Description (see note)							Static Load Range	Speed Range	Inlet Lube Temp. °F	Stability Observation (HFW = Half-Frequency Whirl SW = Synchronous Whirl)		
					Mass Distribution	Journal Diameter			Eccenter Unbalance Degrees								
						A	B	C		S	M					L	
2 Axial	1	2	1	1	x					x			90	HFW at maximum cps each load set			
	1	2	2	100	x					x			90	HFW and SW noted			
	1	2	1	2	x					x			150	HFW at high cps, low loads; SW at high cps, high loads			
	1	2	3	3	x					x			120	HFW at high cps, low loads; SW at high load, all cps			
	1	2	300	300	x					x			120	HFW at maximum cps each load set			
	1	2	1	2	x					x			120	HFW at 8.6 lb. load			
	1	2	4	4	x					x			120	HFW at maximum cps each load set			
	1	2	1	2	x					x			120	HFW at low load; no HFW above 34.4 lb. load			
	1	2	1	2	x					x			120	HFW below 8.6 lbs., 60 cps			
	1	2	1	2	x					x			120	HFW at 0 load, 60 cps			
	2 Axial	1-1/2	3	5	5	x					x			120	CPS limited by amplitude of HFW		
		1-1/2	3	7	7	x					x			75	No whirl at low cps; SW at medium cps; HFW + SW high cps		
1-1/2		3	6	6	x					x			75	HFW at low cps; SW at other cps			
1-1/2		3	600	600	x					x			75	70 psig - HFW at 60 cps; SW > 60 cps			
1-1/2		3	501	501	x					x			120	HFW at high cps all loads; SW at other cps			
1-1/2		3	701	701	x					x			75	HFW at 60 cps < 25.8 lb. load			
1-1/2		3	18	18	x					x			120	HFW at low cps and loads; no HFW with load > 34.4			
1-1/2		3	19	19	x					x			120	HFW at 0 load; HFW + SW above 0 load			
Tilting Pad		1	4	8	8	x					x			120	No HFW; predominantly SYN. whirl		
		1	4	9	9	x					x			120	No HFW; predominantly SYN. whirl		
		1	4	10	10	x					x			120	No HFW; predominantly SYN. whirl		
		1	4	11	11	x					x			120	No HFW; SYN. whirl > 200 cps		
Three Lobe	1	5			x					x							
Compound Cylindrical	1	6			x					x							
Displaced Elliptical	1	6	14	14	x					x			120	8.6 lb. load, HFW + SW at 350 cps; SW > 8.6 lb. load			
	1	7	15	15	x					x			120	HFW at 0 load - 270 cps; HFW + SW at 0 load - 400 cps			
	1	7	16	16	x					x			120	SYN. whirl - entire range			
	1	7	17	17	x					x			120	HFW at 0 load; HFW + SW at high cps all loads			
	1	7			x					x							

NOTES ON ROTOR DESCRIPTION

- A = Plain Shaft (Fig. 12) with Eccenters (Fig. 31)
B = Plain Shaft (Fig. 12) with End Fly Wheels (Fig. 26)
C = Large Central Mass Shaft (Fig. 27) with Eccenters (Fig. 31)
S = Small Journal Diameter = 1.250 inch
M = Medium Journal Diameter = 1.252 inch
L = Large Journal Diameter = 1.253 inch

Table 9

OVERALL SUMMARY
of
BEARING TESTS

Table 10

Threshold Speed of Half-Frequency Whirl
 2 Axial Groove Bearing
 $L/D = 1$

Test No.	Run No.	Speed Cps	Radial Clearance Mils	Bearing Load Lbs.	Sommerfeld No.		Reynolds' No. Ratio	
					U	L	U	L
1	7	237	1.450	8.60	.783	.854	1.517	1.393
	11	200	"	17.20	.360	.360	1.176	1.176
	17	270	"	25.80	.305	.301	1.689	1.710
	24	320	"	34.40	.258	.255	2.100	2.124
100	5	217	"	8.60	.785		1.416	
	6	206	"	17.20	.440		1.657	
	7	264	"	25.80	.304		1.723	
	8	265	"	25.80	.306		1.730	
	9	322	"	34.40	.279		2.102	
2	4	179	1.320	8.60	.537	.543	1.324	1.310
	8	207	"	17.20	.310	.312	1.533	1.523
	14	279	"	25.80	.281	.279	2.048	2.063
3	4	195	1.390	8.60	.575	.559	1.431	1.471
	7	222	"	17.20	.330	.318	1.616	1.675
	12	300	"	25.80	.305	.293	2.130	2.217
300	4	205	"	0	--	--	1.492	1.526
	7	200	"	8.60	.585	.570	1.478	1.518
	10	220	"	17.20	.317	.312	1.649	1.680
4	3	190	"	8.60	.579	.556	1.349	1.404
	8	215	"	17.20	.325	.312	1.540	1.600
	13	280	"	25.80	.280	.271	2.022	2.084
12	19	350	"	34.40	.264	.254	2.507	2.605
	2	60	"	8.60	.173	.173	.446	.447
	3	192	"	8.60	.555	.555	1.428	1.429
	4	226	"	17.20	.329	.324	1.669	1.693
	7	189	"	8.60	.550	.543	1.396	1.416
	13	254	"	25.80	.252	.247	1.831	1.877
	14	321	"	34.40	.232	.229	2.388	2.421

Table 11

Threshold Speed of Half-Frequency Whirl

2 Axial Groove Bearing

 $L/D = 1.5$

Test No.	Run No.	Speed Cps	Radial Clearance Mils	Bearing Load Lbs.	Sommerfeld No.		Reynolds' No. Ratio	
					U	L	U	L
5	4	156	2.385	17.20	.1099	.1094	2.726	2.772
	8	140	"	8.60	.2136	.2093	2.259	2.315
	12	180	"	25.80	.0887	.0867	2.997	3.080
	17	212	"	34.40	.0784	.0771	3.529	3.605
	18	245	"	34.40	.0959	.0916	3.850	4.052
	25	313	"	43.00	.0955	.0930	5.050	5.216
	26	350	"	43.00	.1043	.1006	5.783	6.024
7	7	300	1.450	8.60	1.9146	2.0216	1.485	1.407
	13	307	"	17.20	.9930	1.0486	1.500	1.420
	14	60	"	25.80	.1443	.1404	.263	.270
	19	300	"	25.80	.6382	.6558	1.485	1.446
	20	338	"	25.80	.7094	.7489	1.696	1.607
	27	320	"	34.40	.5037	.5318	1.606	1.521
	34	327	"	43.00	.4174	.4231	1.619	1.597
	35	350	"	43.00	.4290	.4290	1.804	1.804

Table 12
Threshold Speed of Half-Frequency Whirl
2 Axial Groove Bearing
L/D=1 1/2

Test No.	Run No.	+Speed cps	Radial Clearance Mils	Bearing Load Lbs.	Sommerfeld No.		Reynolds' Ratio	
					U	L	U	L
6	2	64	0.932	43.00	.1716	.1754	.157	.154
	4	100		8.60	1.6994	1.6441	.232	.241
	13	110		17.20	.9219	.9293	.259	.258
	20	112		25.80	.6344	.6395	.260	.259
	22	150		25.80	.8381	.8448	.353	.352
	29	124		34.40	.5268	.5238	.288	.291
	35	101		34.40	.3433	.3508	.234	.230
	42	107		8.60	1.6839	1.6767	.267	.268
	48	60		17.20	.9972	.9929	.284	.285
600	55	100	0.932	8.60	1.7081	1.6324	.230	.241
	63	92		17.20	.7645	.7509	.218	.221
	72	90		25.80	.5040	.4939	.211	.215
	80	92		34.40	.3864	.3735	.216	.223
	86	98		43.00	.3248	.3227	.233	.234

+Speed at which HFW disappears as speed is increased for constant load.

Table 13
Threshold Speed of Half-Frequency Whirl
2 AXIAL GROOVE BEARING $L/D = 1-1/2$

Test No.	Run No.	Speed cps	Rad Cl. Mils	Bearing Load Lbs.	Sommerfeld No.		Reynold's No. Ratio	
					u	l	u	l
18	12	*90	.941/.970	8.60	.6033	.5408	.353	.388
	17	**299		8.60	2.0414	1.7602	1.151	1.315
	20	*83		17.20	.2782	.2494	.325	.358
	25	**291		17.20	.9842	.8512	1.131	1.288
	26	*344		17.20	1.1239	1.0004	1.384	1.531
	28	*98		25.80	.2252	.1963	.374	.422
	32	**302		25.80	.6525	.5855	1.225	1.344
	33	*318		25.80	.6768	.6165	1.309	1.415
	6	**60	.986/.969	8.60	.3515	.3563	.263	.262
	16	**141		17.20	.4162	.4215	.613	.611
	19	**60		25.80	.1163	.1188	.265	.262
19	21	**170		34.40	.2550	.2523	.727	.742
	22	**280		51.60	.2714	.2736	1.236	1.237
	23	**330		77.40	.2148	.2163	1.446	1.449

* - HFW Stops

** - HFW Starts

WATER VISCOSITY vs TEMPERATURE

Source: H. Schlichting
Boundary Layer Theory
McGraw-Hill, 1960

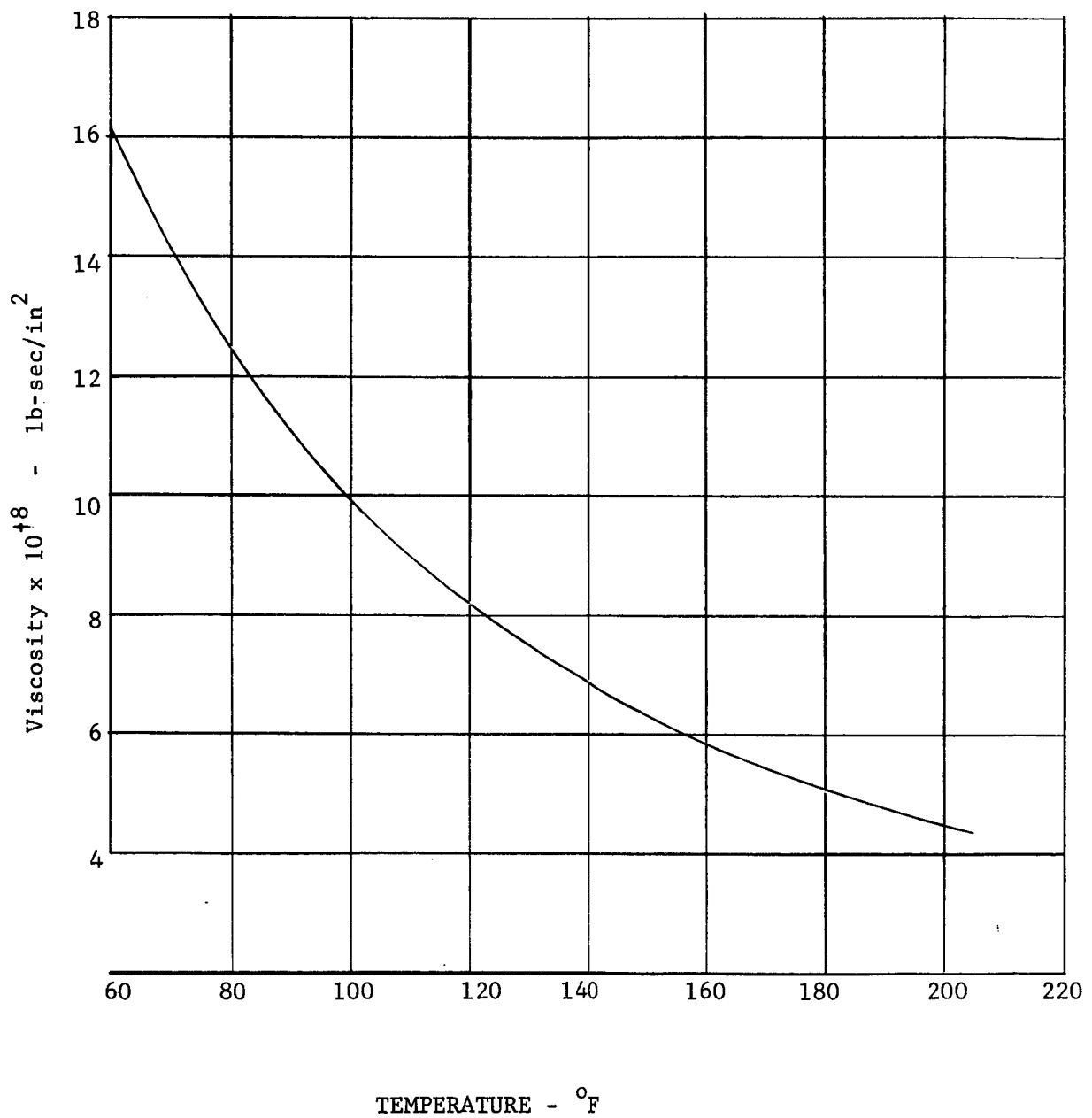


Figure 8

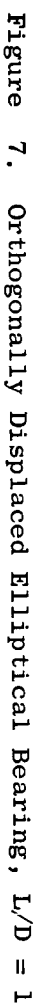


Figure 7. Orthogonally Displaced Elliptical Bearing, $L/D = 1$



Figure 6. Compound Cylindrical Bearing, $L/D = 1$



Figure 5. Three Lobed Bearing
L/D = .5 -1.0

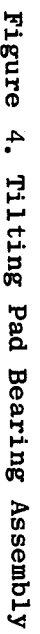




Figure 3. Two-Axial-Groove Cylindrical Bearing

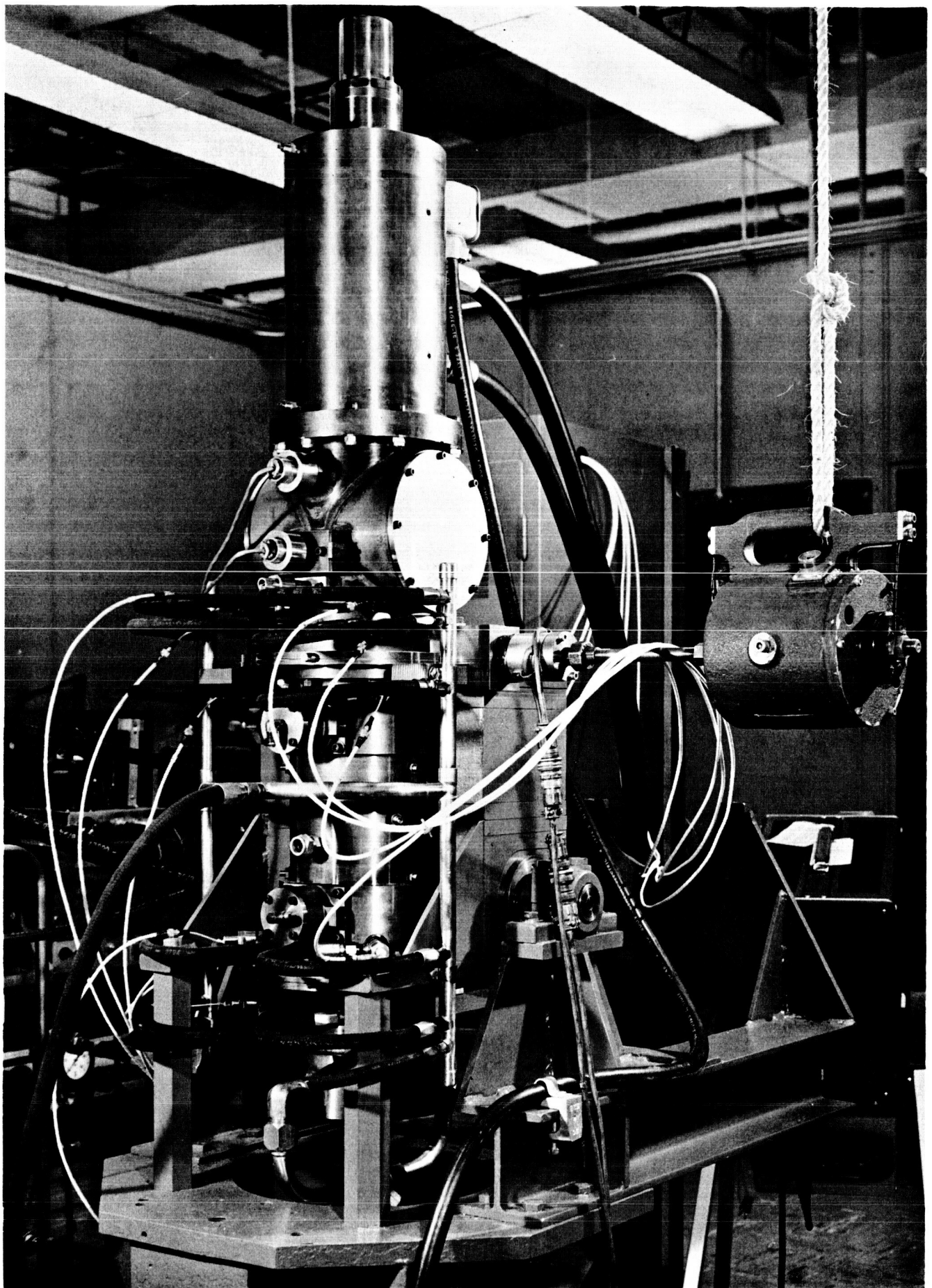


Figure 1. Close-up View of Test Rig Assembly

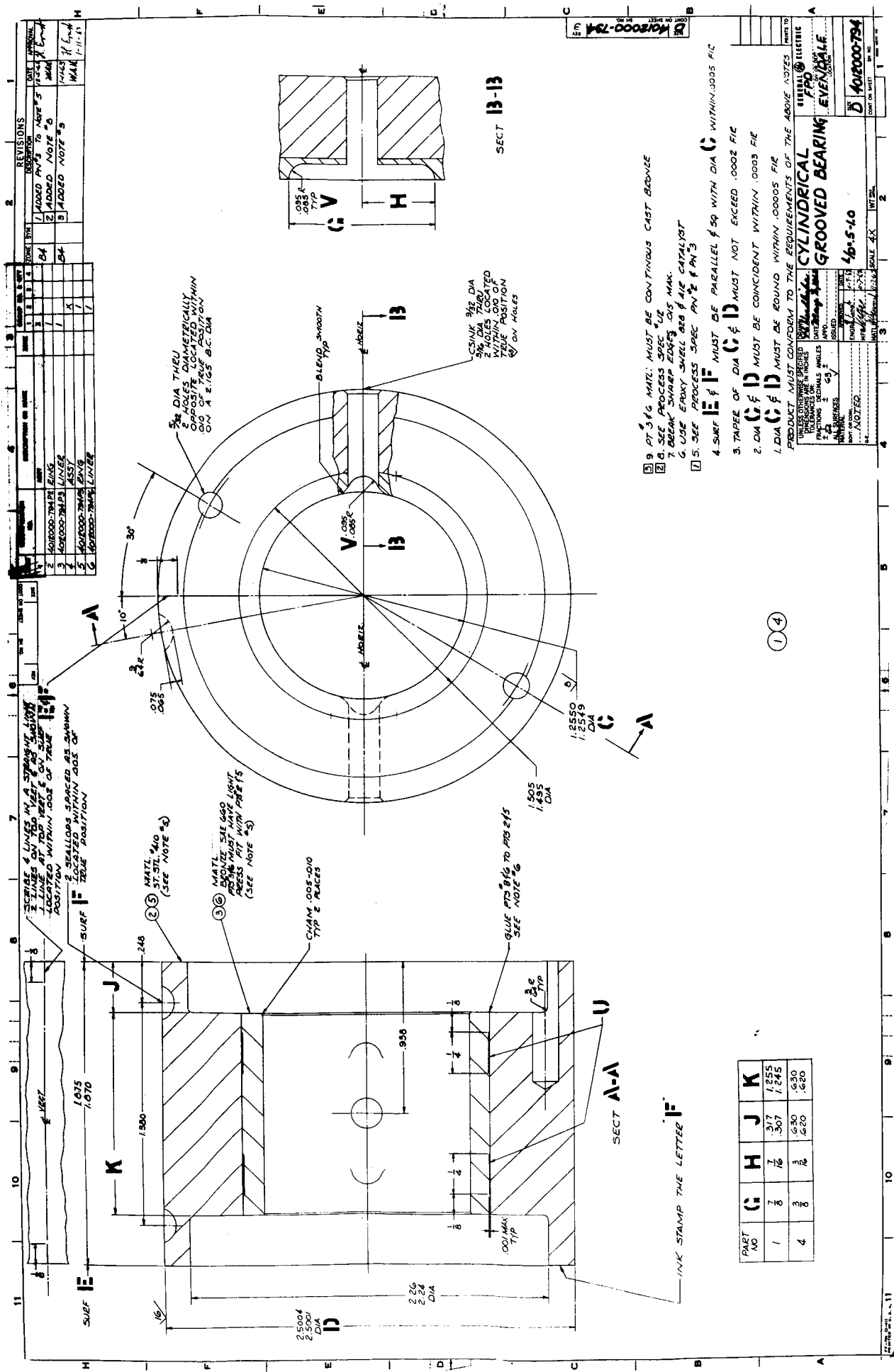


Figure 2. Two-Axial-Groove Cylindrical Bearing
L/D = .5 -1.0

CLEARANCE RATIO BETWEEN POTASSIUM & WATER LUBRICATED
BEARINGS FOR EQUAL SOMMERFELD NUMBERS

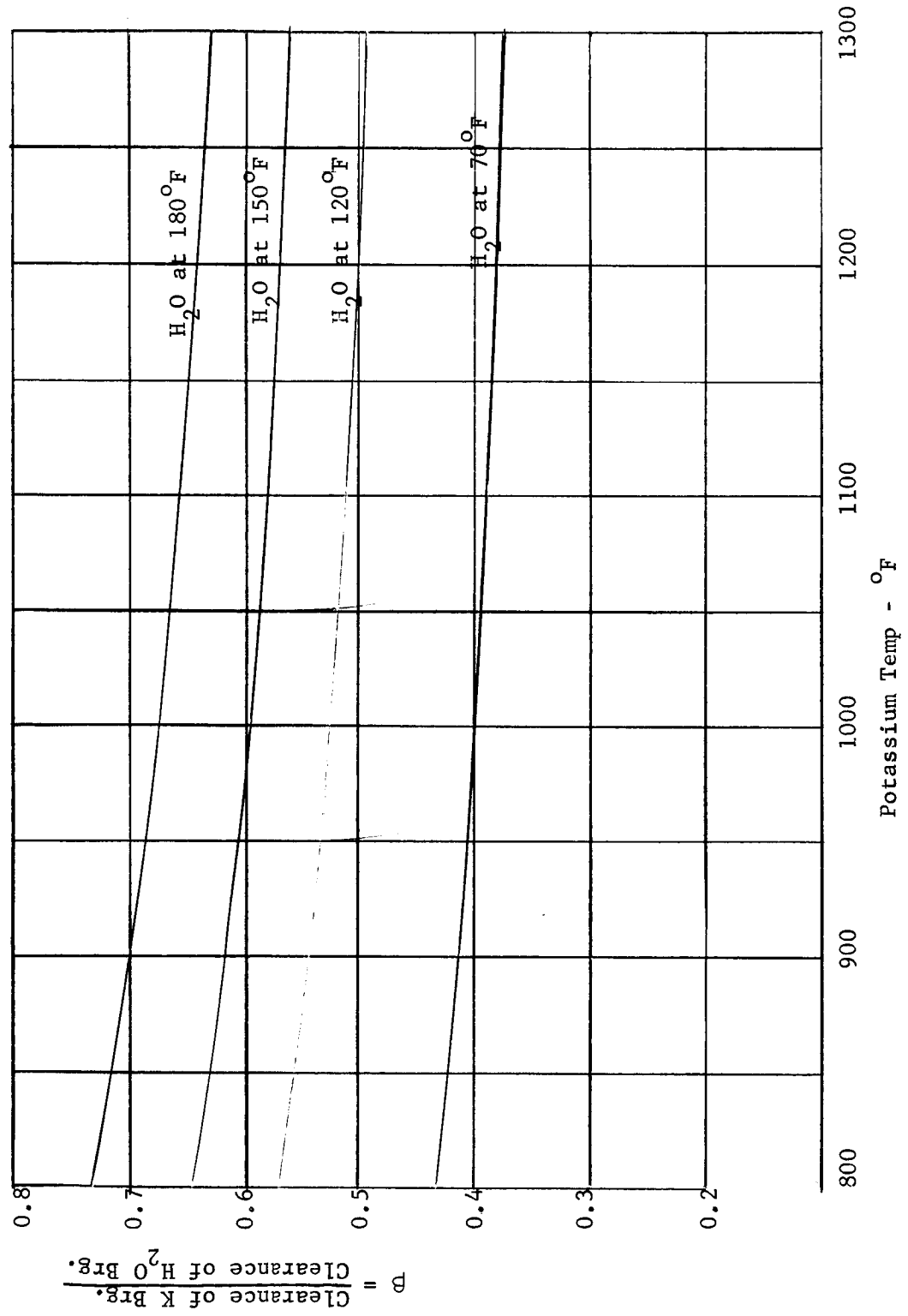
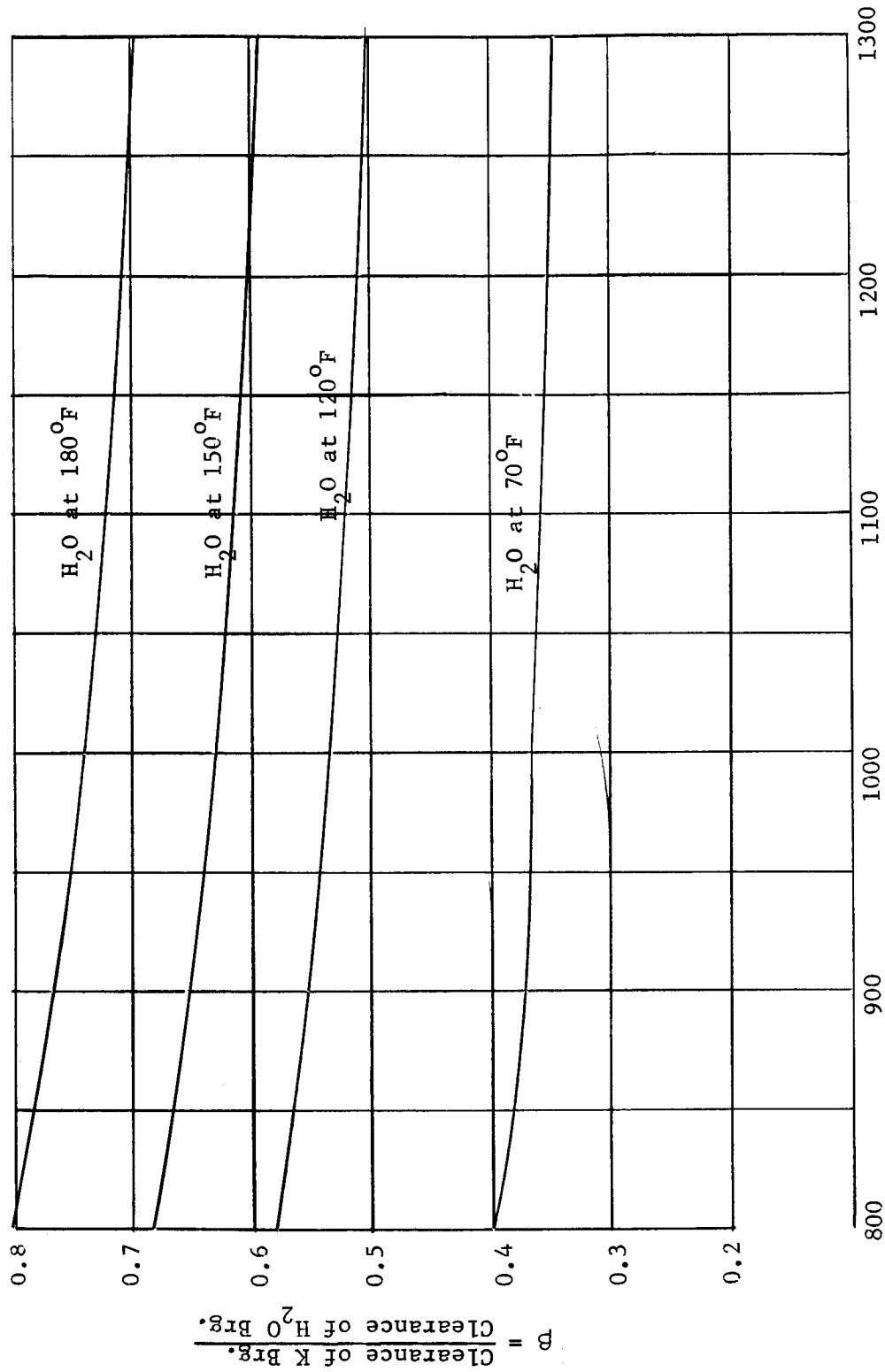


Figure 9

CLEARANCE RATIO BETWEEN POTASSIUM & WATER LUBRICATED
BEARINGS FOR EQUAL TAYLOR NUMBERS



Potassium Temp - $^{\circ}F$
Figure 10

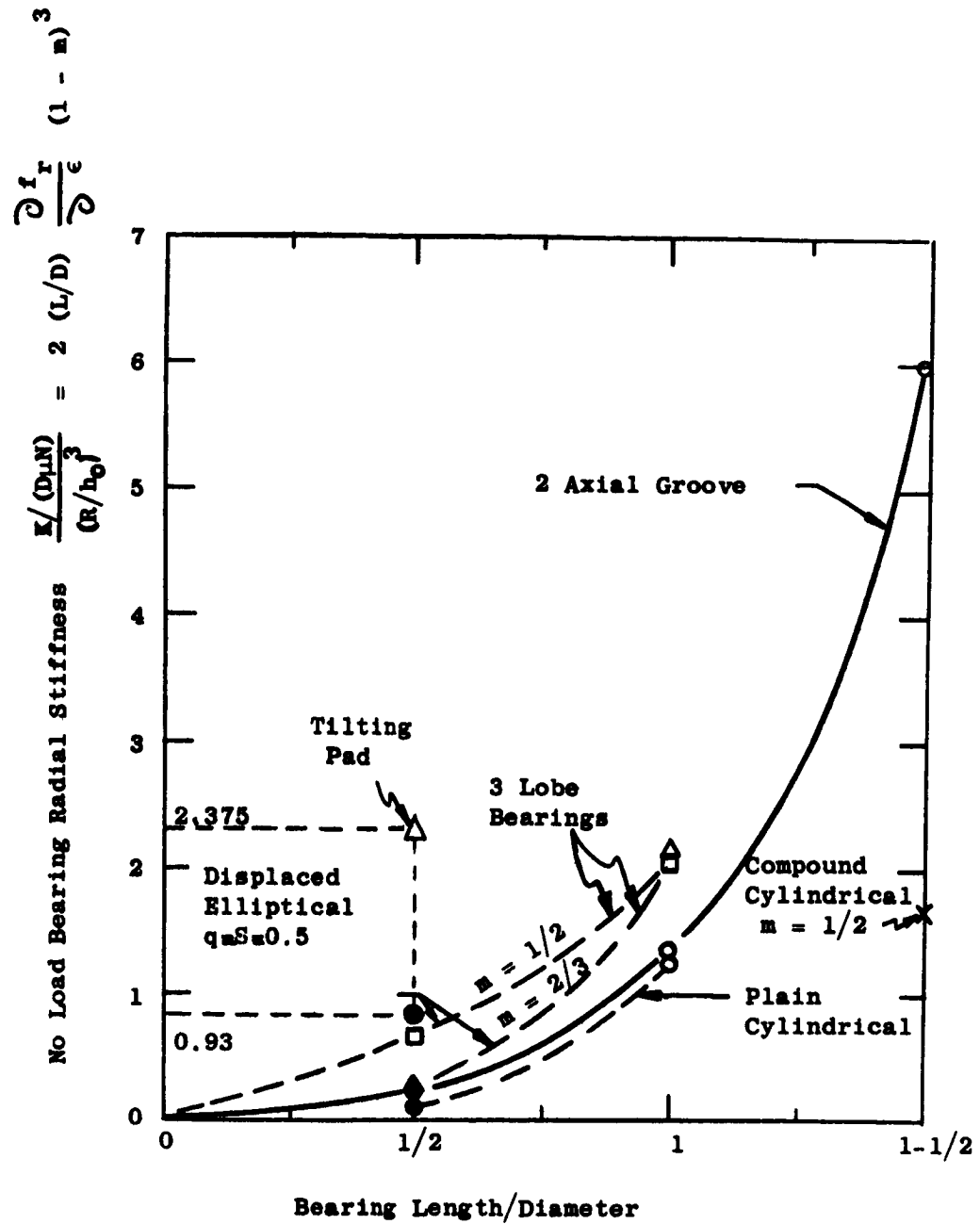


Figure 11. No Load Bearing Radial Stiffness $\frac{K}{(D\mu N)} \frac{2(L/D)}{(R/h_0)^3} (1-m)^3$ vs. Bearing Length/Diameter.

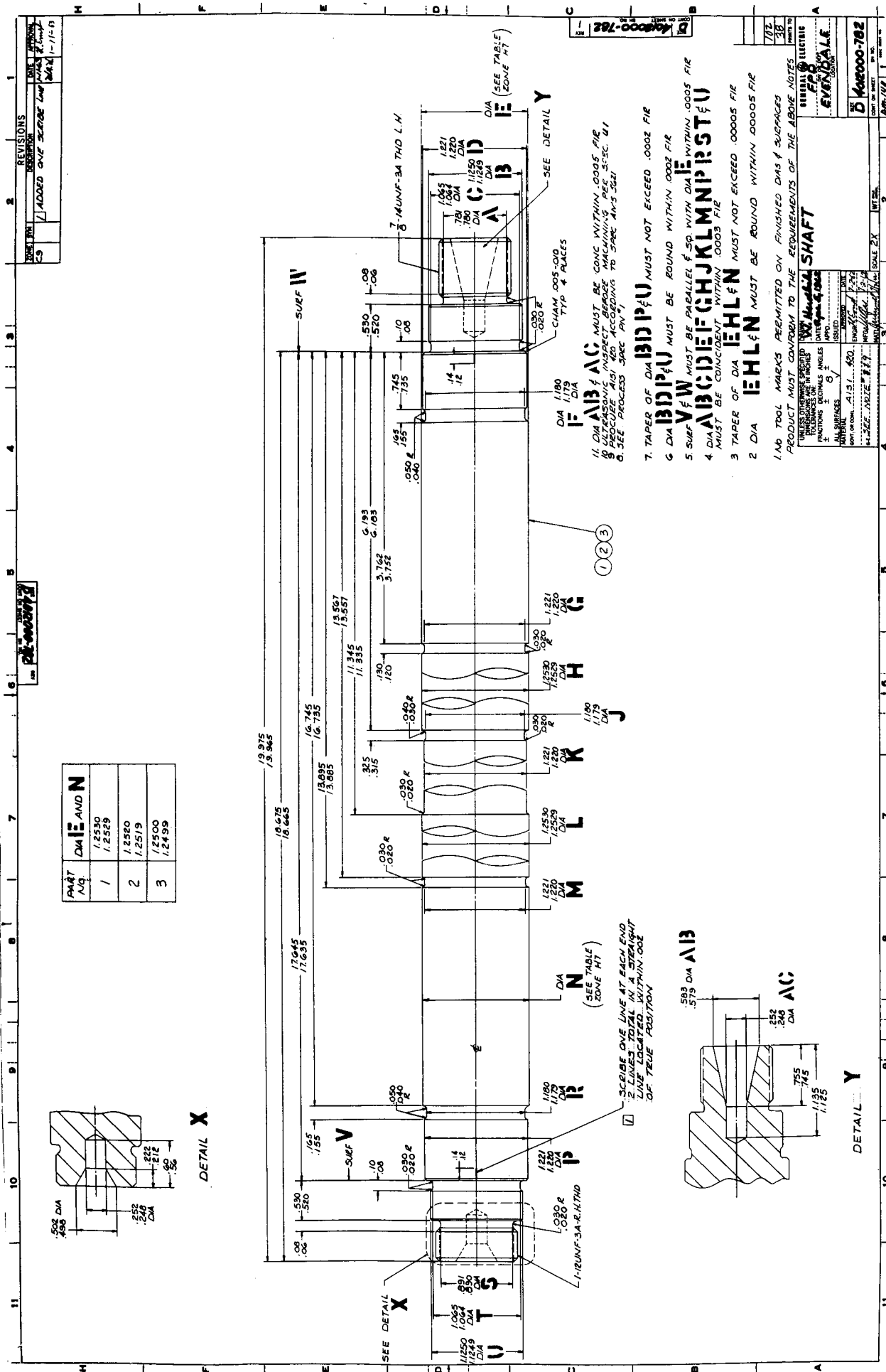


Figure 12. Test Shaft, Long Version
Bearing Centerline Distance = 12.5 Inch

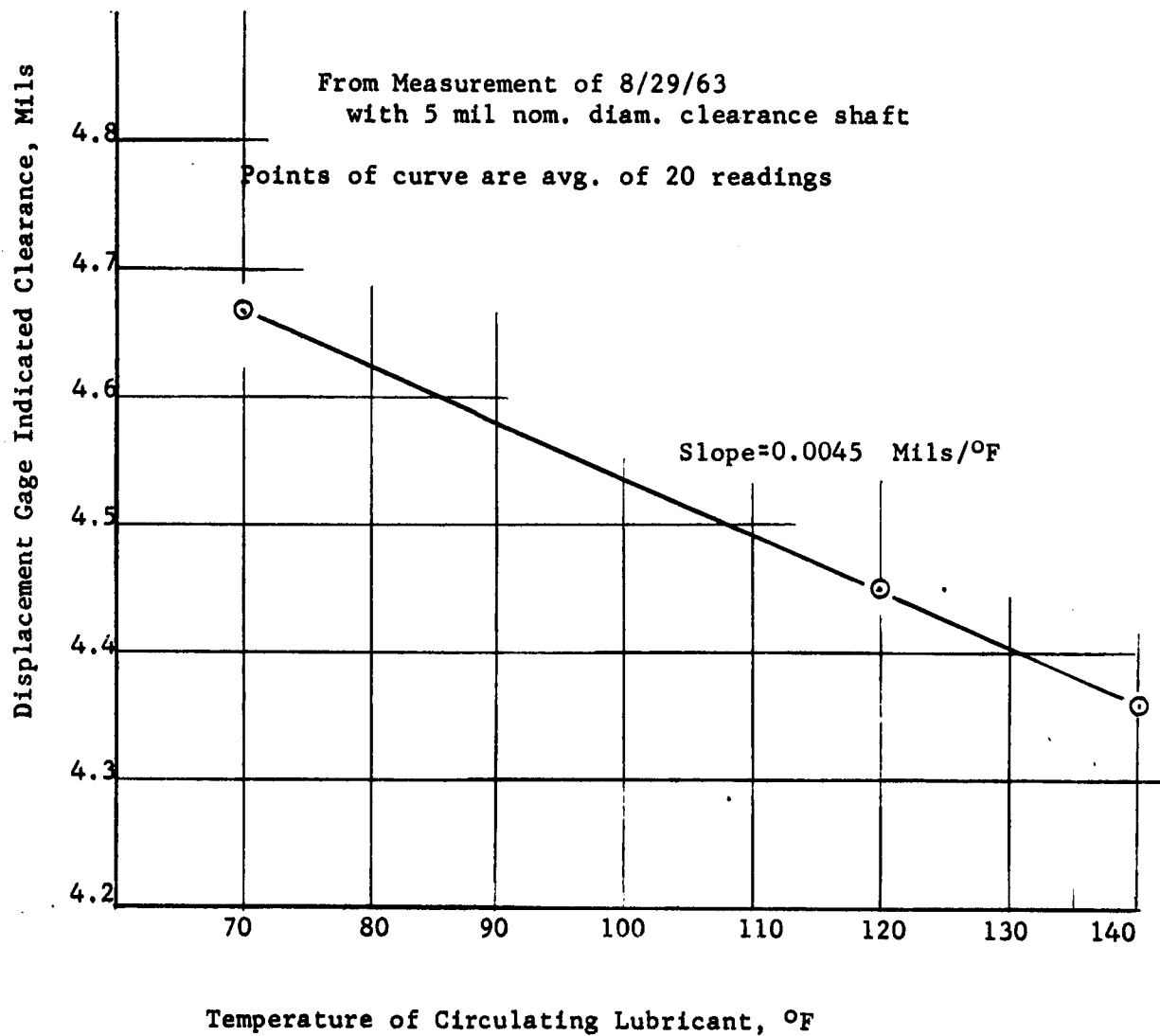


Figure 13 Effect of Temperature on Shaft-Bearing Clearance

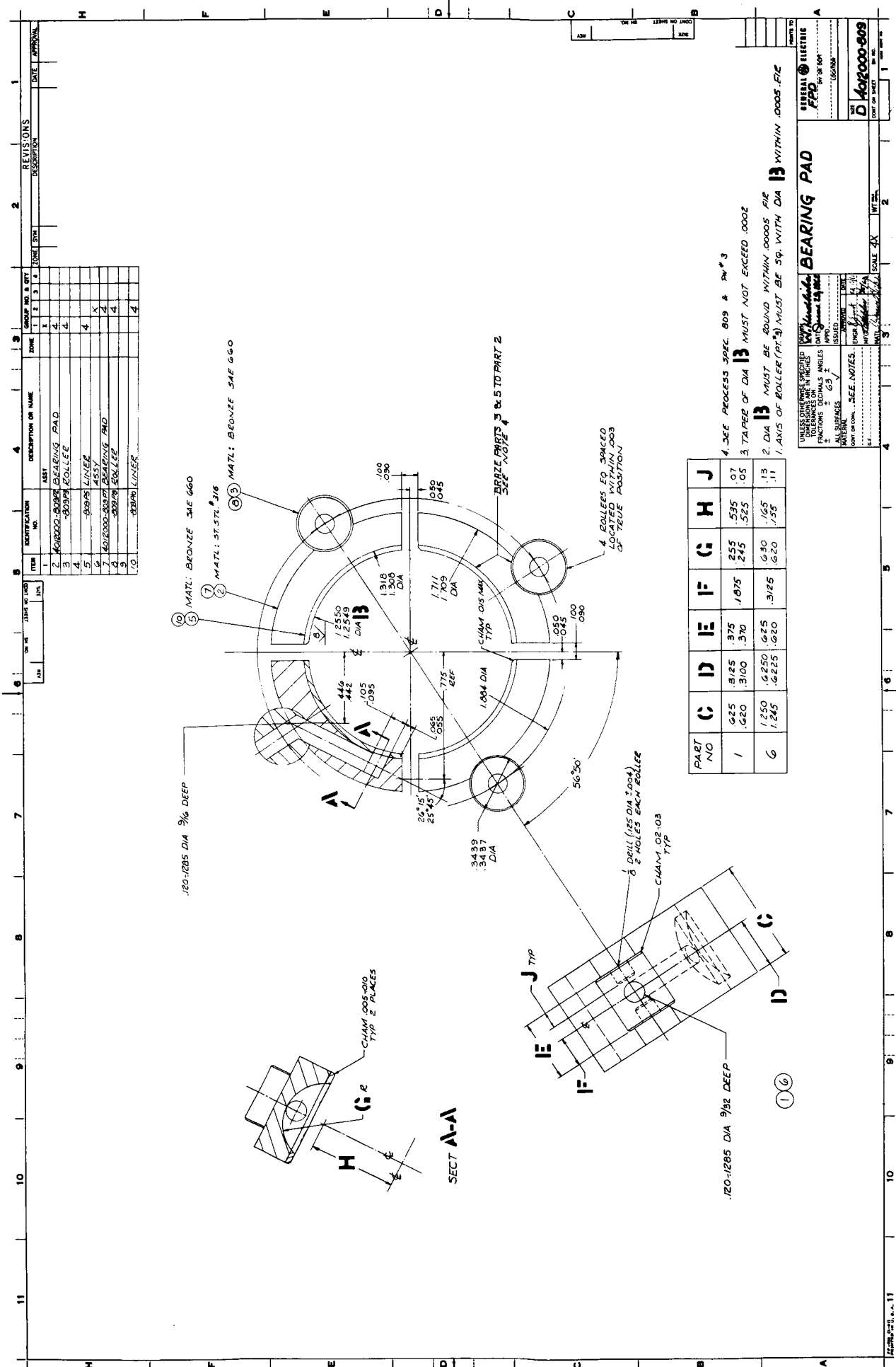
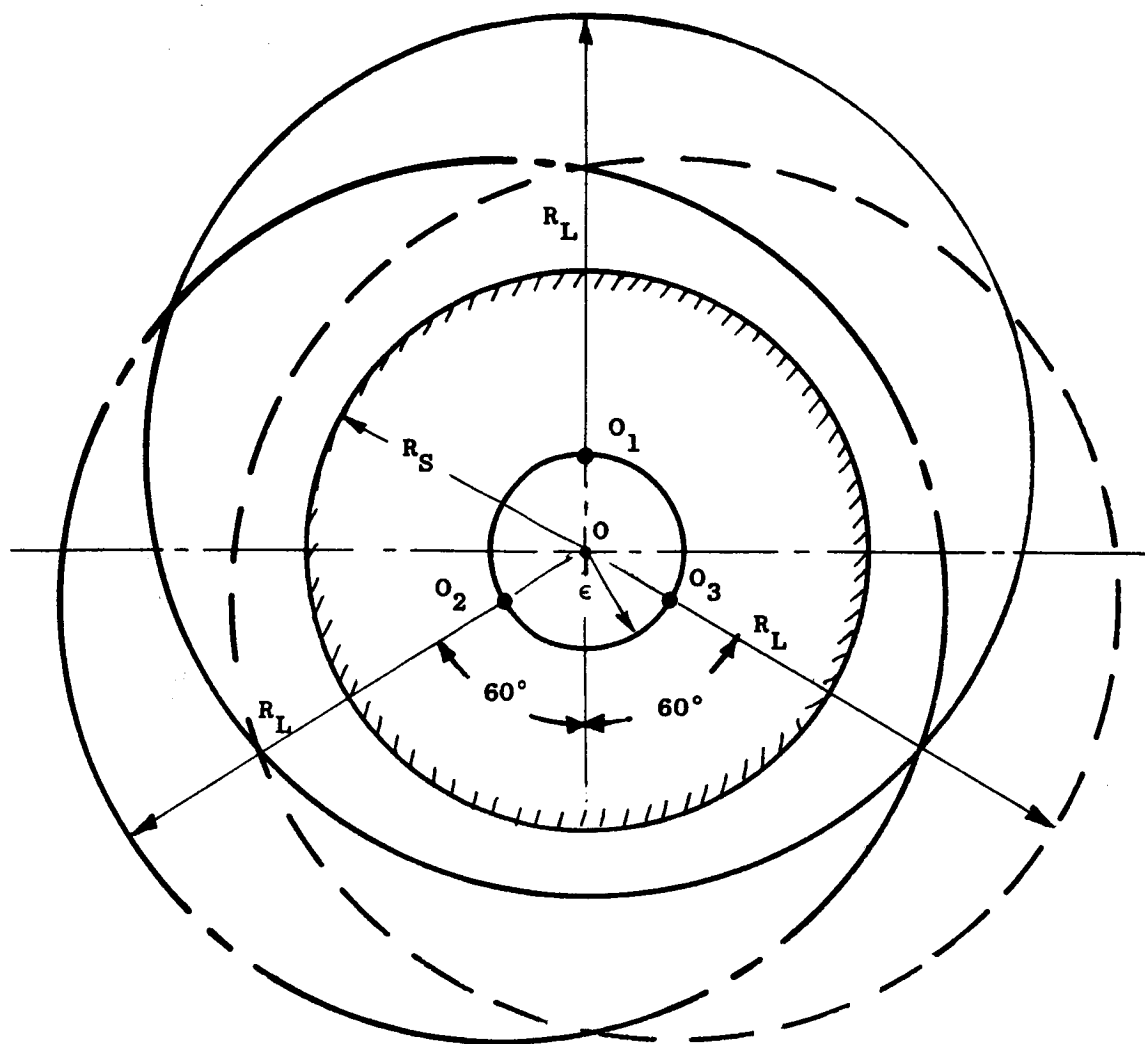


Figure 14. Tilting Pad Bearing--Pad Details



R_S = Shaft Radius

R_L = "Lobe" Radius

ϵ = Ellipticity = Distance from Bearing Center O to Centers of Lobe Radii O_1 , O_2 , O_3 .

$\frac{C}{2}$ = $(R_L - R_S)$ = Lobe Clearance

m = Ellipticity Ratio = $\frac{2\epsilon}{C}$

Figure 15. Compound Cylindrical and Three Lobe Bearing Geometry

AT 895

AT 415

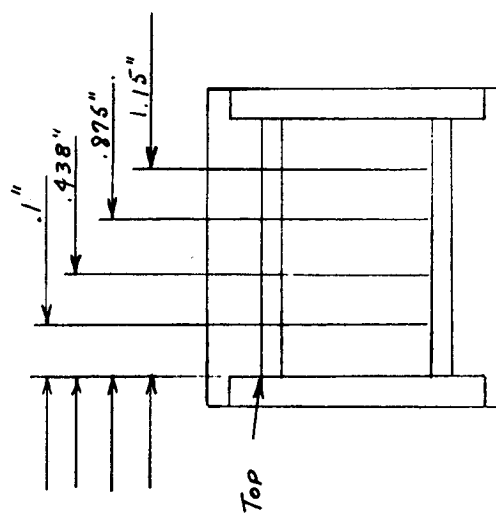
OIL HOLES

AT 438

Q

AT 1

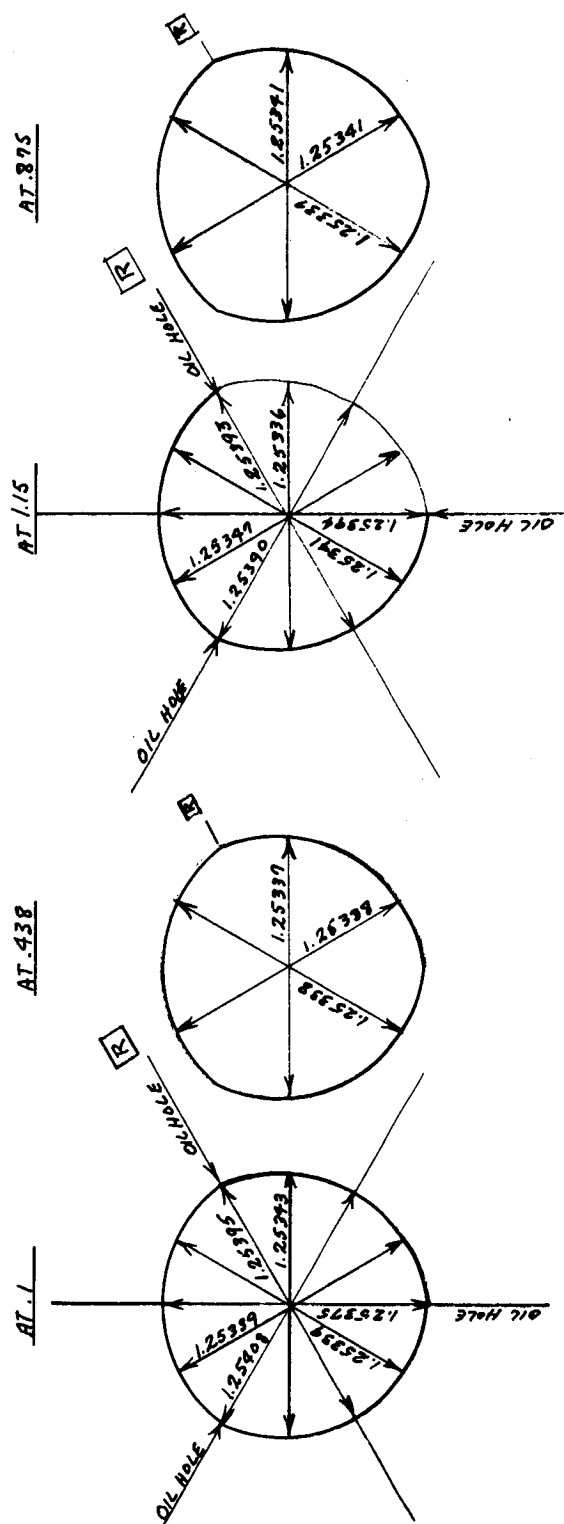
OIL HOLES



Diameters of the Bore

Figure 16
Three Lobed Bearing - 796

#2.



Dias. of the Bore

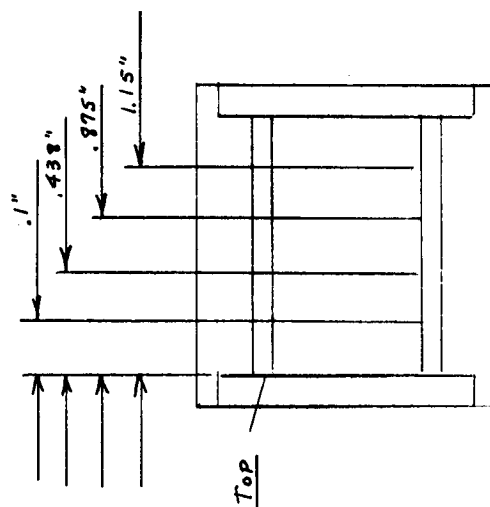


Figure 17

Three Lobed Bearing - 796

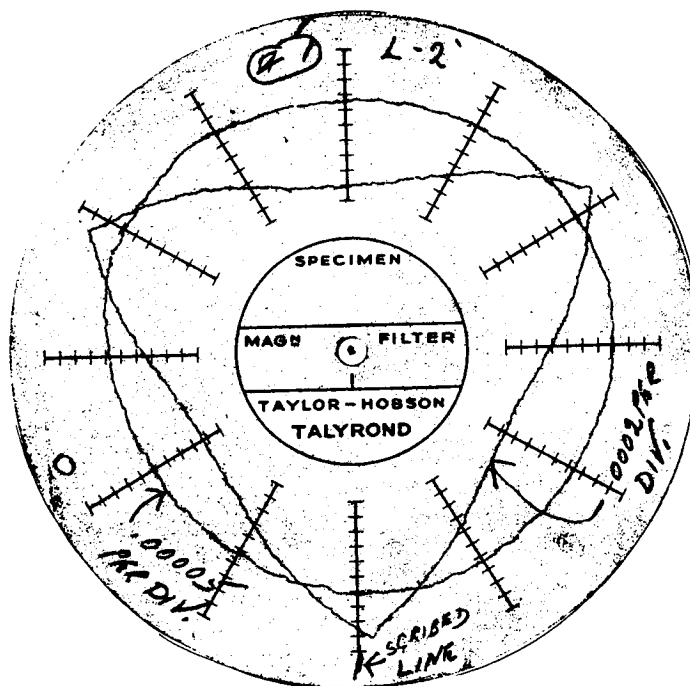
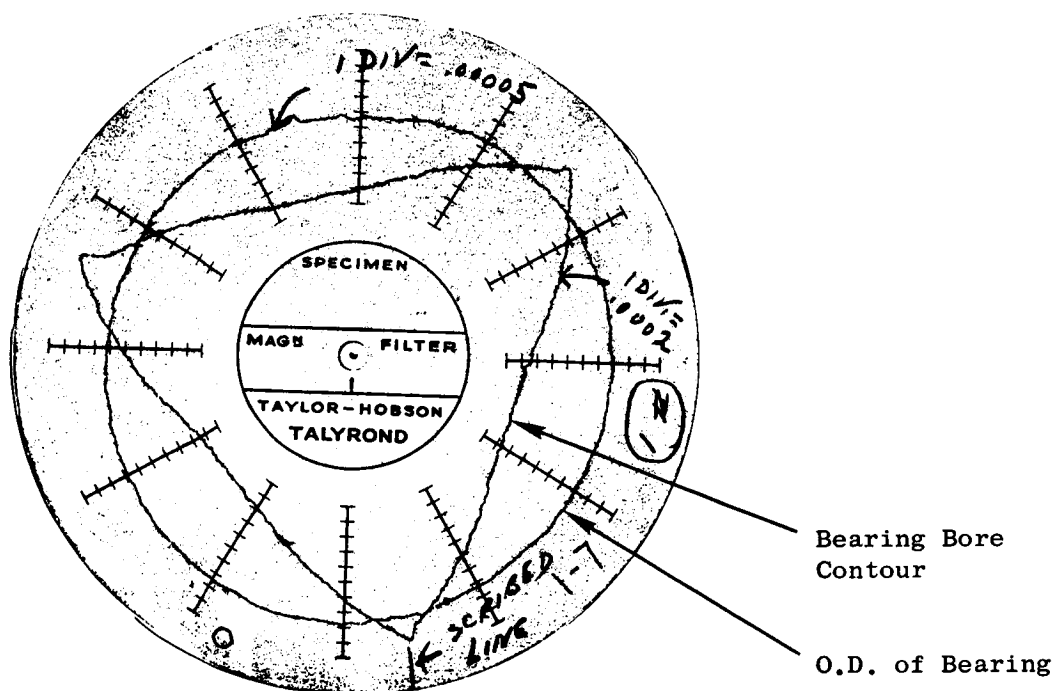


FIGURE 18. Three Lobed Bearing

BORE DIAMETERS

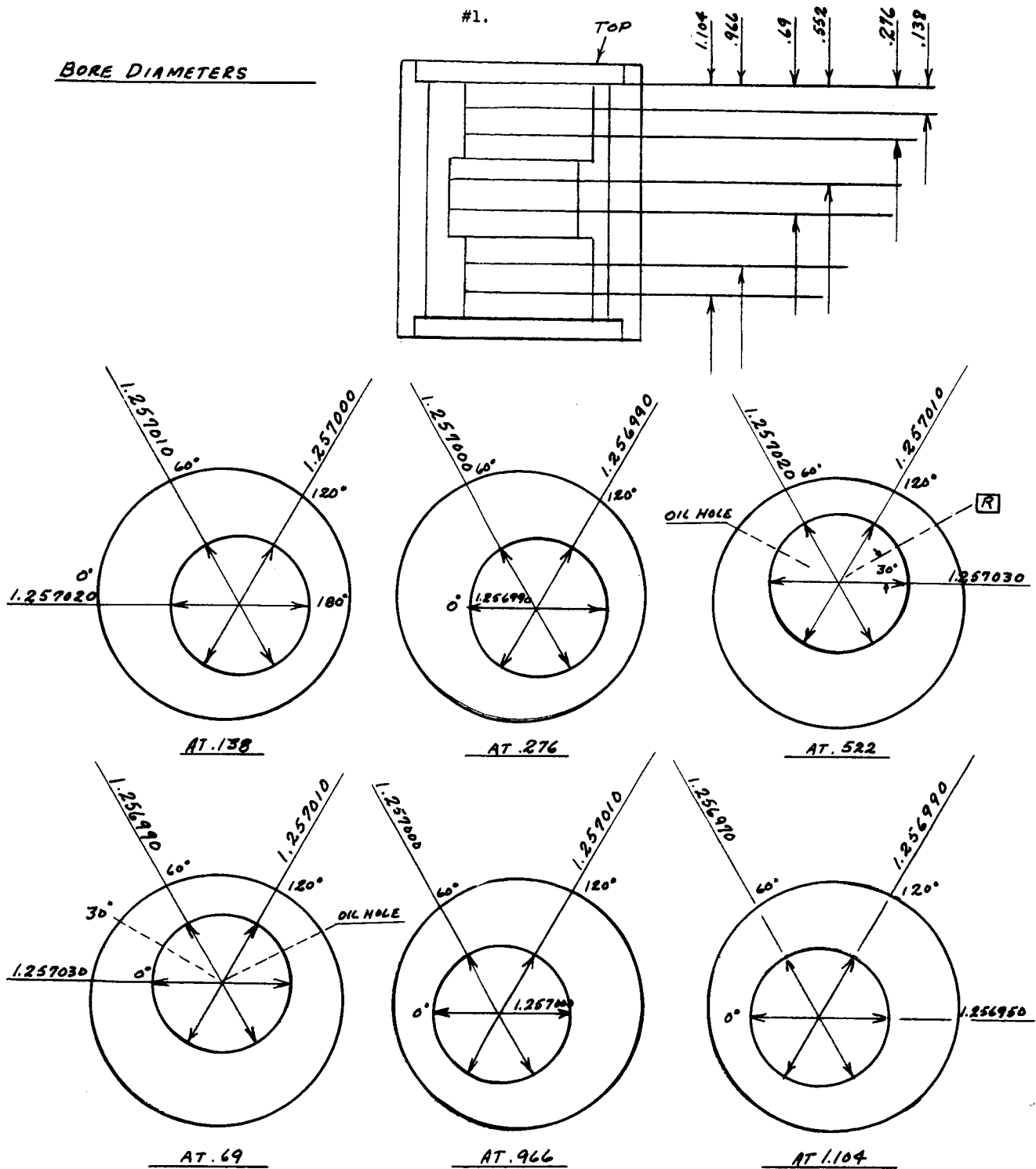


Figure 19

Cylindrical Bearing - 802

BORE DIAMETERS

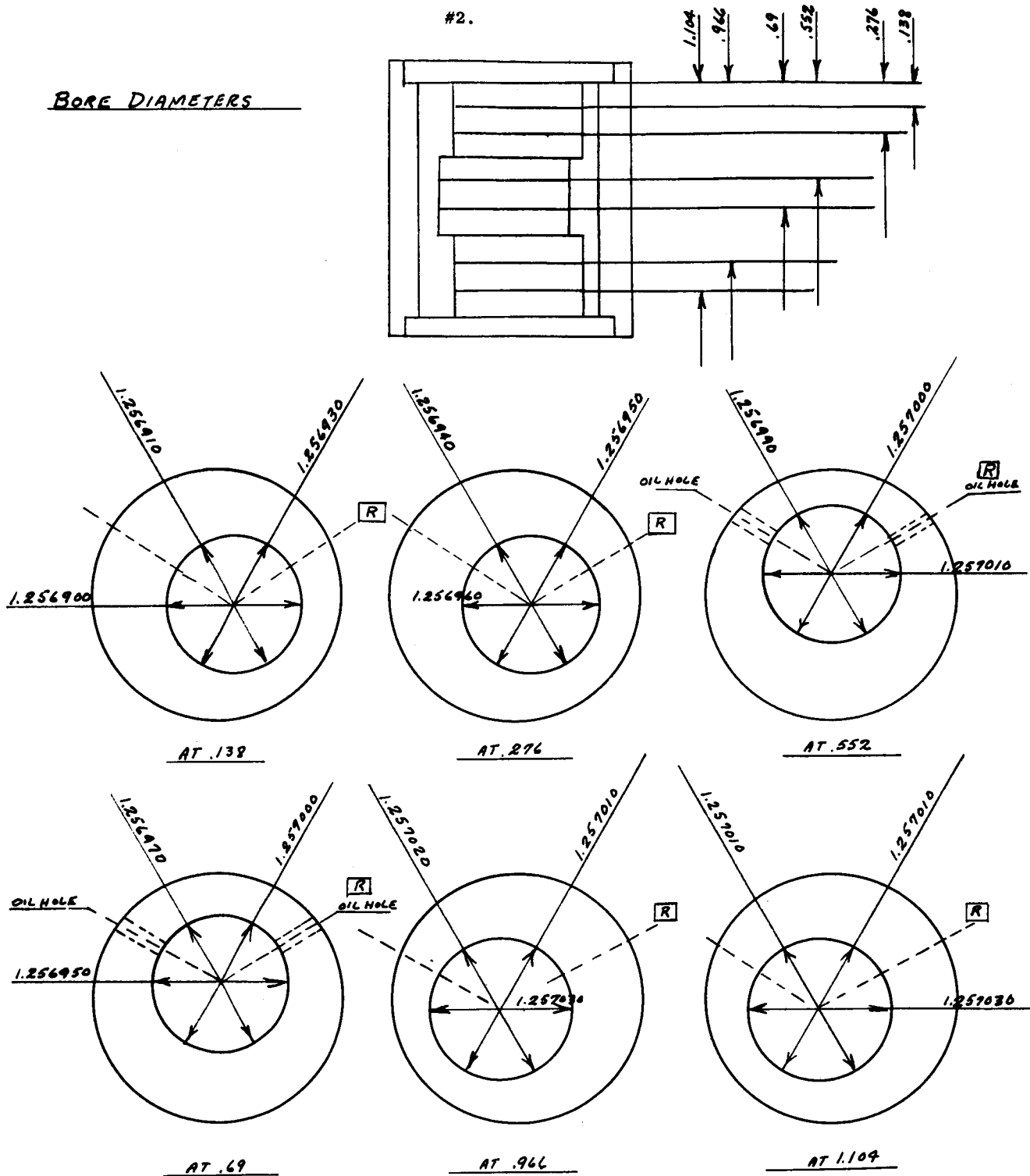
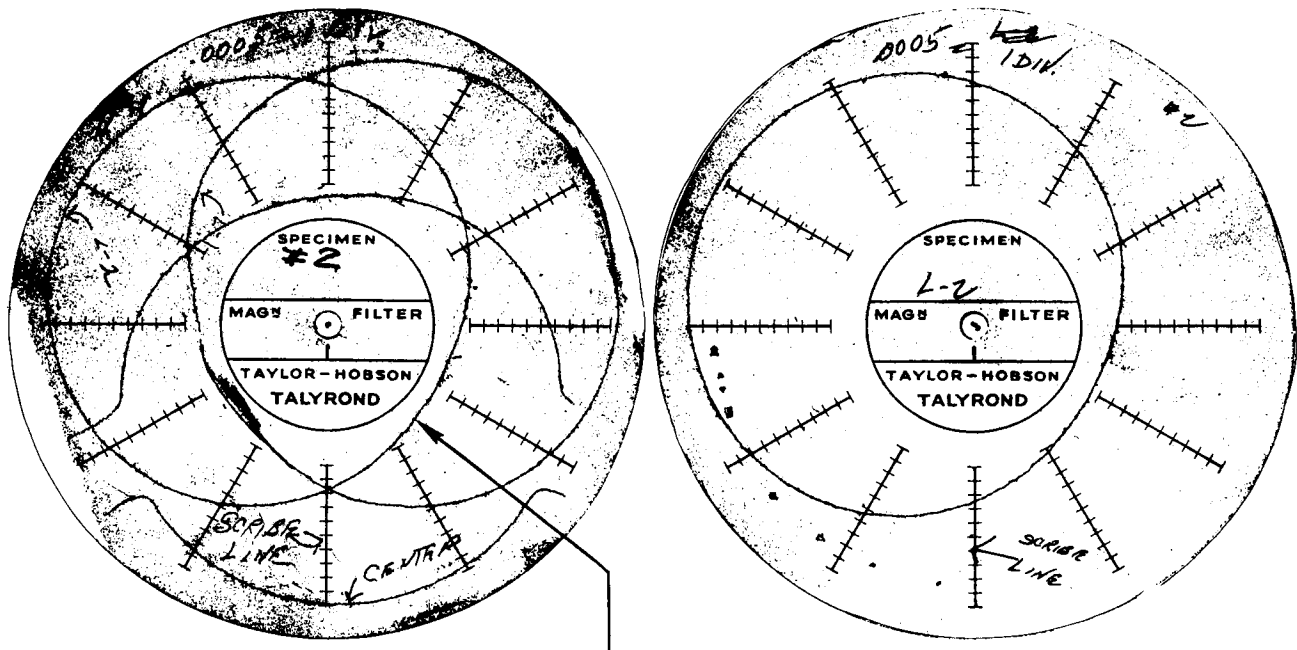


Figure 20

Cylindrical Bearing - 802



Contour of Compound Cylindrical Bearing Bore Consisting of Three Off-set Cylindrical Bearing Segments.

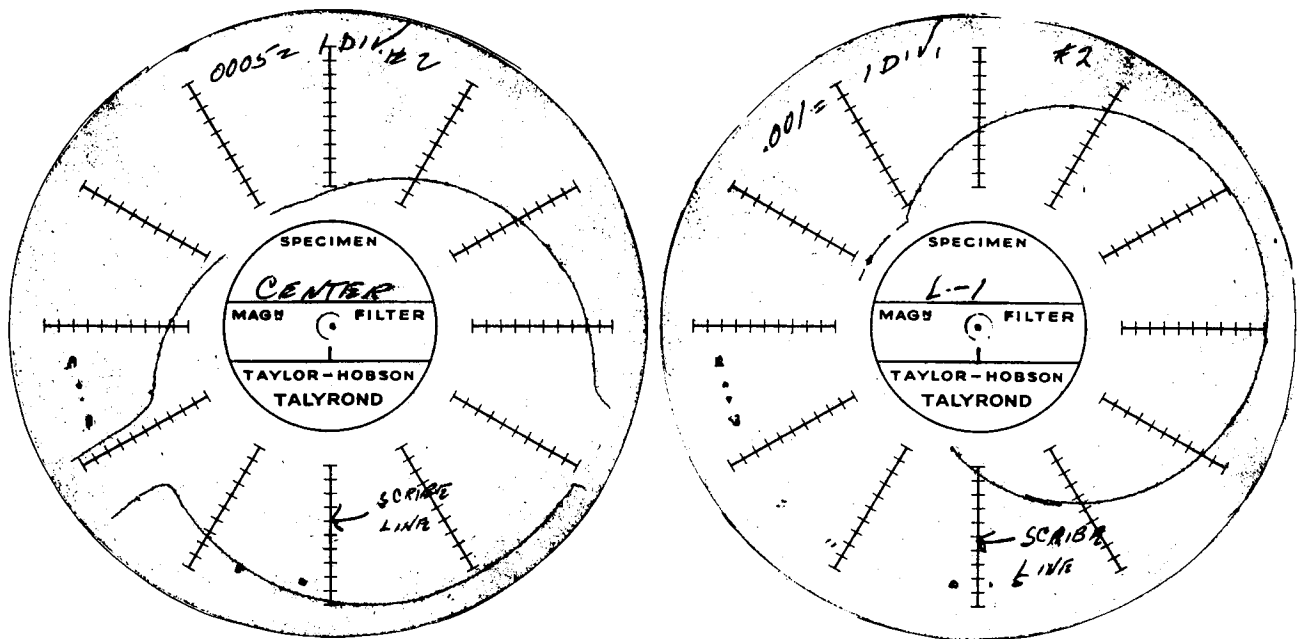
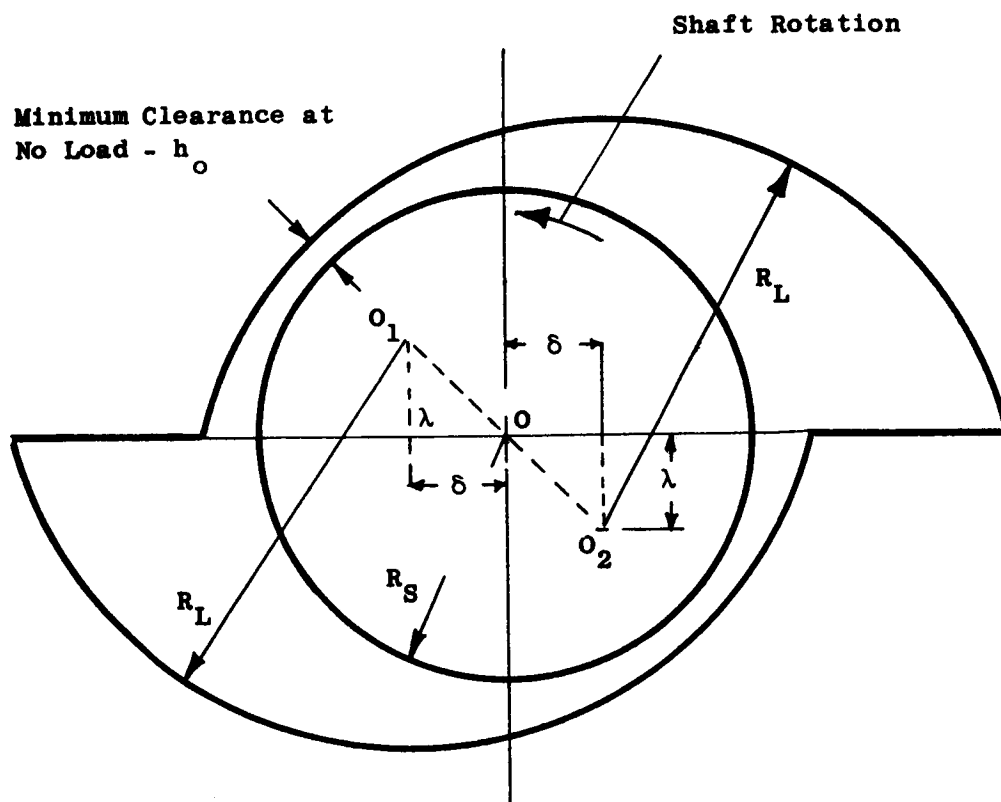


FIGURE 21. Displaced Cylindrical Bore of Bearing Segment



R_L = Lobe Radius

R_S = Shaft Radius

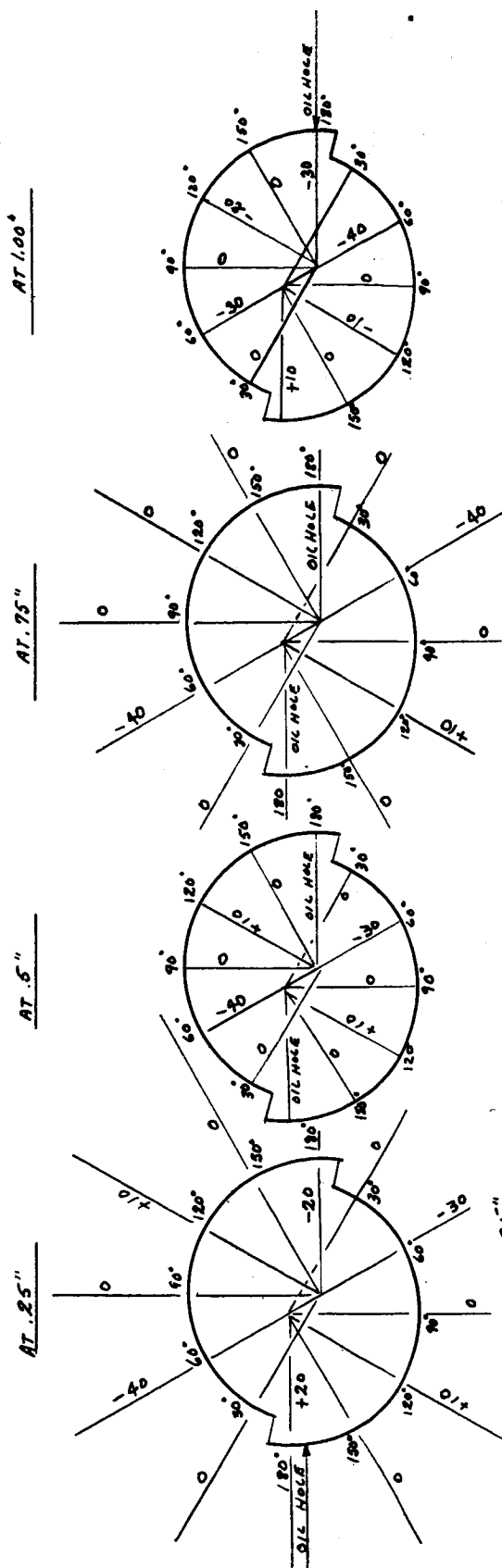
λ, δ = Displacement of Lobe Centers

$C/2 = R_L - R_S$ = Lobe Radial Clearance

$q = \frac{2\lambda}{C}$; $s = \frac{2\delta}{C}$ = Displacement Ratios

Figure 22. Orthogonally Displaced Elliptical Bearing Geometry

#1.



Uniformity of Roundness
In Millionths of an Inch.

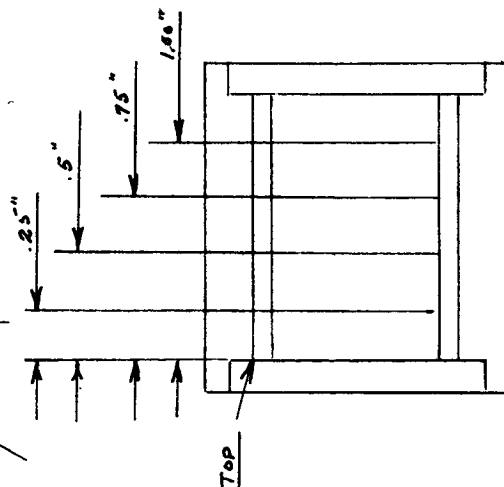
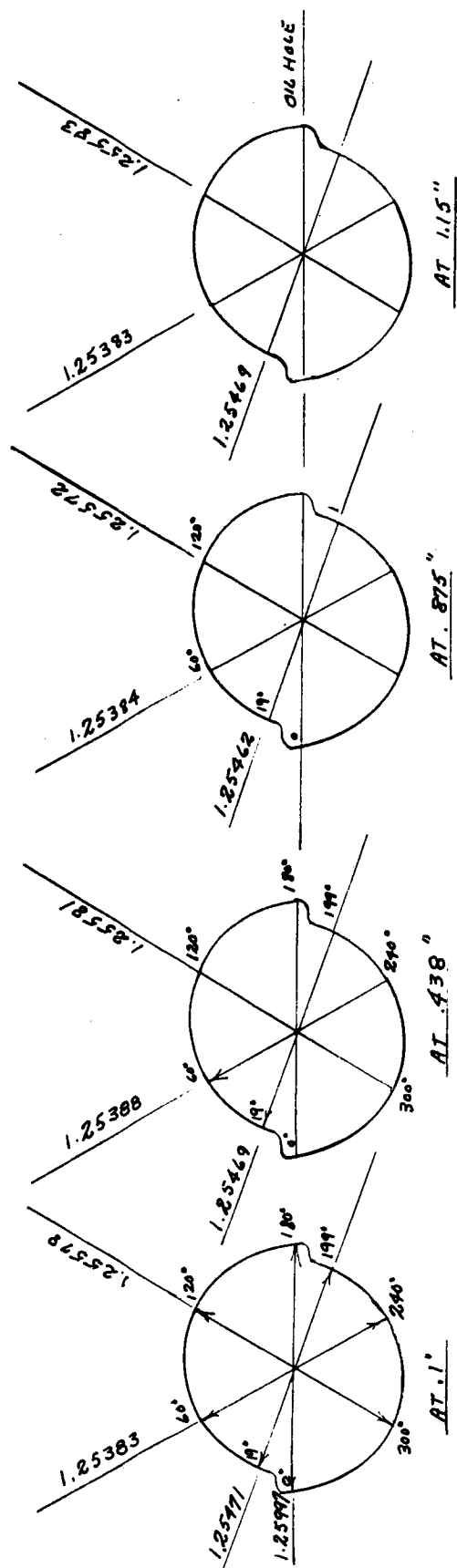
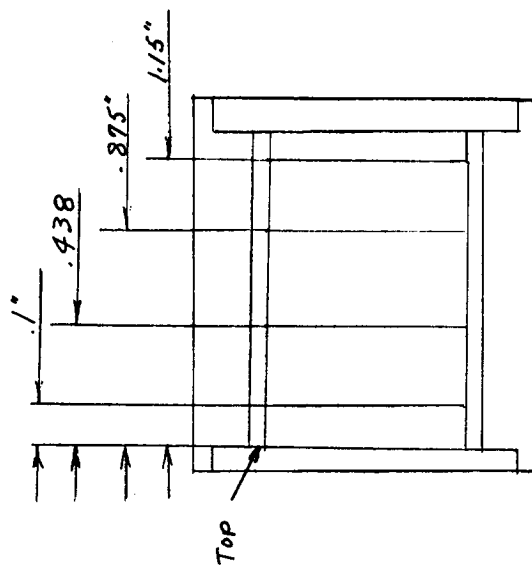


Figure 23
Displaced Elliptical Bearing - 795



Diameters of the Bore

Figure 24
DISPLACED ELLIPTICAL BEARING
Part No. 4012000-795



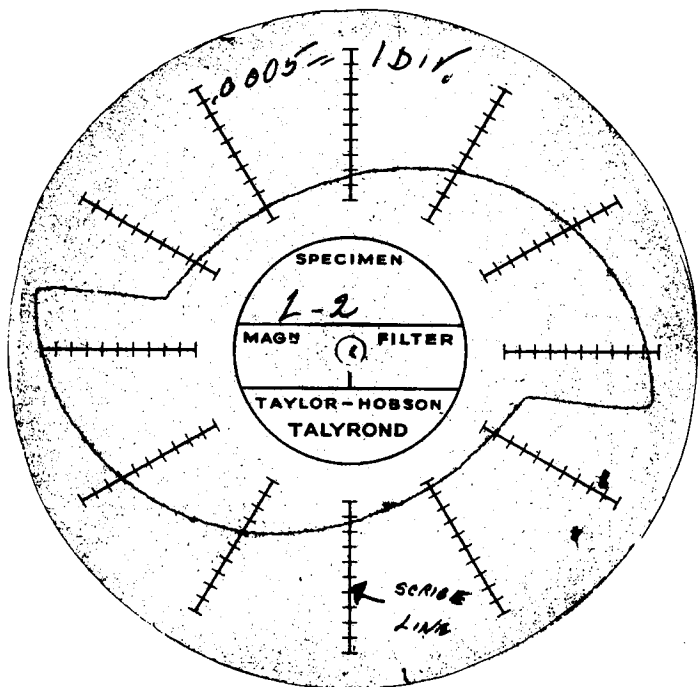
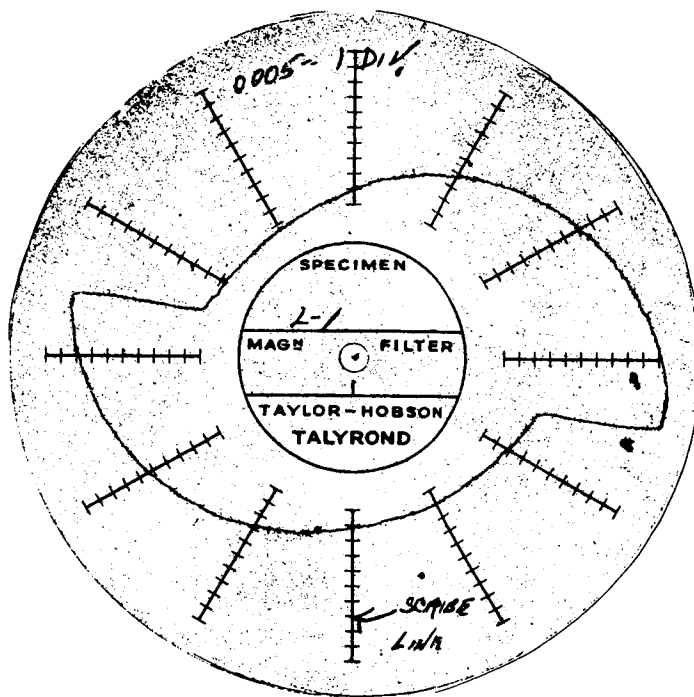


FIGURE 25. Bore Contour Plot - Orthogonally Displaced Elliptical Bearing

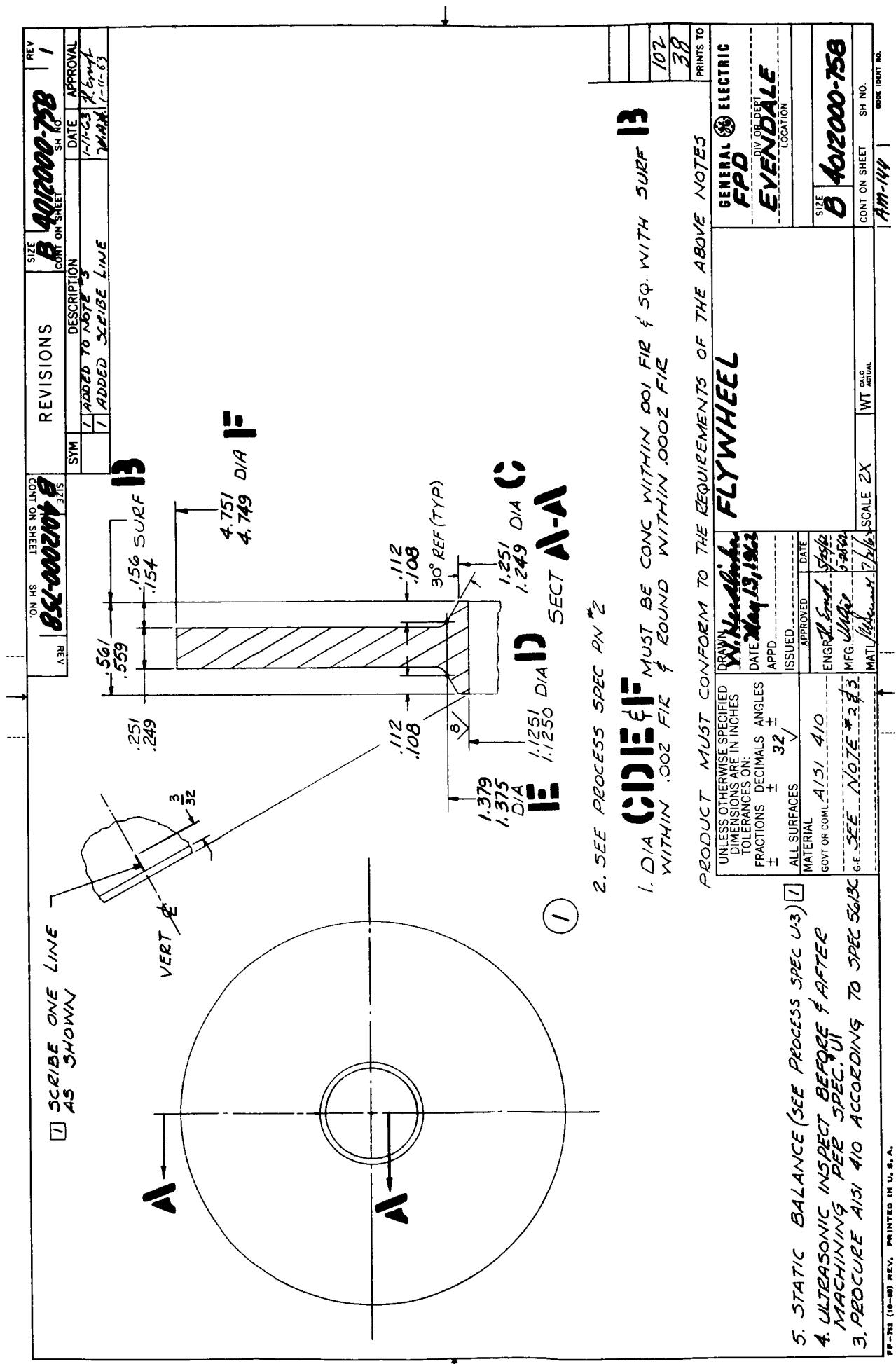


Figure 26. Rotor End Flywheel

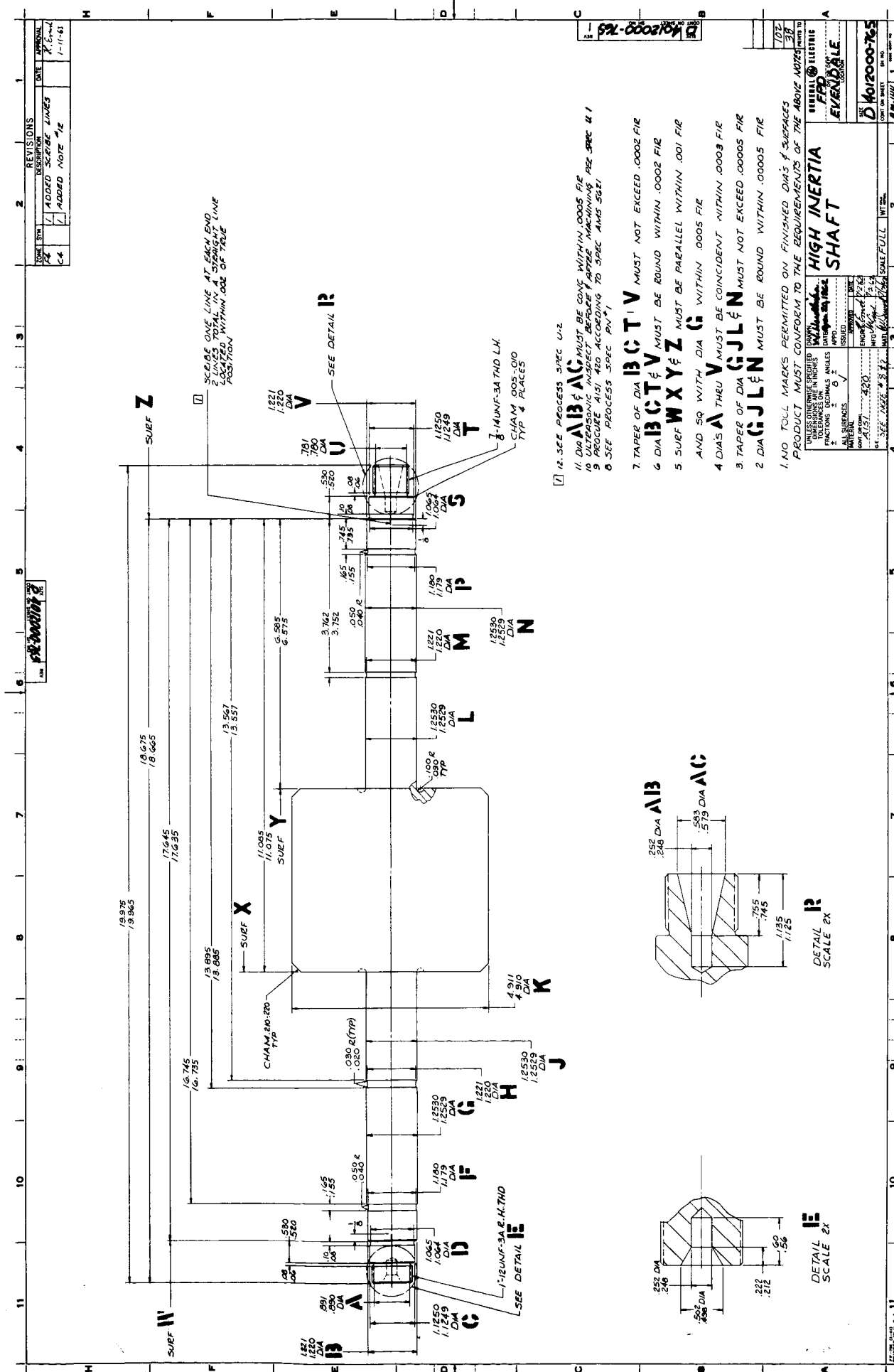


Figure 27. High Inertia Shaft

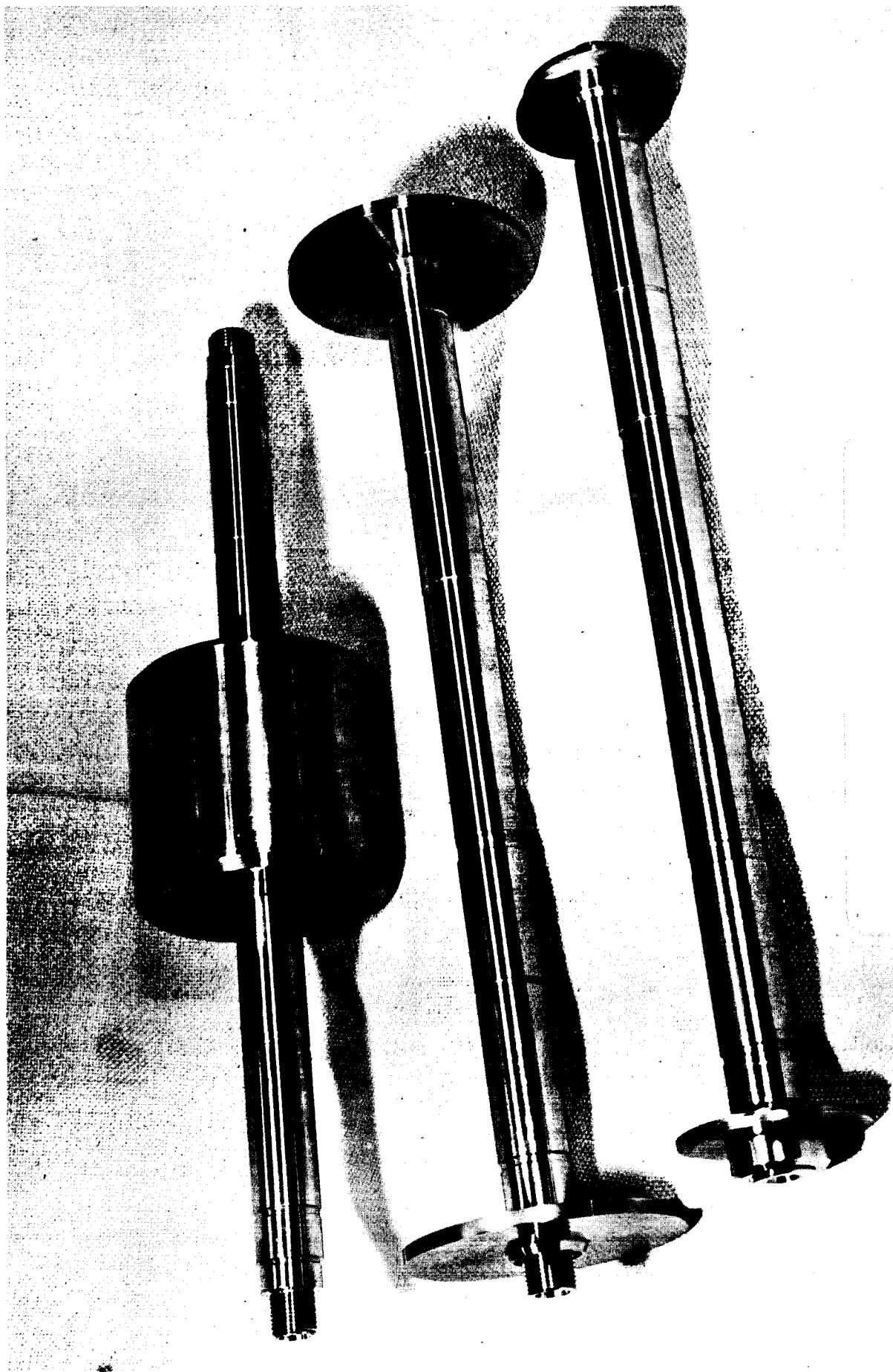
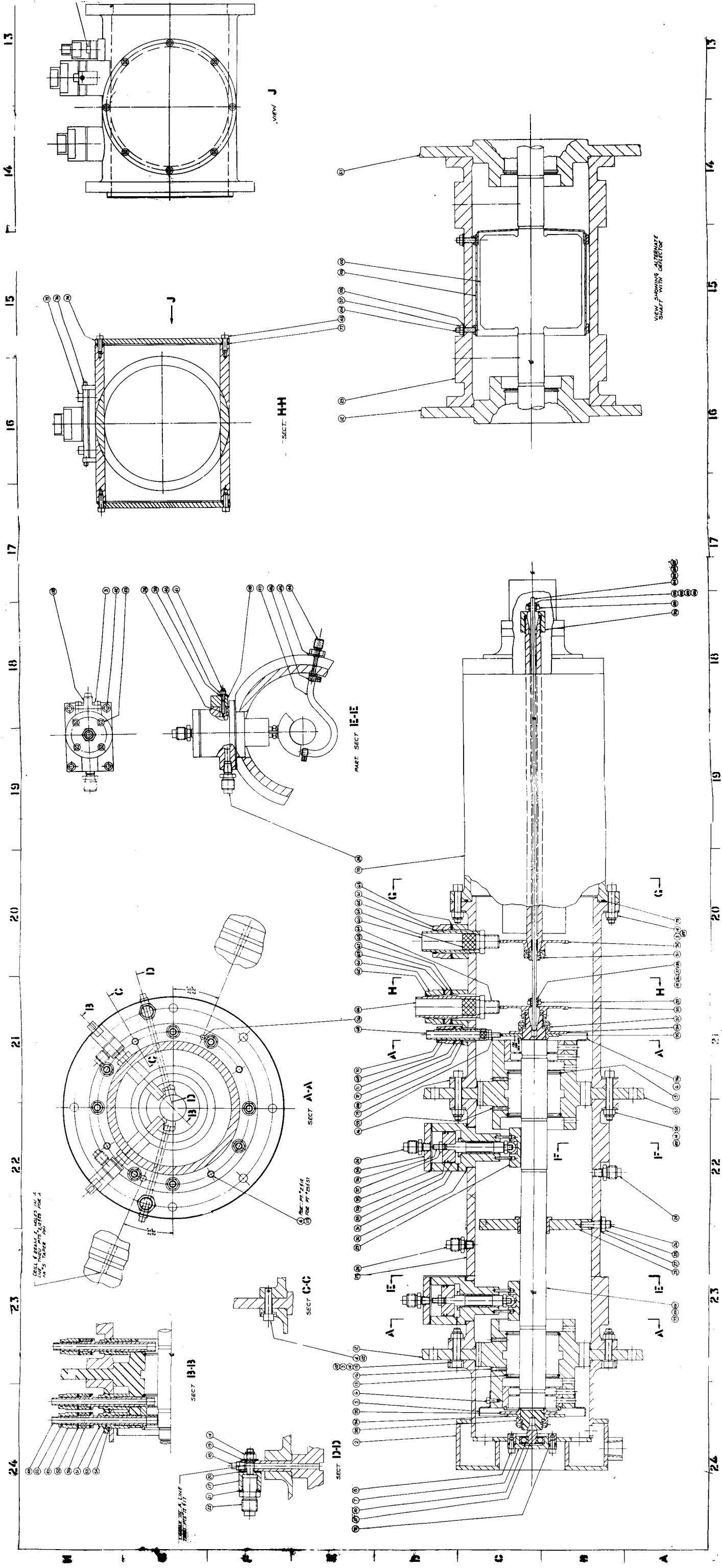
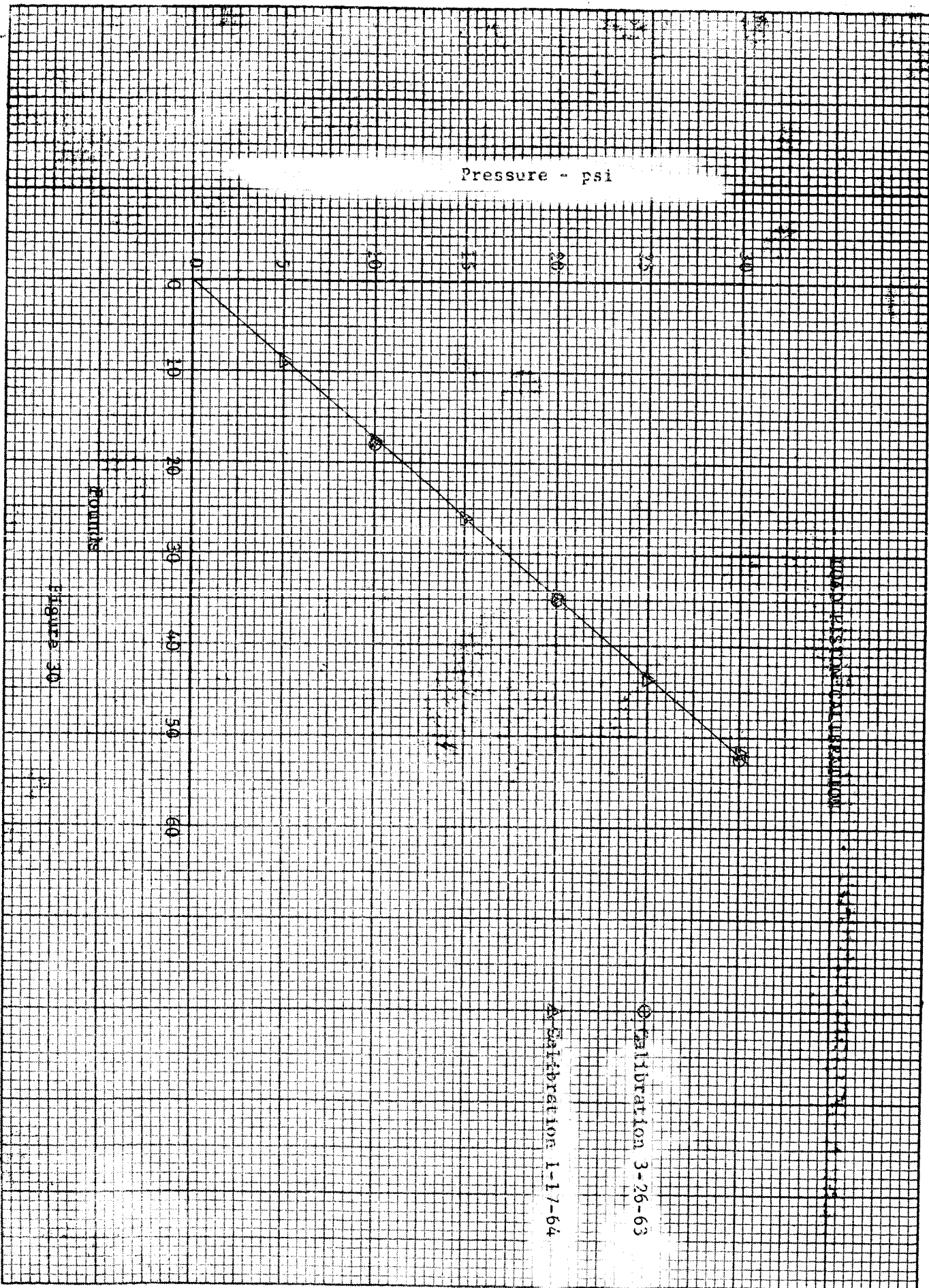


Figure 28. View of Three Test Shafts





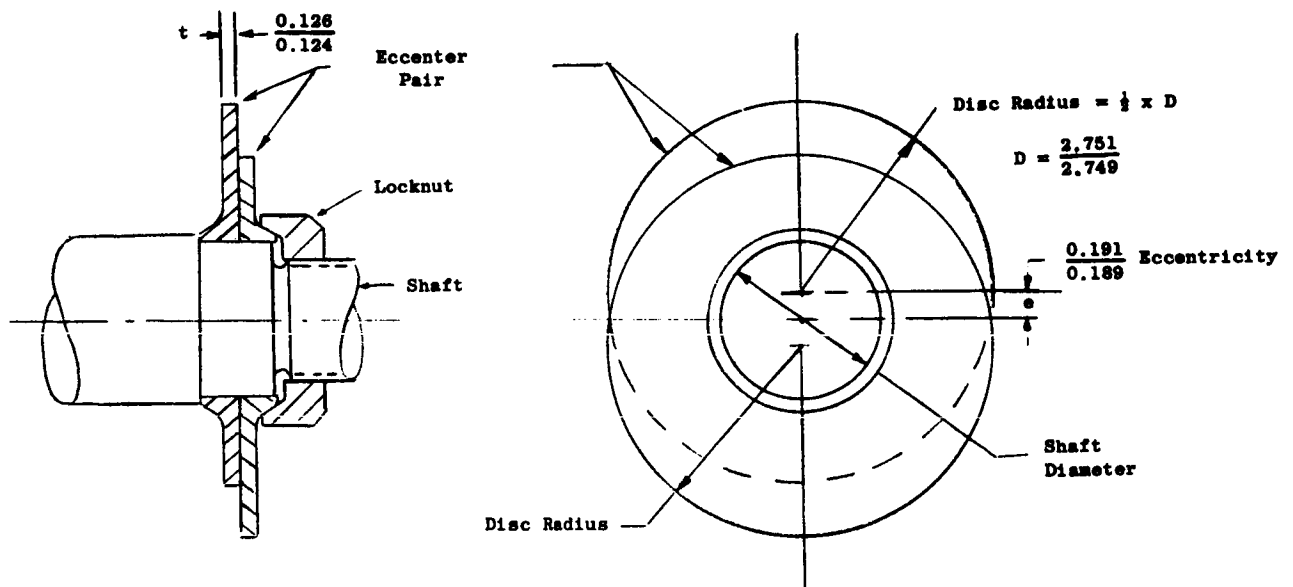


Figure 31. Eccenters for Dynamic Load Application
(Zero Unbalance Shown)

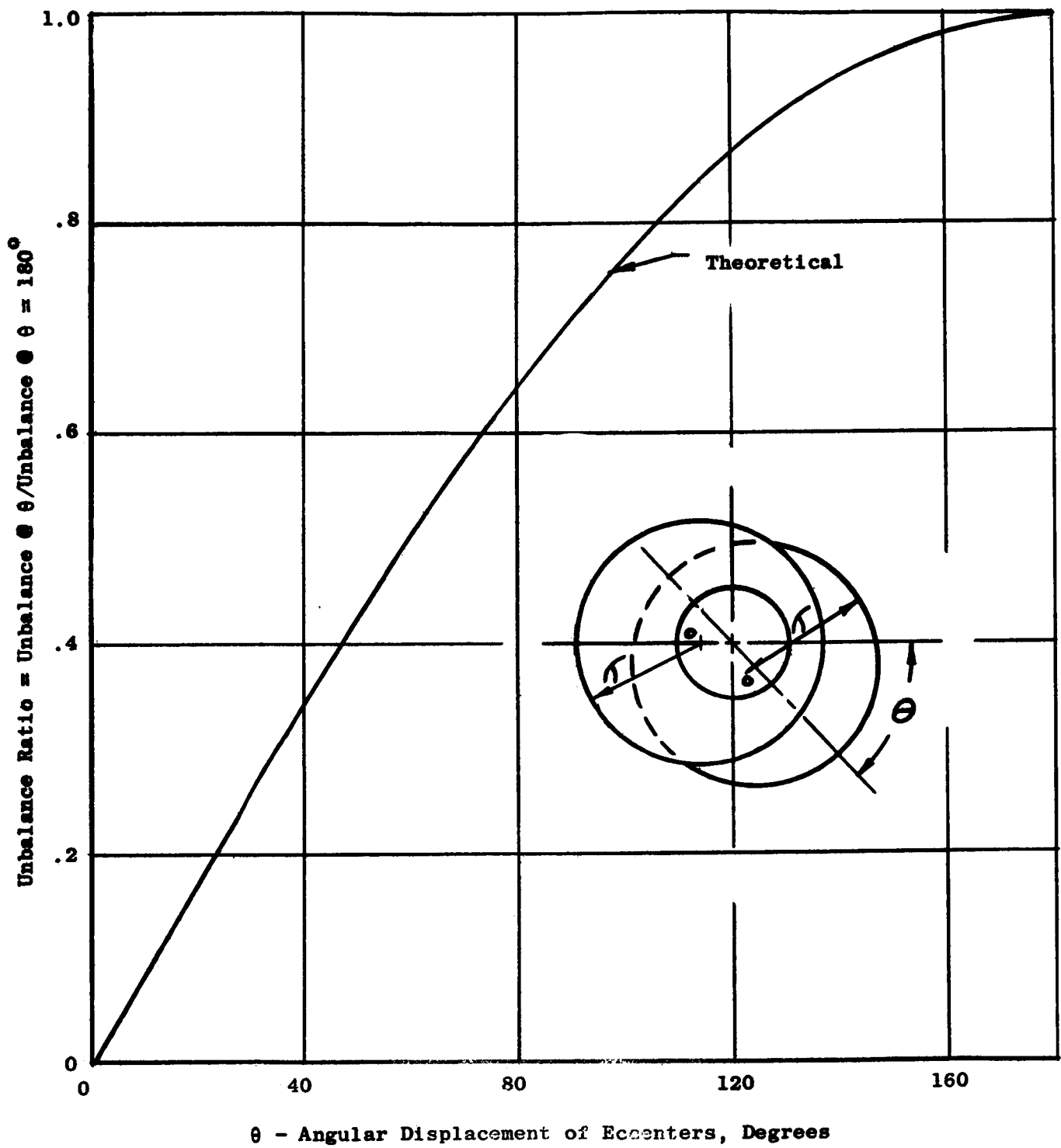
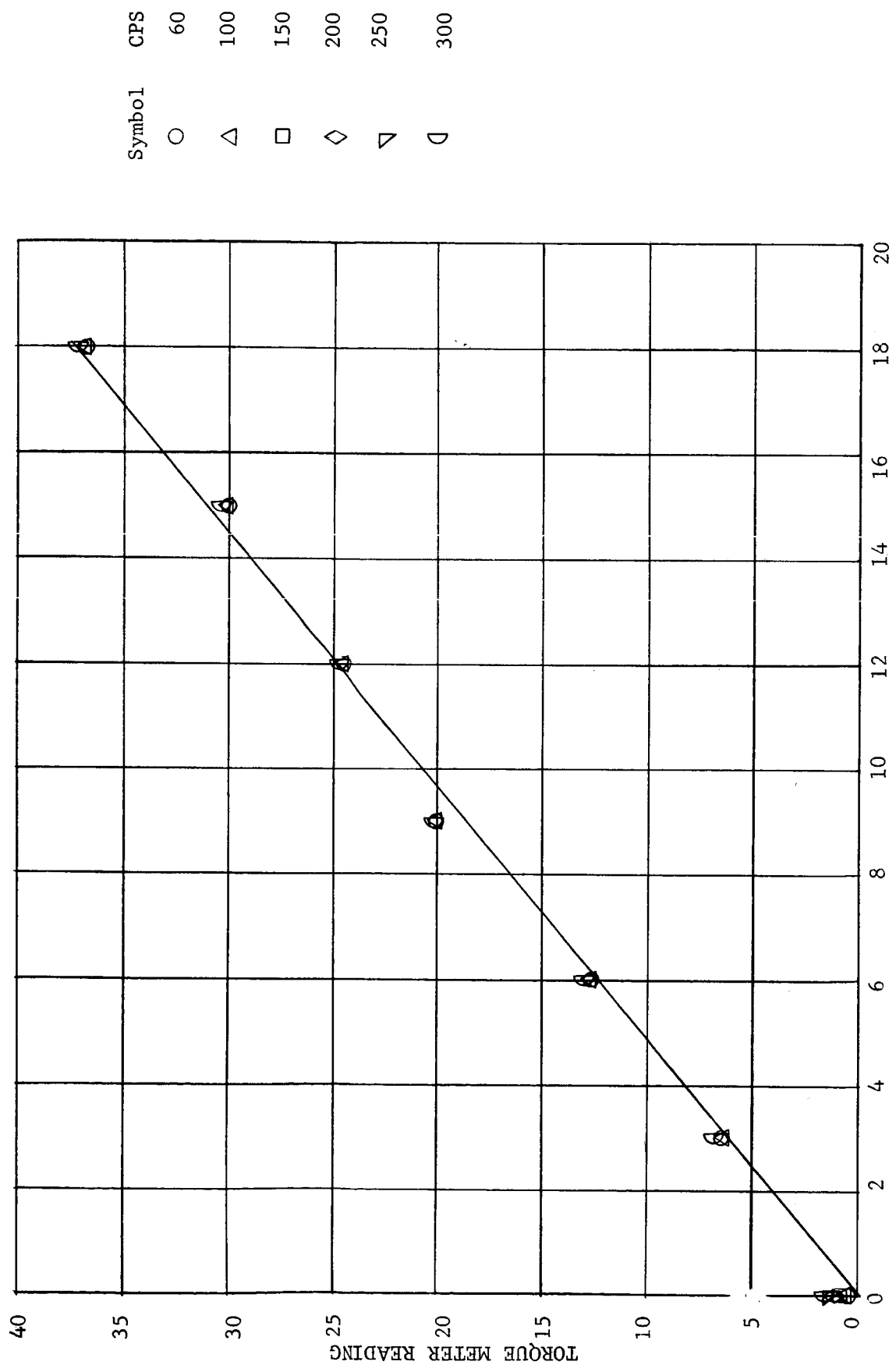


Figure 32. Eccenter Unbalance Ratio at Different Angular Settings



ANGLE - DEGREES
FIGURE 33 - TORQUE READOUT SYSTEM CALIBRATION

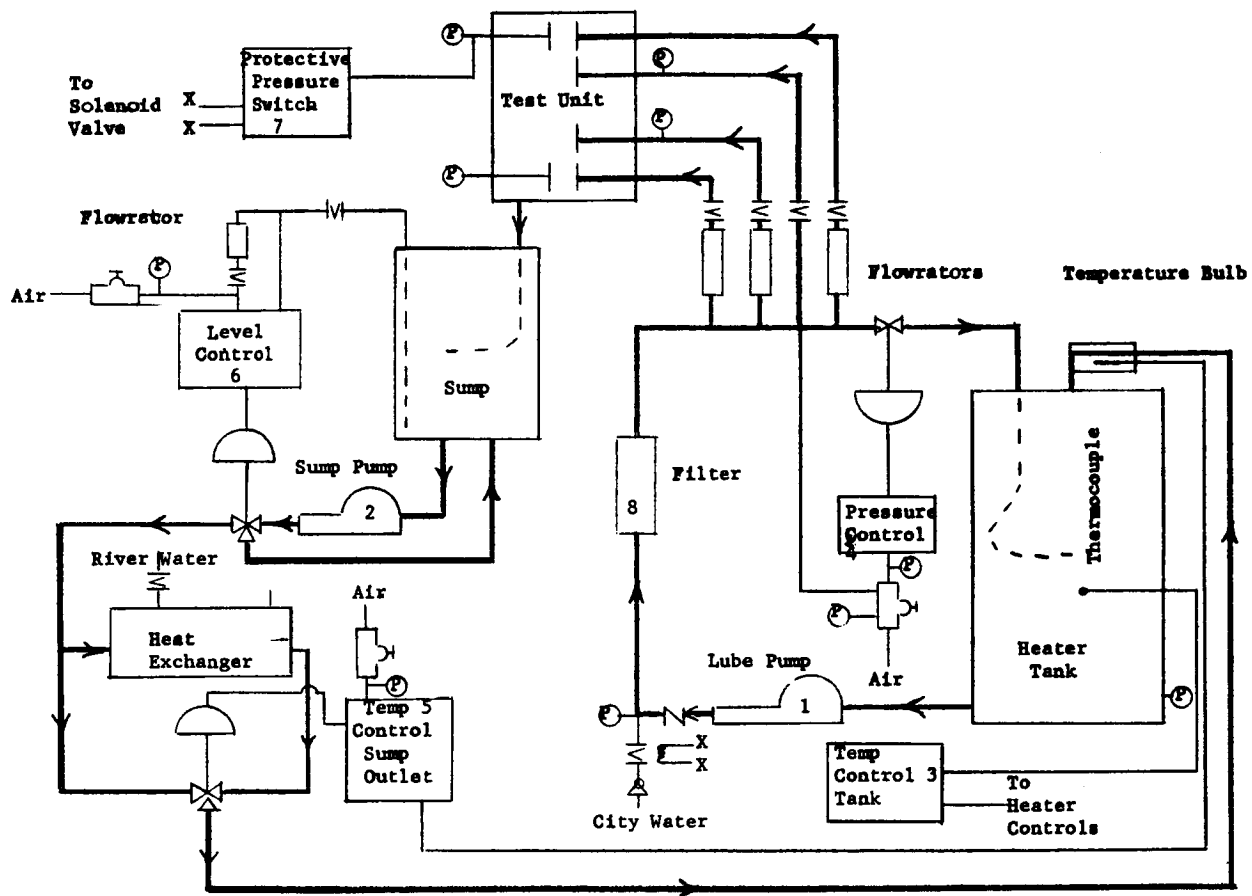
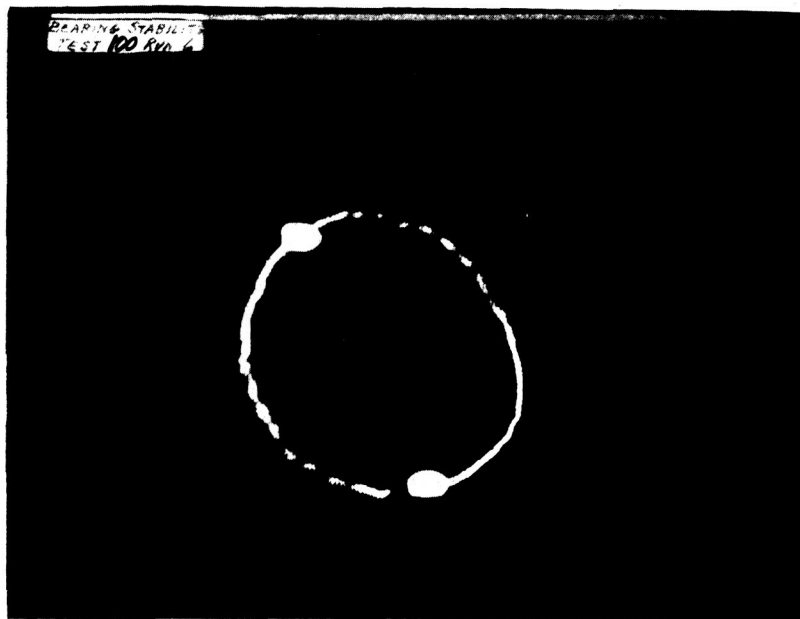


Figure 34. Diagram of Lubricant Loop



(b) Test No.100 Run No. 6 Speed 254 CPS.
Static Load 17.2 Lbs. (0.2 Volts/cm)



(a) Test No.100 Run No. 10 Speed 393 CPS.
Static Load 34.4 Lbs.

Figure 35. Oscilloscope Traces of Half-Frequency and Synchronous Whirl. 2 Axial Groove Bearing, $L/D = 1$, 3 mil Nom. Diam. Clear., 90°F nom. Lubricant Temp.

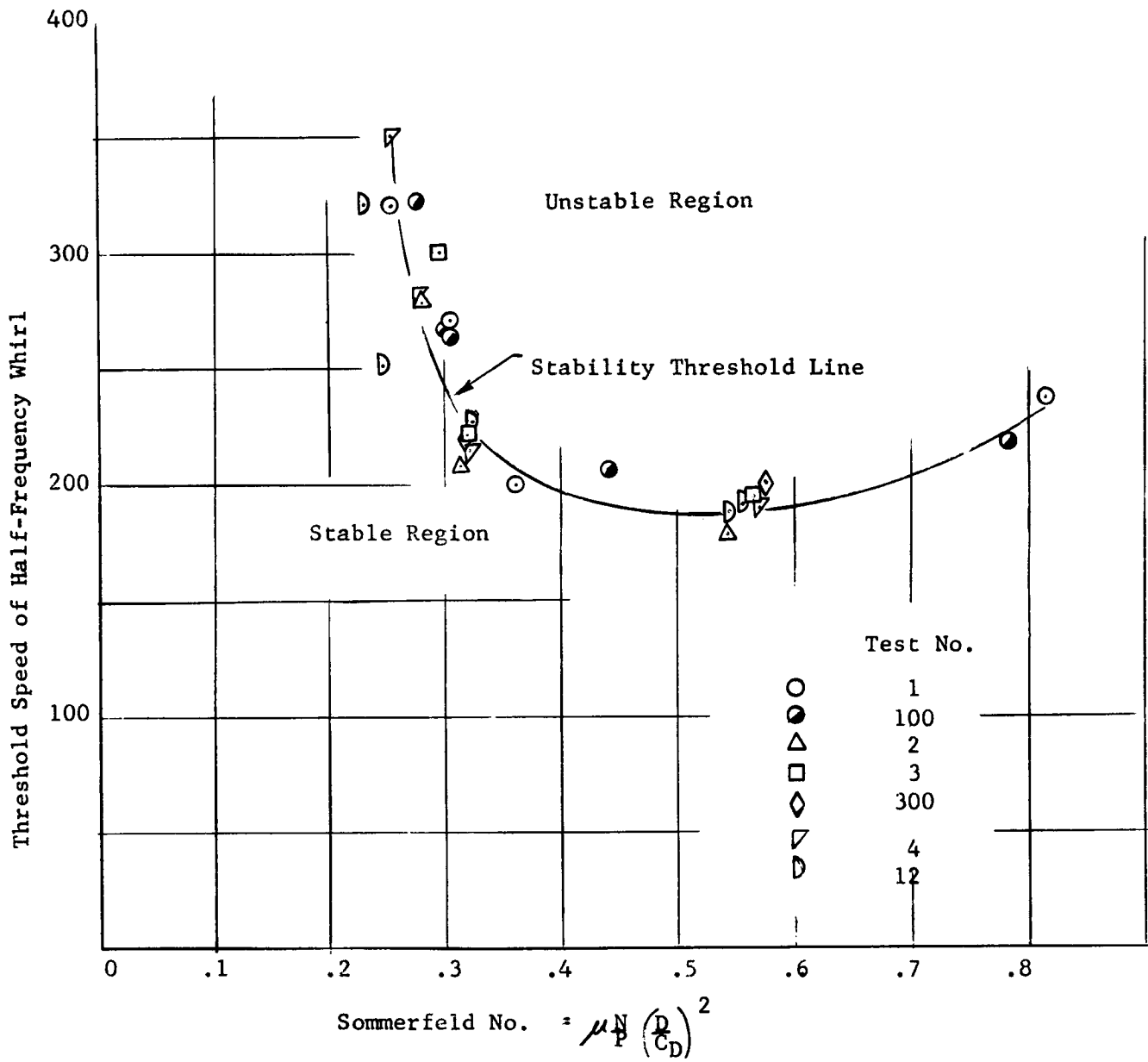


Figure 36. Threshold Speed of HFW vs Sommerfeld No.
 2 Axial Groove Bearing $L/D=1$
 3 Mil Nom. Diam. Clearance

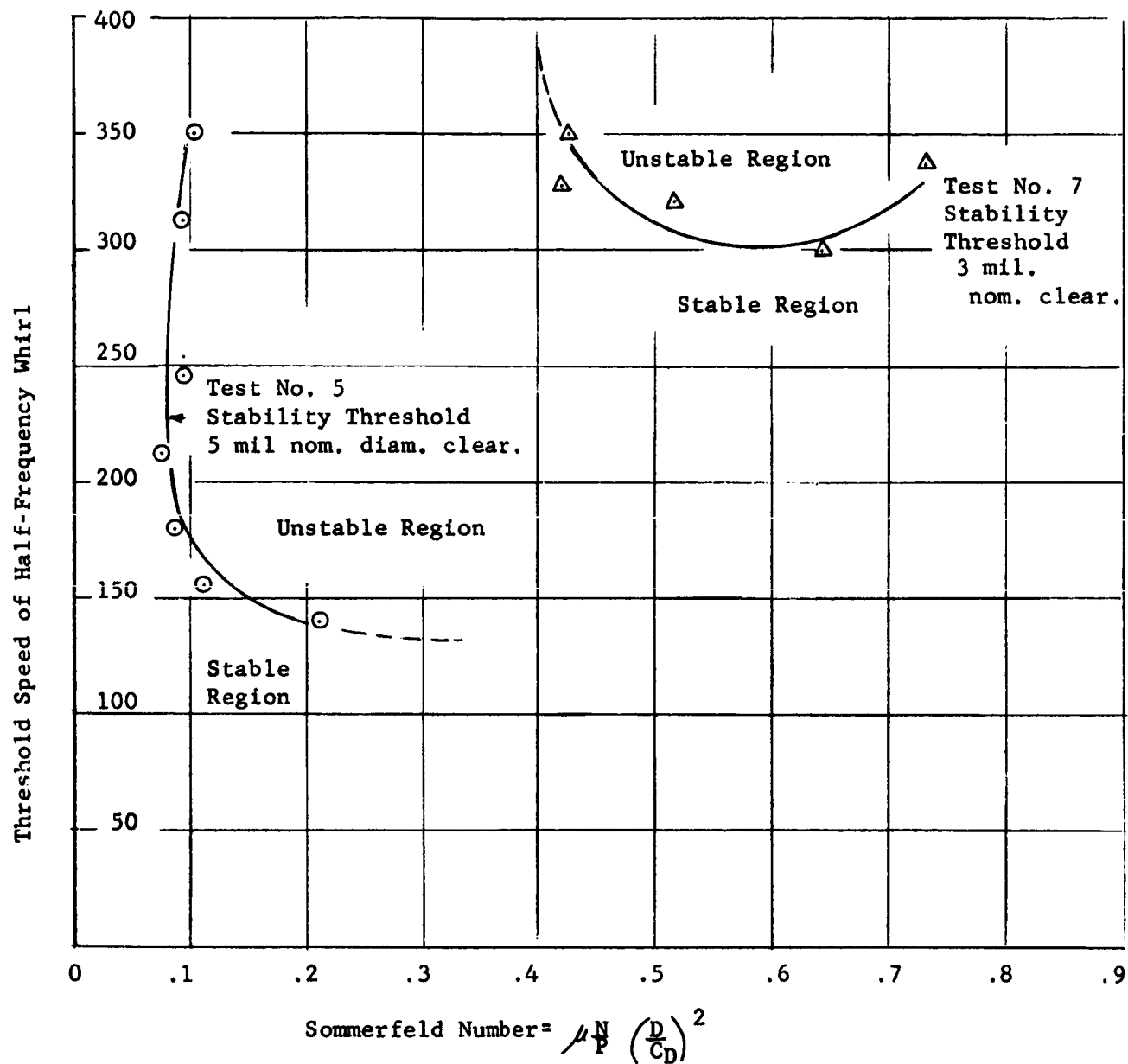


Figure 37. Threshold Speed of Half-Frequency Whirl
vs Sommerfeld Number

2 Axial Groove Bearing, $L/D=1\frac{1}{2}$

TILTING PAD BEARING

Test No. 8 Run 43,44
Plain Shaft with Eccenters (Fig. 12)

Max. Journal Diam.
120° Lubricant 77.4 lbs. Static Load



300 CPS

Gage #2&4

Gage #1&3



Lower Bearing



Upper Bearing

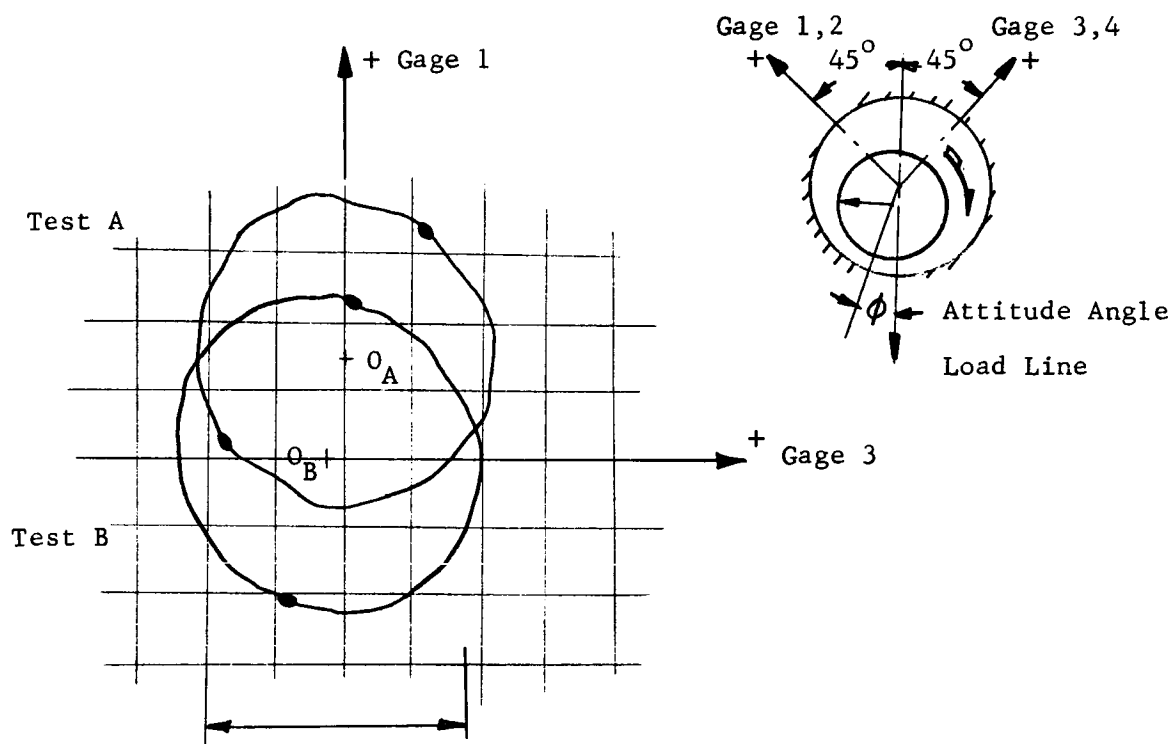


350 CPS

Gage #2&4

Gage #1&3

Figure 38. Oscilloscope Traces of Shaft Orbit in Tilting Pad Bearing.



Calculated Brg. Diametral Clearance = 3 mils
 0.2 volt/Cm. Scope sensitivity; 0.25 volts/mil gage-scope
 calib.

Gage zero shift with speed

Two axial groove bearing $L/D = 1$

3 mil diametral clearance shaft

Data of November 4, 1963

Test A - Half frequency whirl at 17.5 cps shaft speed

D.C. voltmeter readings

#1 gage - 1.8V calibration .09628 mils/volt

#3 gage - 2.3V calibration .09706 mils/volt

Test B - Half frequency whirl at 168 cps shaft speed

D.C. Voltmeter readings

#1 gage - 13.2V

#3 gage - 3.8V

Figure 39. Gage Zero Shift with Speed

Test No. 3

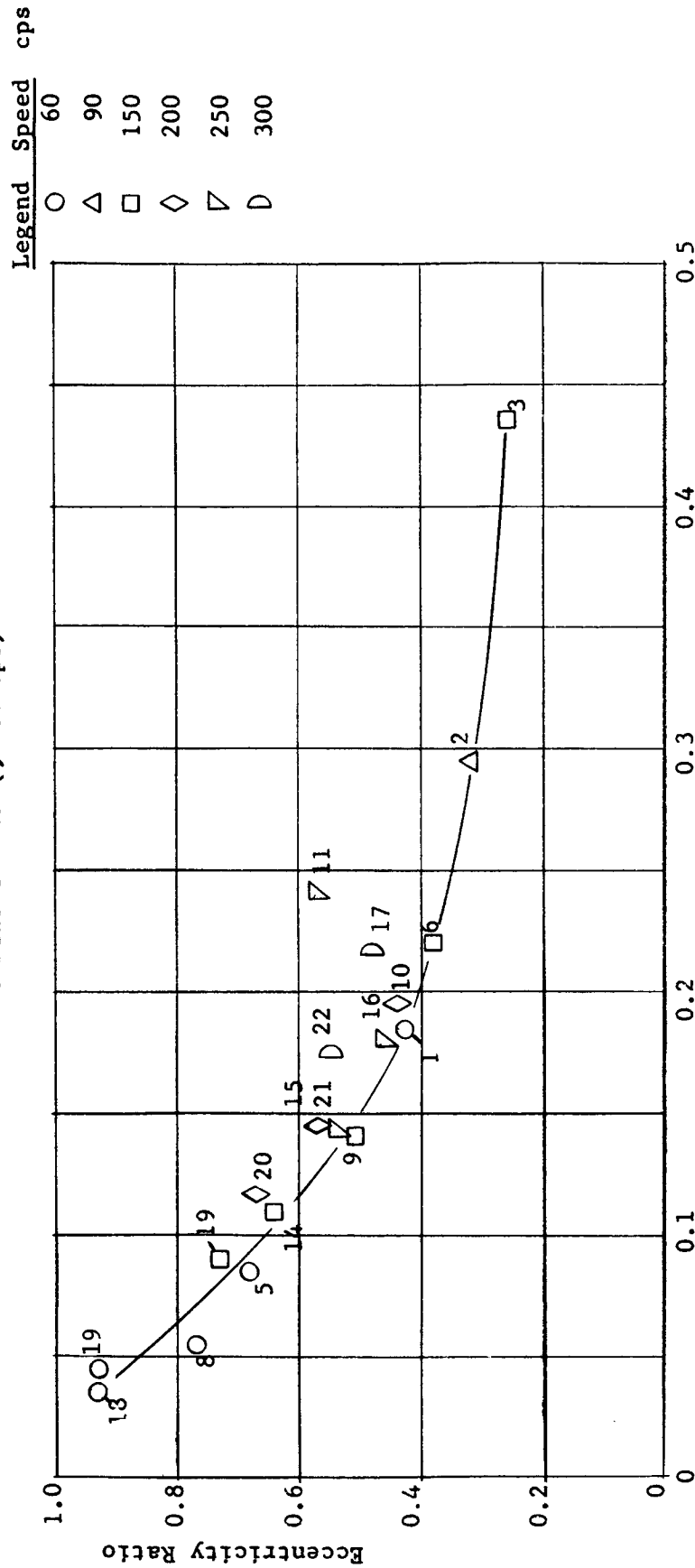
Lower Bearing

2 Axial Groove $L/D=1$

3 Mil Nom. Diam. Clearance

120°F Nom. Water-Lube. Temp.

Gage zero positions based on avg. zero Runs 1 & 18 (60 cps)
& Runs 3 & 19 (> 60 cps)



$$\text{Sommerfeld No. } S = \mu N \left(\frac{D}{C_D} \right)^2$$

Figure 40. Eccentricity Ratio vs Sommerfeld No.
Test No. 3, Lower Bearing

2 Axial Groove Brg., I/D=1
 3 Mil Nom. Dia. Clear.
 120°F Lube. Temp.

Gage zeros based on
 Avg. of runs 1 & 18 for 60 cps
 Avg. of runs 3 & 17 for 60 cps
 Load Line

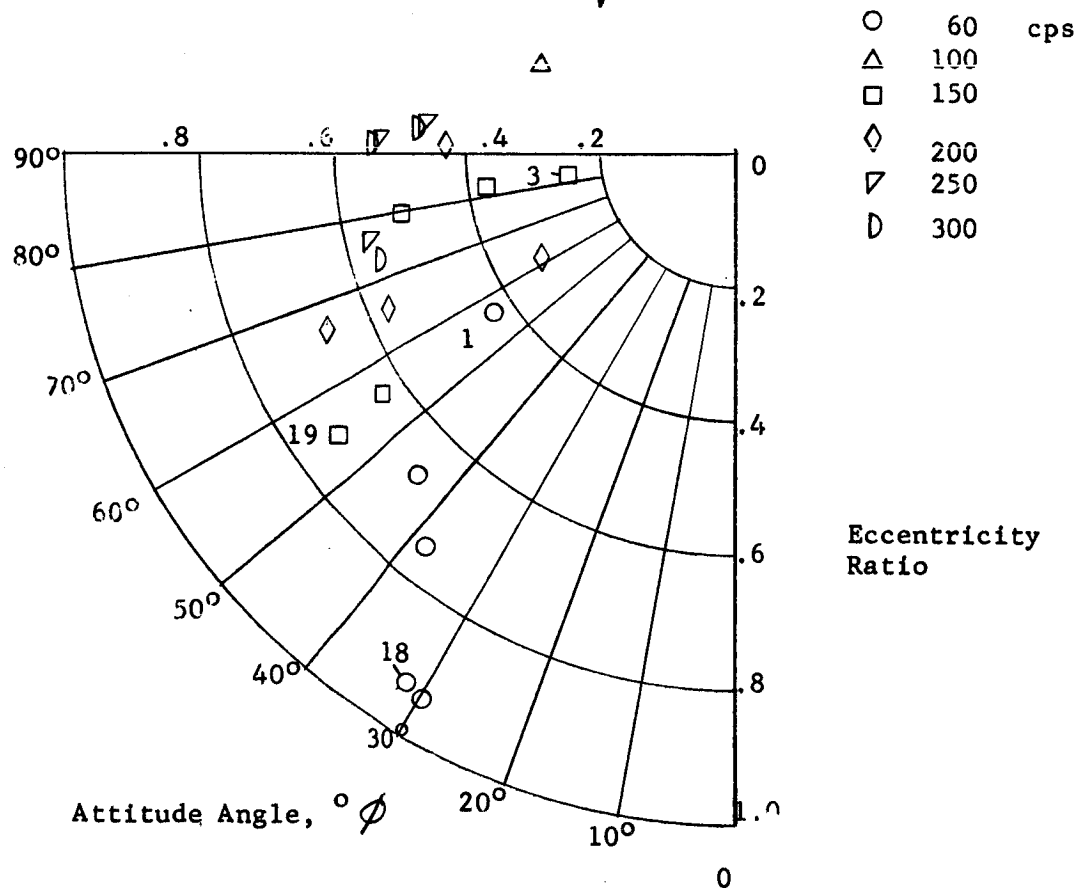
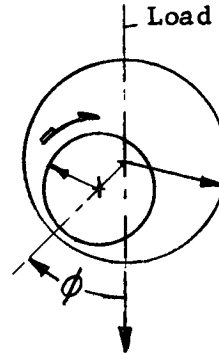


Figure 41 . Eccentricity Ratio vs Attitude Angle
 Test No. 3, Lower Bearing

Test No. 4, Lower Bearing
 2 axial groove brg, L/D=1, 120°F nom. lube. temp.
 3 mil. nom. diam. clear.

Gage zeros based on:

Avg. of Runs 9, 14, 21 for 60 cps

Avg. of Runs 2, 22 for > 60 cps

○ 60 cps
 △ 100
 □ 150
 ◇ 200
 ▽ 250
 D 300
 O 350

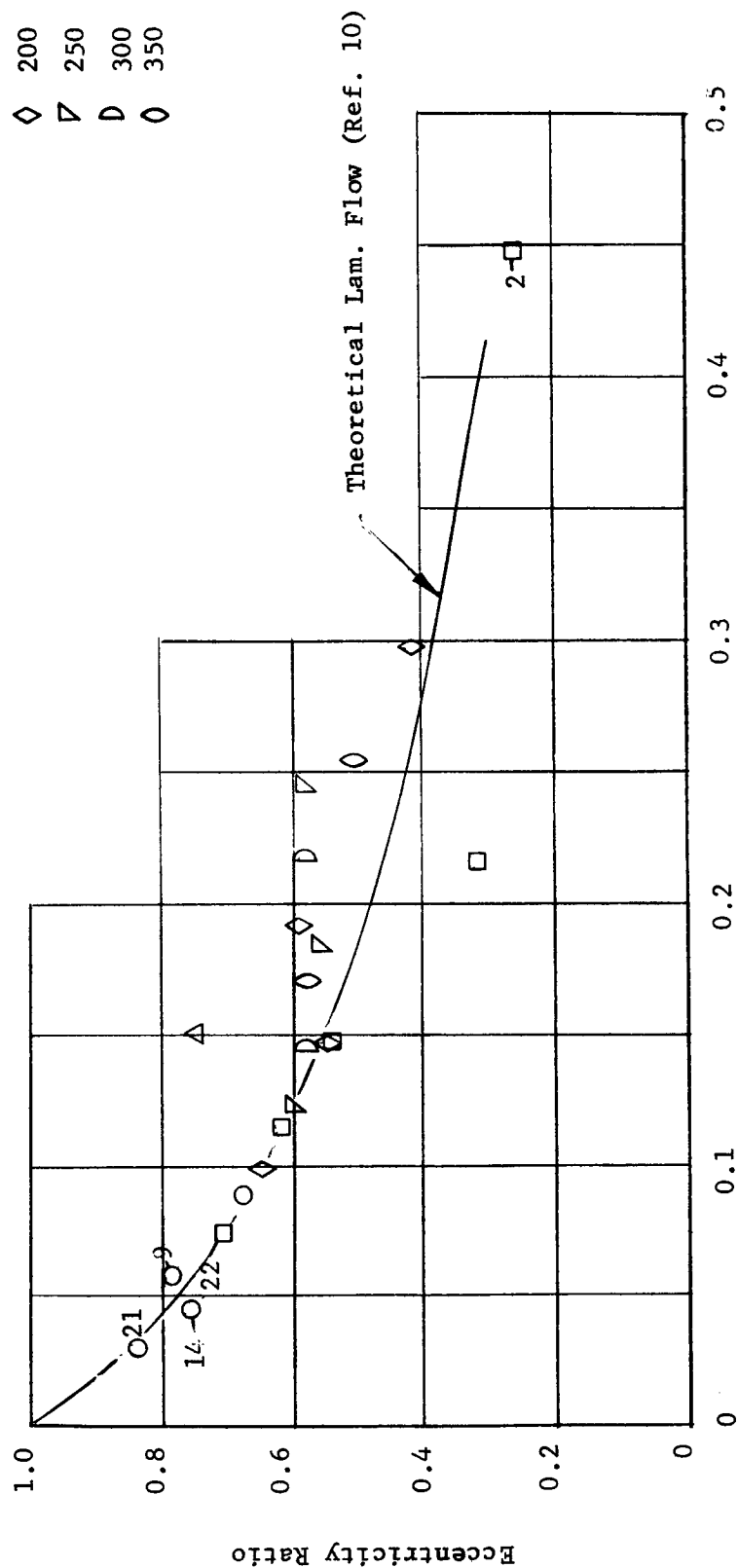


Figure 42 Eccentricity Ratio vs Sommerfeld No.
 Test No. 4, Lower Bearing

$$\text{Sommerfeld No. } S = \frac{\mu N}{P} \left(\frac{D}{C} \right)^2$$

Test No. 4, Lower Bearing
 2 Axial Groove, $L/D=1$
 3 Mil nom. diam. clear.
 120° F Lube. Temp.

Gage zeros based on:
 Avg. of Runs 9, 14, 21 for 60 cps
 Avg. of Runs 2, 22 for 60 cps

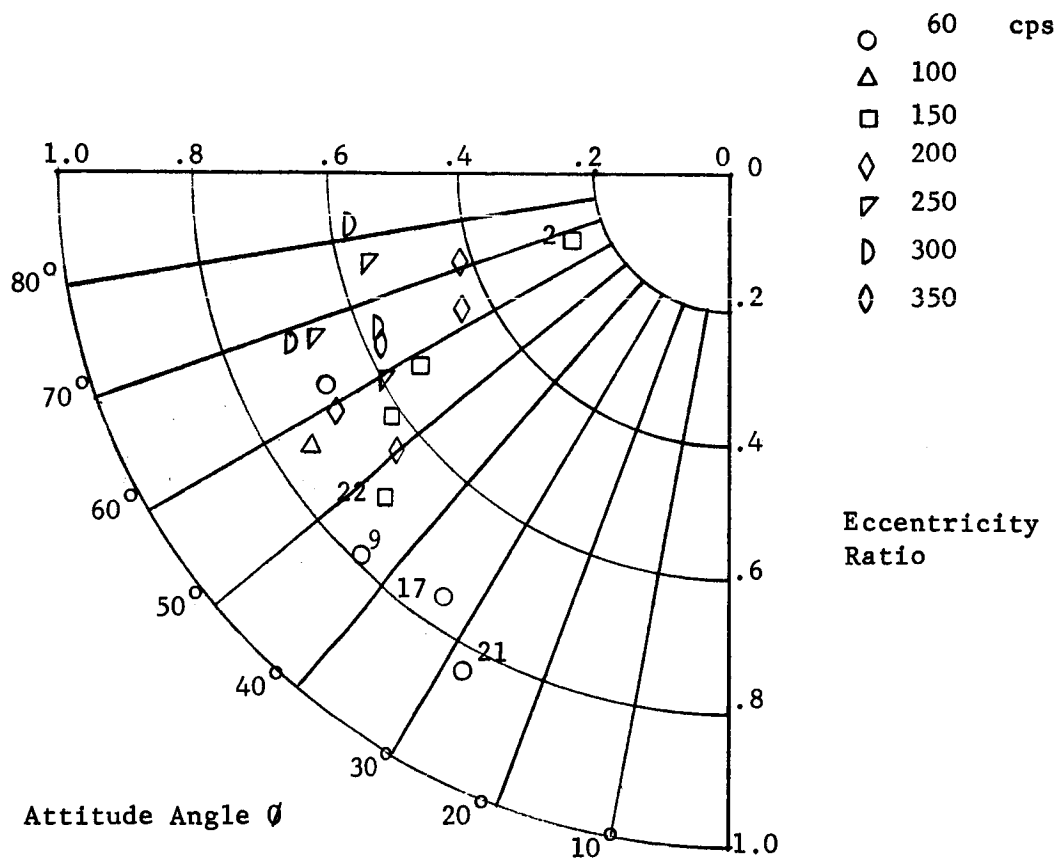


Figure 43 Eccentricity Ratio vs Attitude Angle
 Test No. 4, Lower Bearing

Test No. 3, Upper Bearing

2 axial groove brg., L/D=1, 120°F Nom. Lub. Temp
 3 Mil Diam. Clearance Gage zero based on Run 18,
 (Assumed eccentricity ratio 1.0, $\phi = 330^\circ$)

Runs at 60 cps only

Run No.	Brg. Load, Lbs
1	8.6
5	17.2
8	25.8
13	34.4
18	43.0

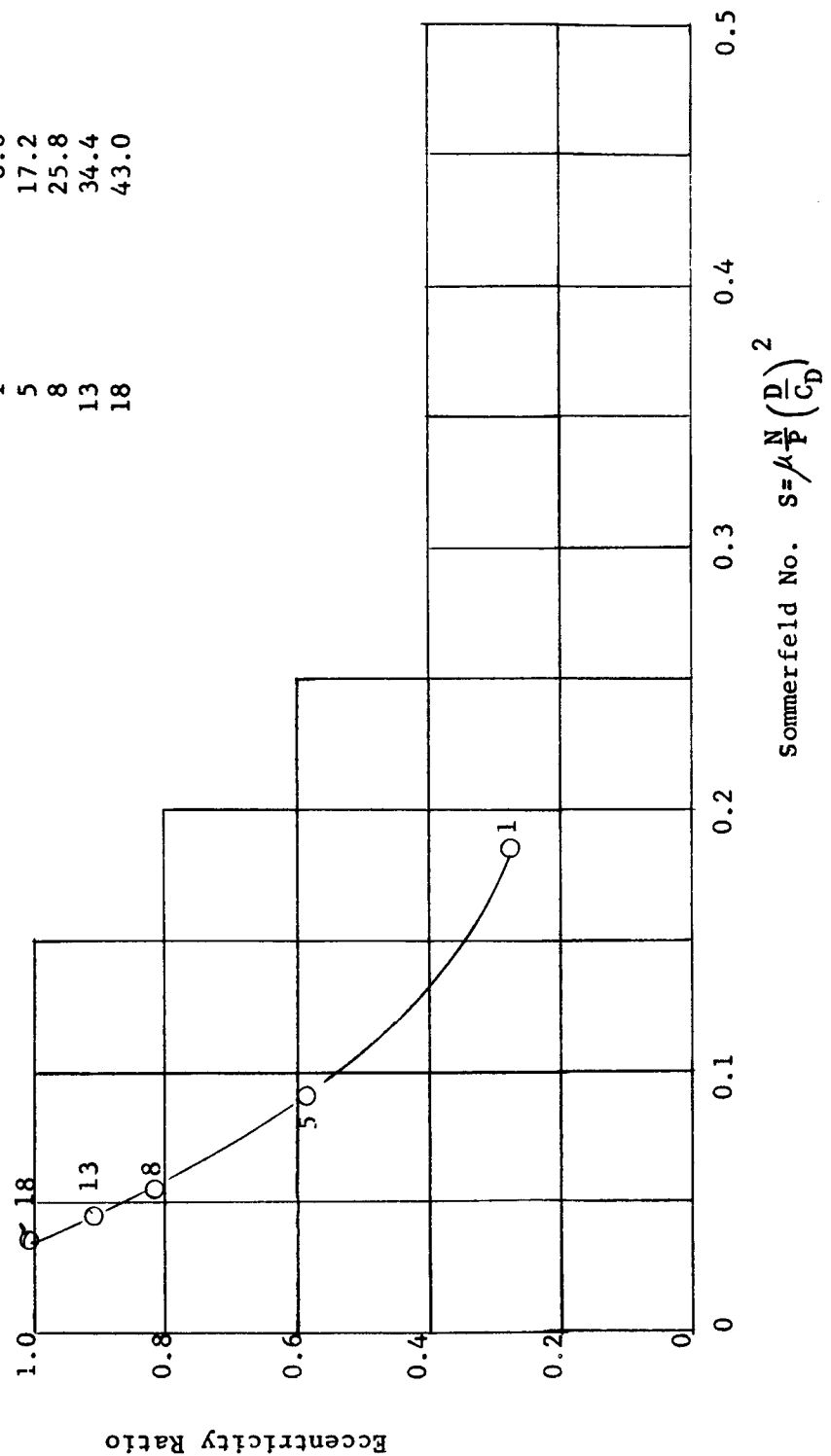
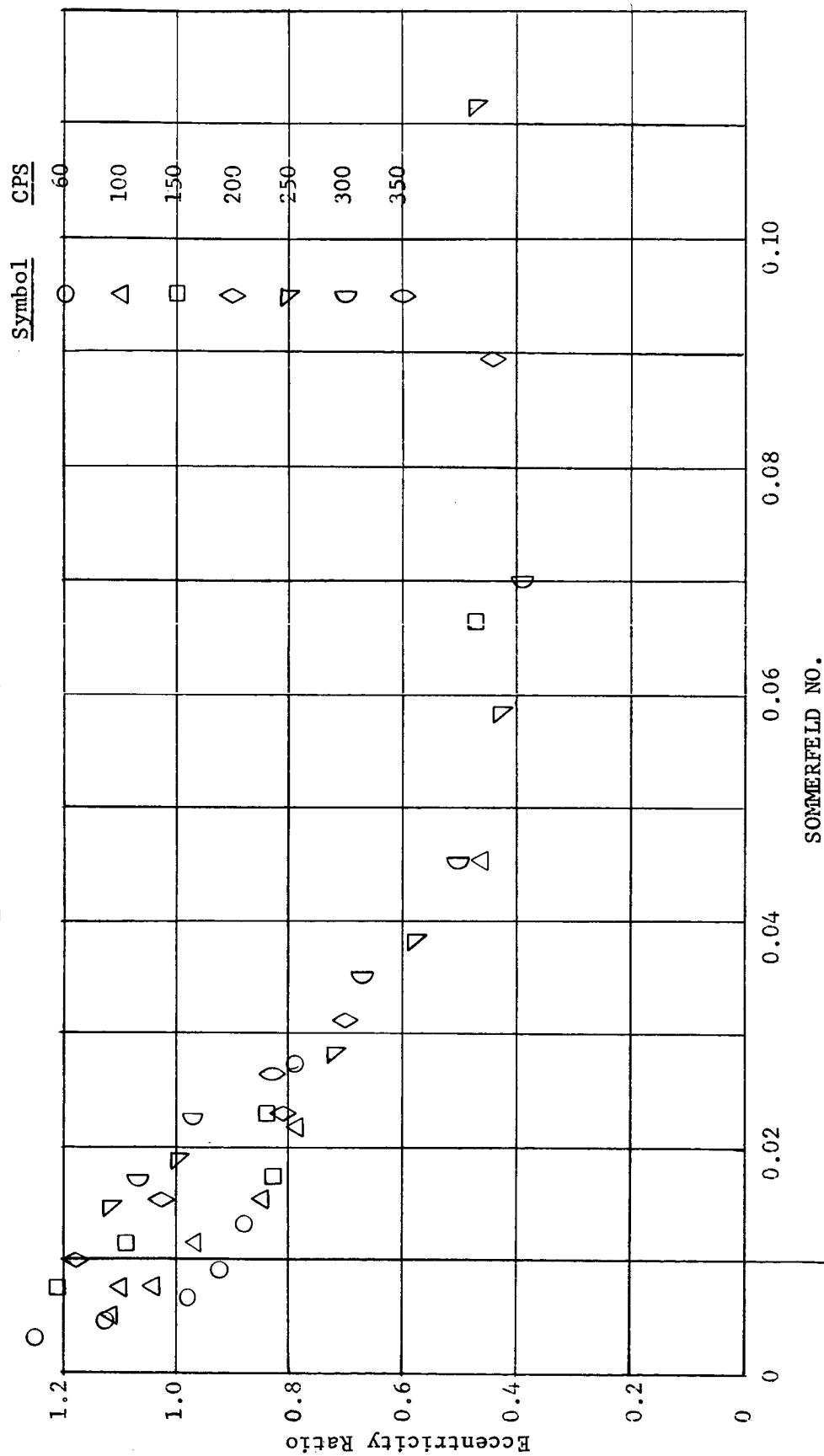


Figure 44. Eccentricity Ratio vs Sommerfeld No.
 Test No. 3, Upper Bearing, 60 cps run

FIG. 45

Test No. 9
 Tilting Pad Bearing $L/D = 1$
 5 Mil Nom. Dia. Clearance
 120°F Nom. Lube Temperature
 UPPER BEARING
 Based on Measured Gauge Zeros
 Load on Pivot of One Pad



Test No. 3

2 Axial Groove $L/D = 1$
 3 Mil Nom. Diam. Clearance
 120°F Nom. Lube Temperature

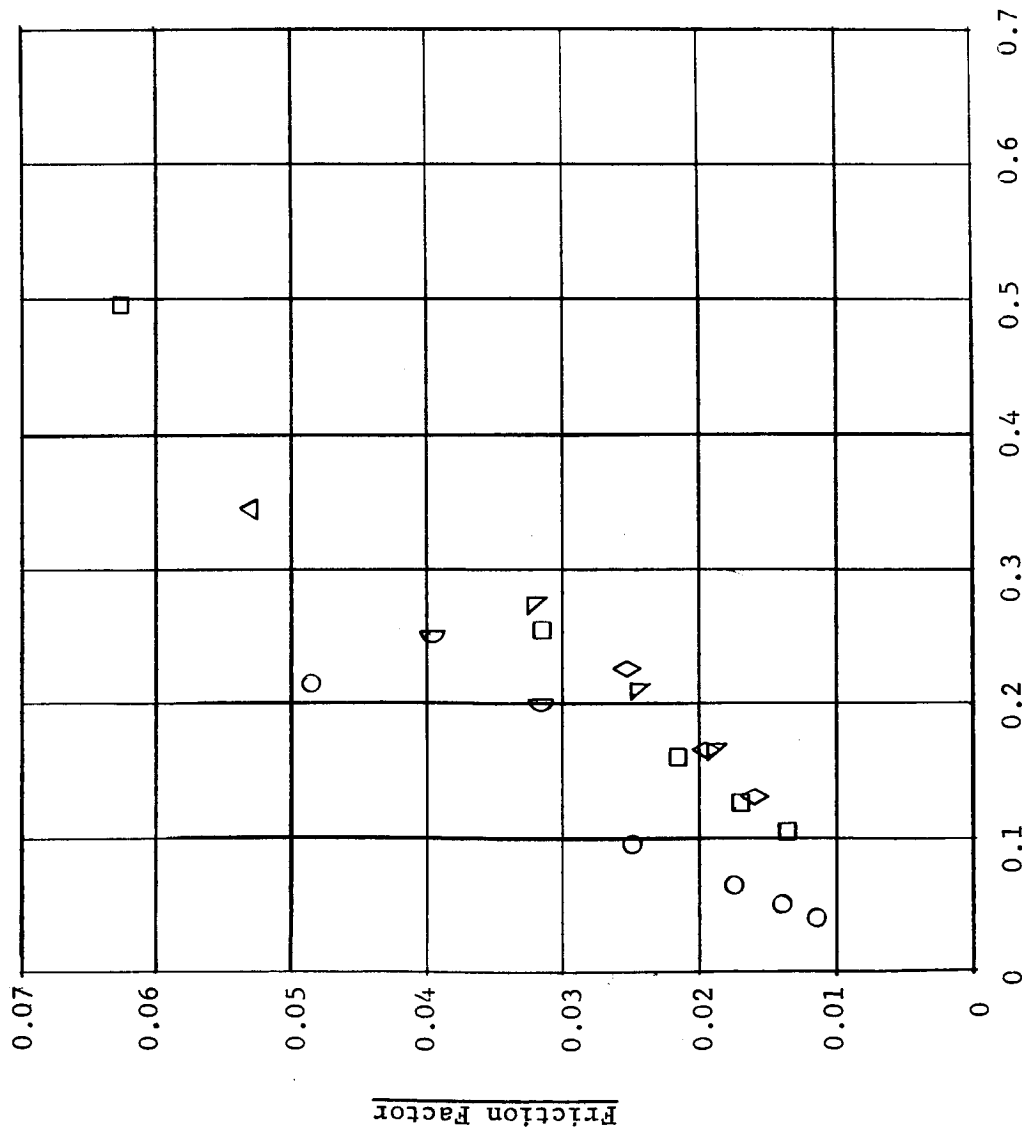


FIGURE 46 - SOMMERFELD NUMBER VS. FRICTION FACTOR

Test No. 300

2 Axial Groove L/D = 1
 3 Mil Nom. Diam. Clearance
 120°F Nom. Lube Temperature

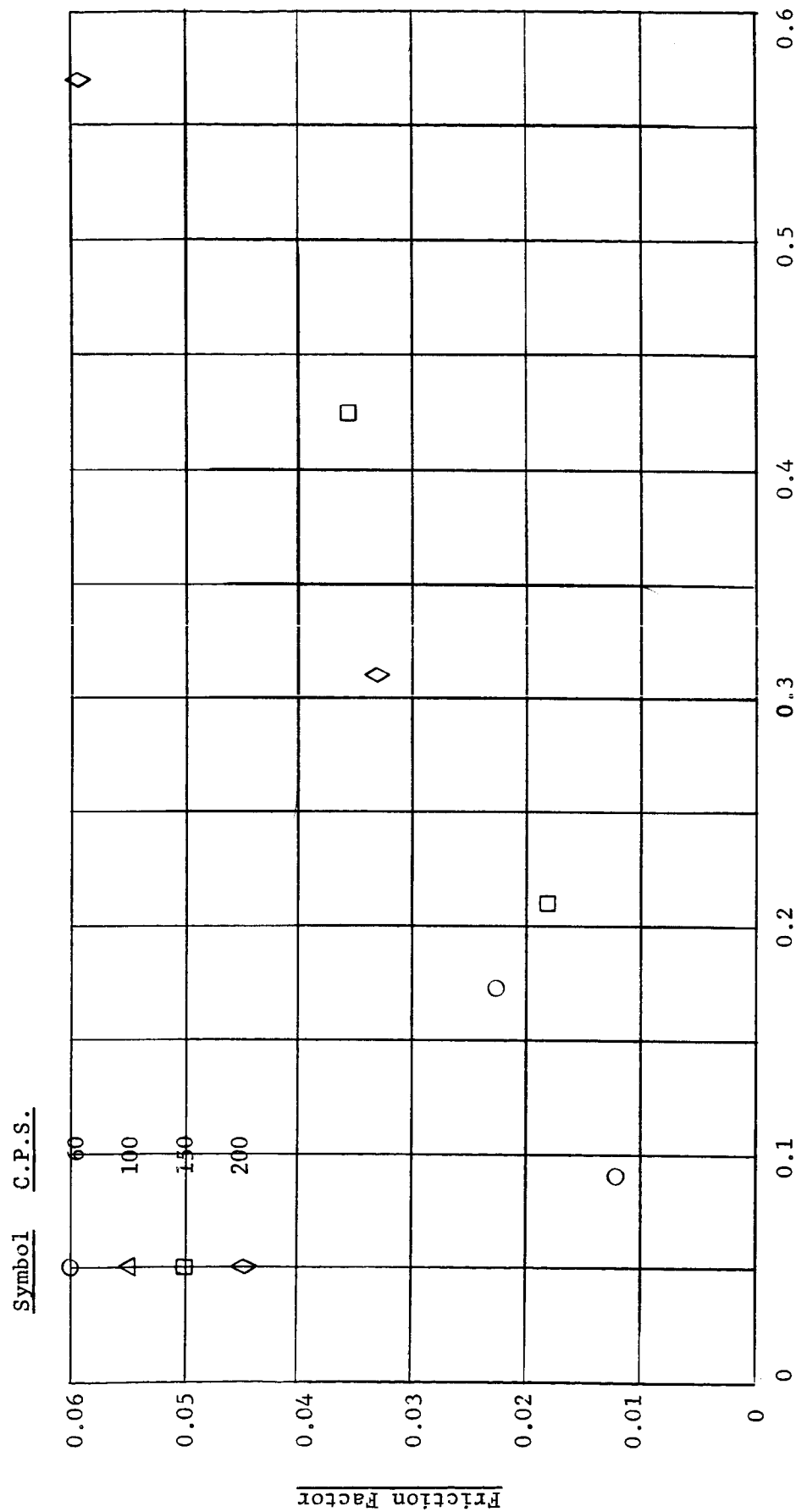


FIGURE 47 - SOMMERFELD NUMBER VS. FRICTION FACTOR

Test No. 301

2 Axial Groove L/D = 1
3 Mil Nom. Diam. Clearance
120°F Nom. Lube Temperature

Symbol C.P.S.

○ 60

△ 100

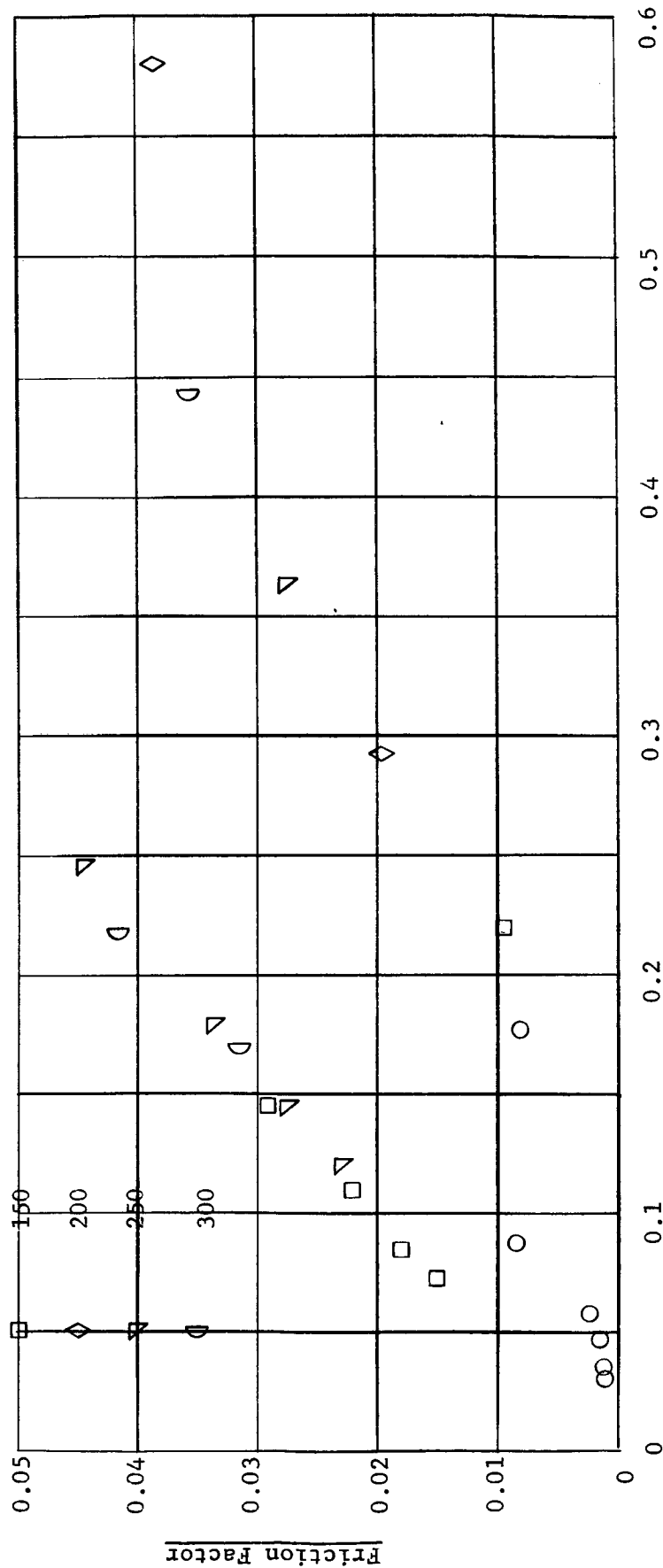


FIGURE 48 - SOMMERFELD NUMBER VS. FRICTION FACTOR

Test No. 302

2 Axial Groove $L/D = 1$
 3 Mil Nom. Diam. Clearance
 120°F Nom. Lube Temperature

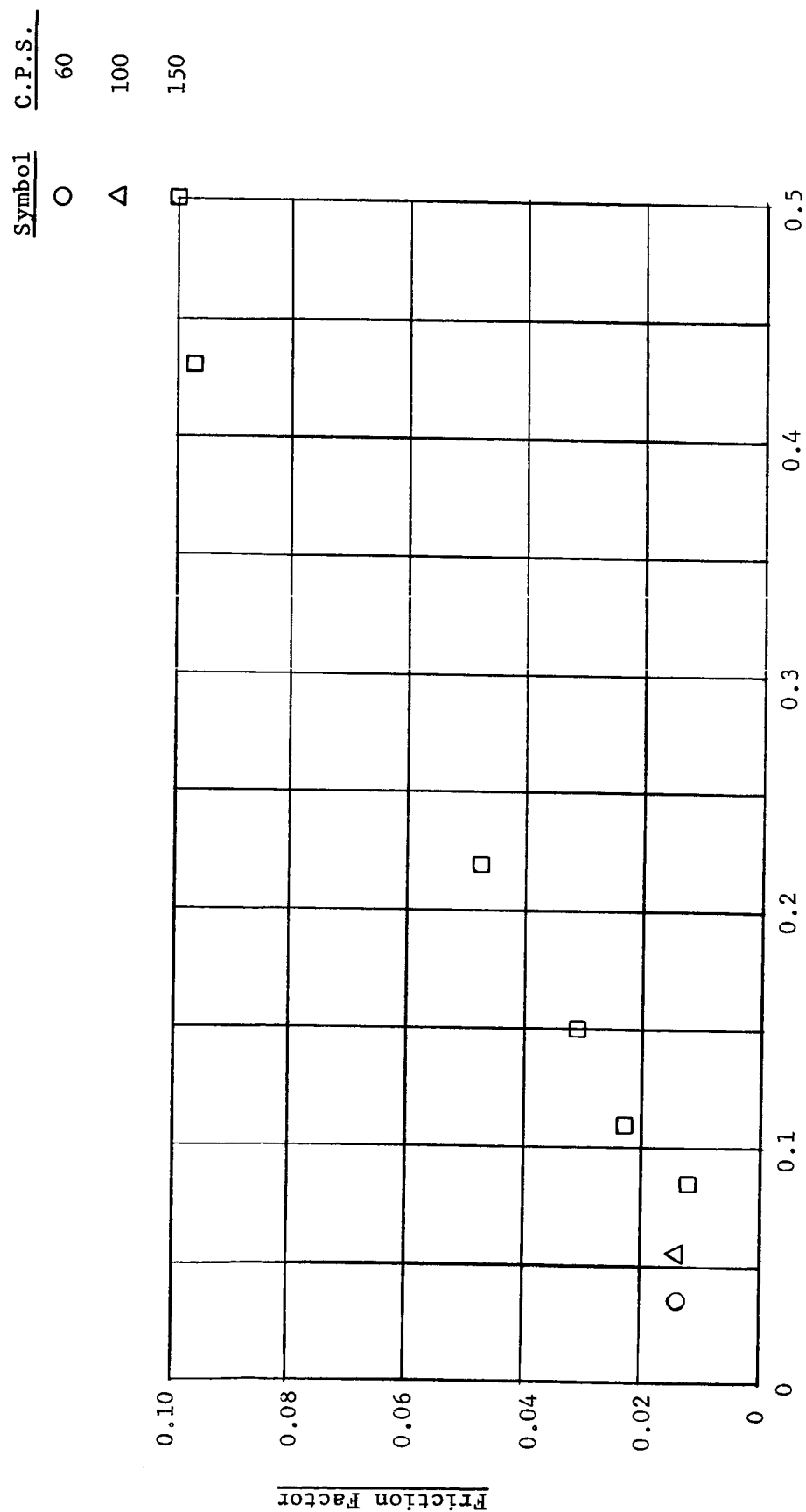


FIGURE 49 - SOMMERFELD NUMBER VS. FRICTION FACTOR

Test No. 4

2 Axial Groove $L/D = 1$
 3 Mil Nom. Diam. Clearance
 120°F Nom. Lube Temperature

Symbol	C.P.S.
○	60
△	100
□	150
◇	200
▽	250
⊖	300

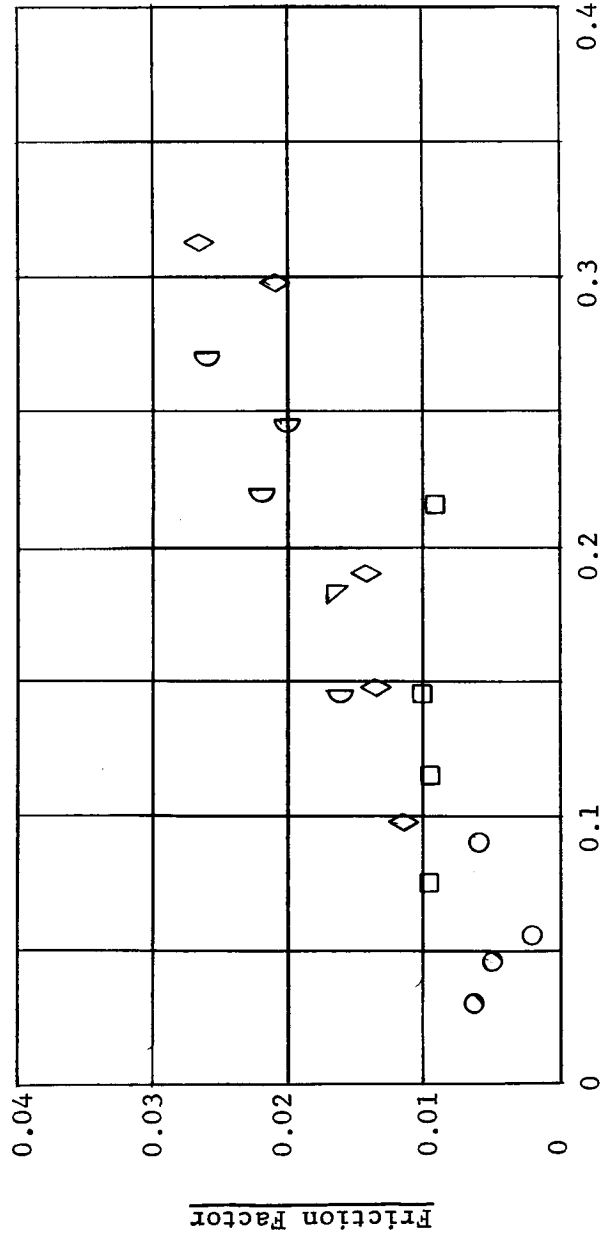


FIGURE 50 - SOMMERFELD NUMBER VS. FRICTION FACTOR

Test No. 5

2 Axial Groove $L/D = 1.5$
 5 Mil Nom. Diam. Clearance
 120°F Nom. Lube Temperature

<u>Symbol</u>	<u>C.P.S.</u>
○	60
△	100
□	150
◇	200
▽	250
∩	300
∅	350

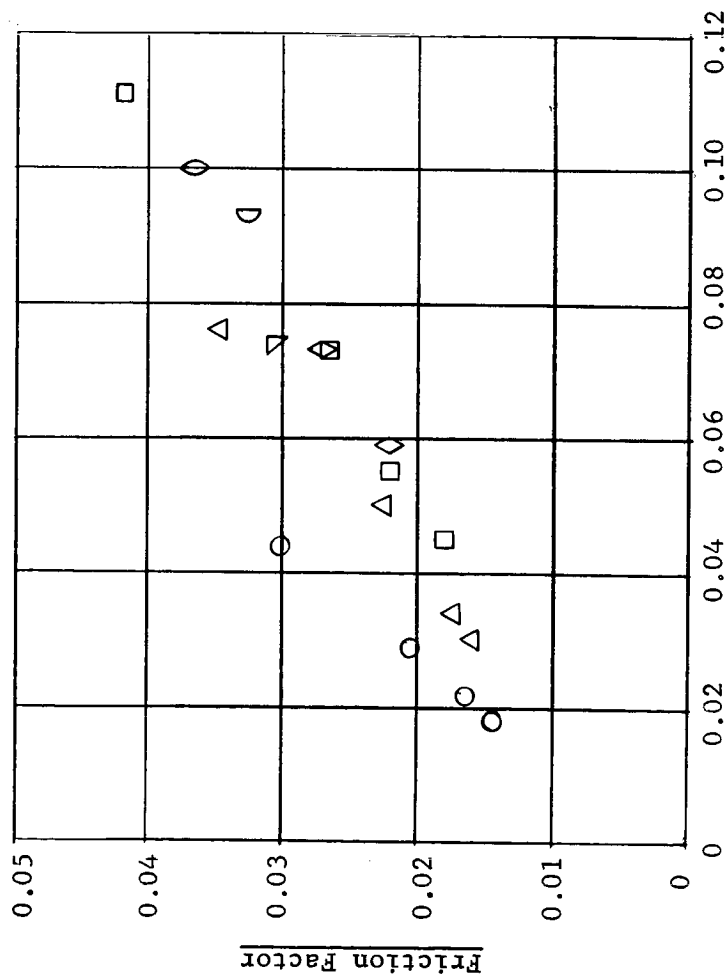


FIGURE 51 - SOMMERFELD NUMBER VS. FRICTION FACTOR

Test No. 501

2 Axial Groove L/D = 1.5
 5 Mil Nom. Diam. Clearance
 120°F Nom. Lube Temperature

<u>Symbol</u>	<u>C.P.S.</u>
○	60
△	100
□	150
◇	200

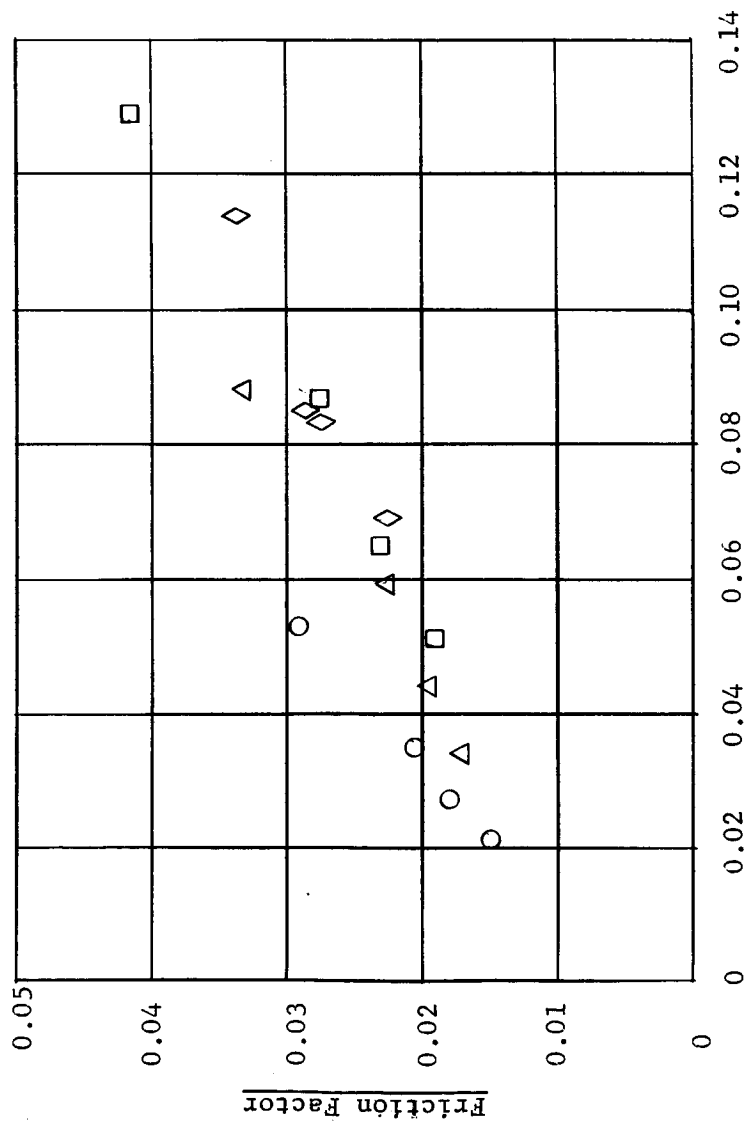
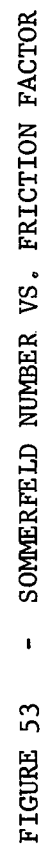


FIGURE 52 - SOMMERFELD NUMBER VS. FRICTION FACTOR

2 Axial Groove 40 = 1.5
2 Mil Nom. Diam. Clearance
75°F Nom. Lube Temperature



Test No. 600

2 Axial Groove L/D = 1.5
 2 Mil Nom. Diam. Clearance
 75°F Nom. Lube Temperature

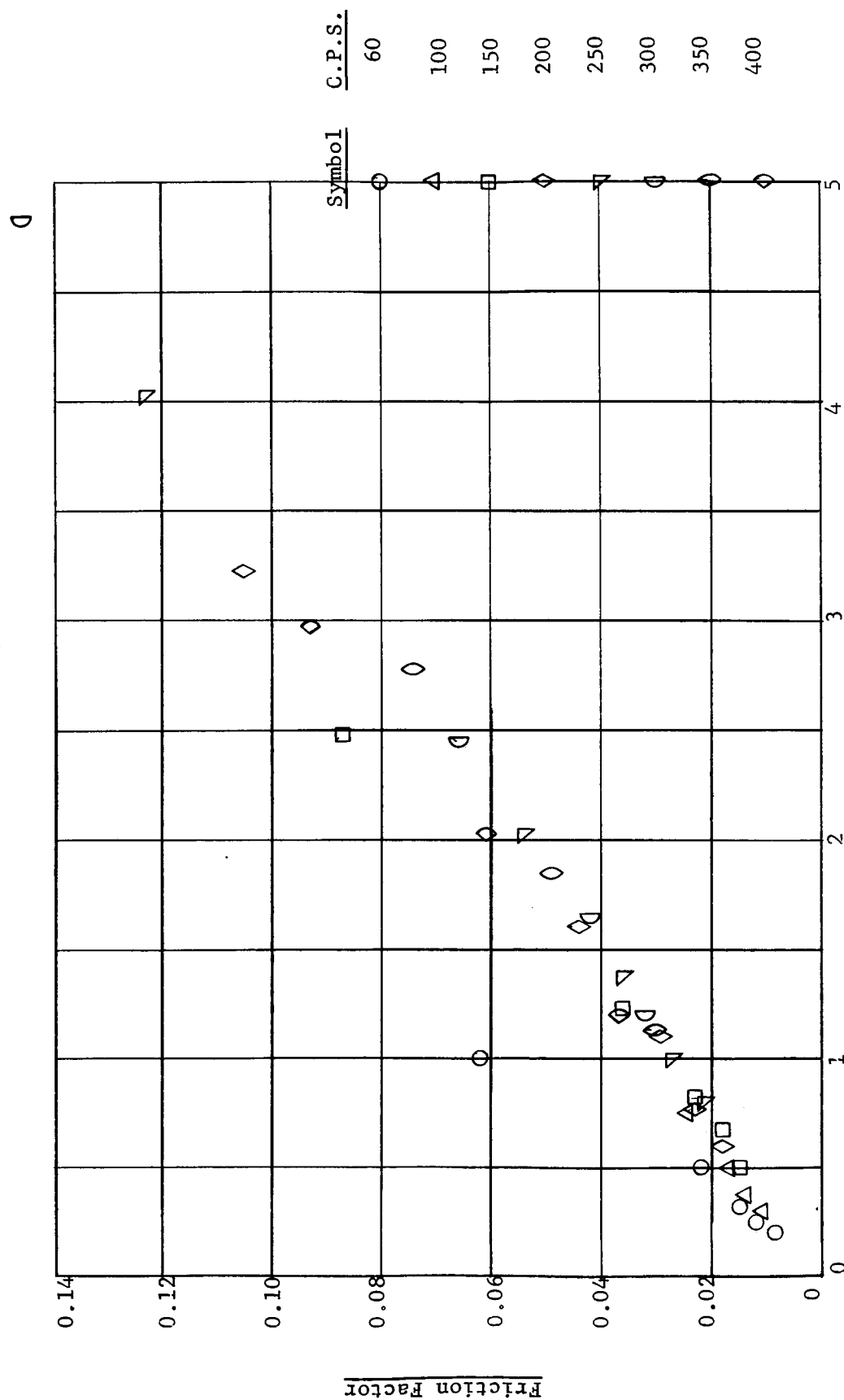


FIGURE 54 - SOMMERFELD NUMBER VS. FRICTION FACTOR

Test No. 7

2 Axial Groove $L/D = 1.5$
 3 Mil Nom. Diam. Clearance
 75°F Nom. Lube Temperature

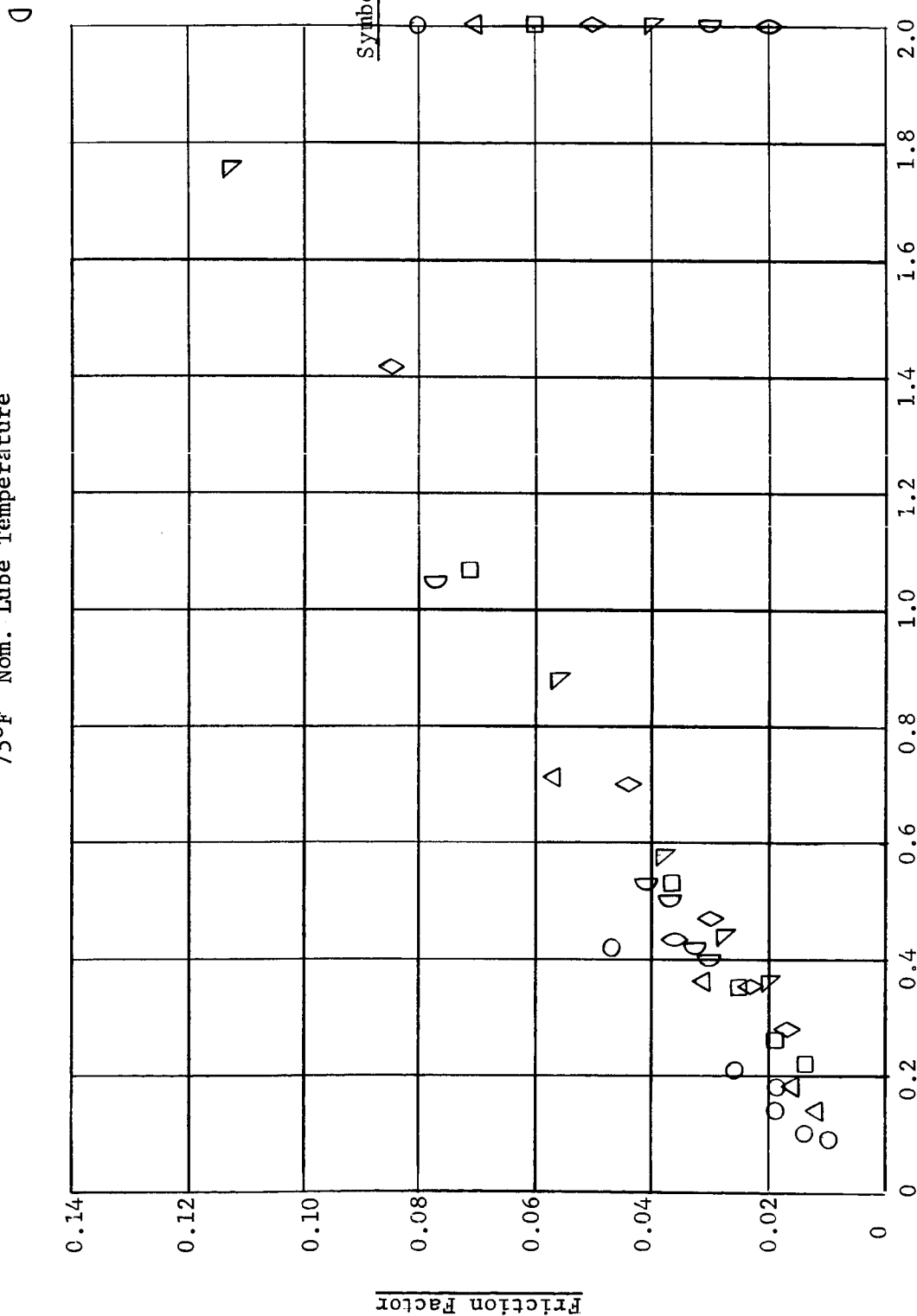


FIGURE 55 - SOMMERFELD NUMBER VS. FRICTION FACTOR

Test No. 701

2 Axial Groove $L/D = 1.5$
 3 Mil Nom. Diam. Clearance
 75°F Nom. Lube Temperature

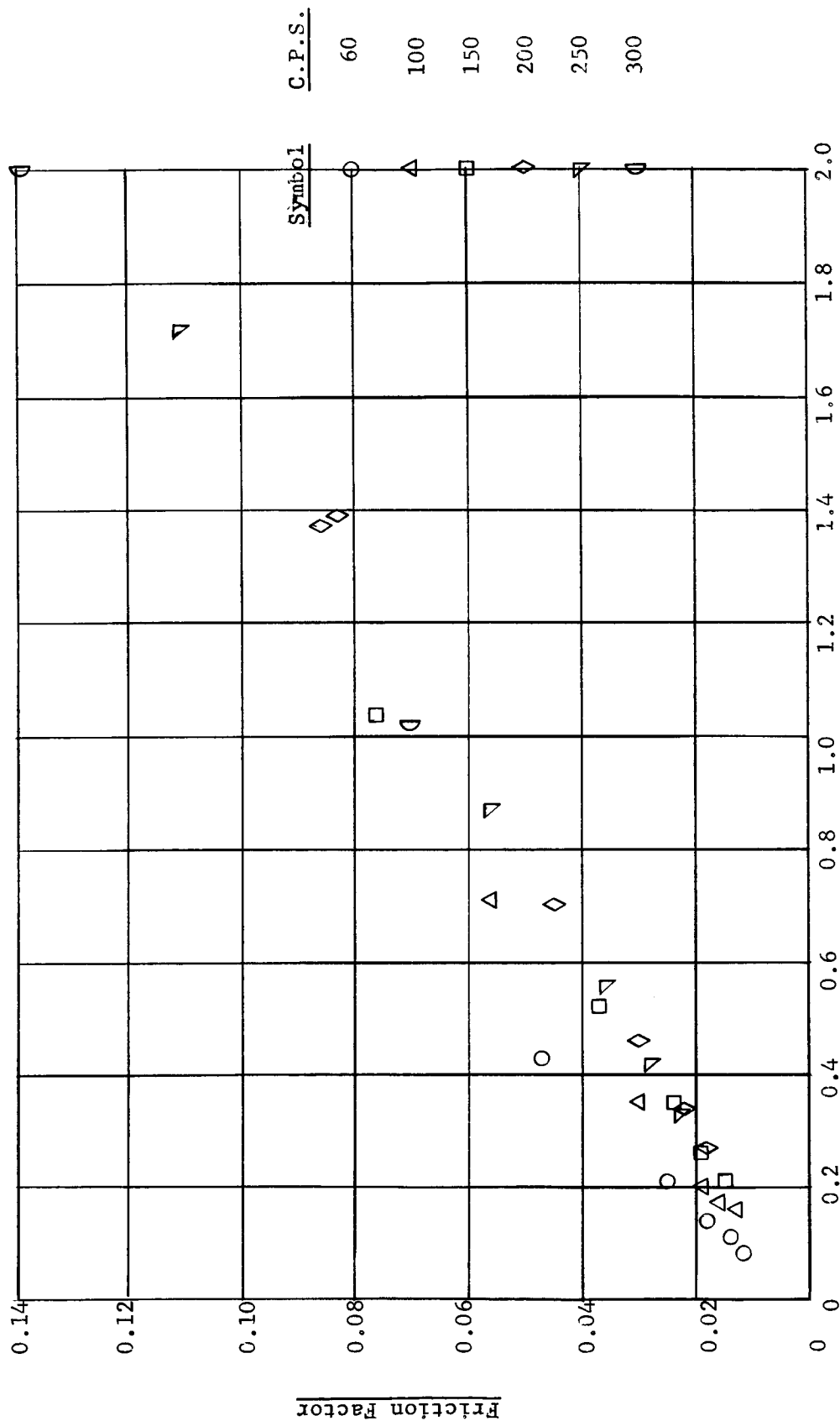


FIGURE 56 - SOMMERFELD NUMBER VS. FRICTION FACTOR

Test No. 12

2 Axial Groove L/D = 1
 3 Mil Nom. Diam. Clearance
 120°F Nom. Lube Temperature

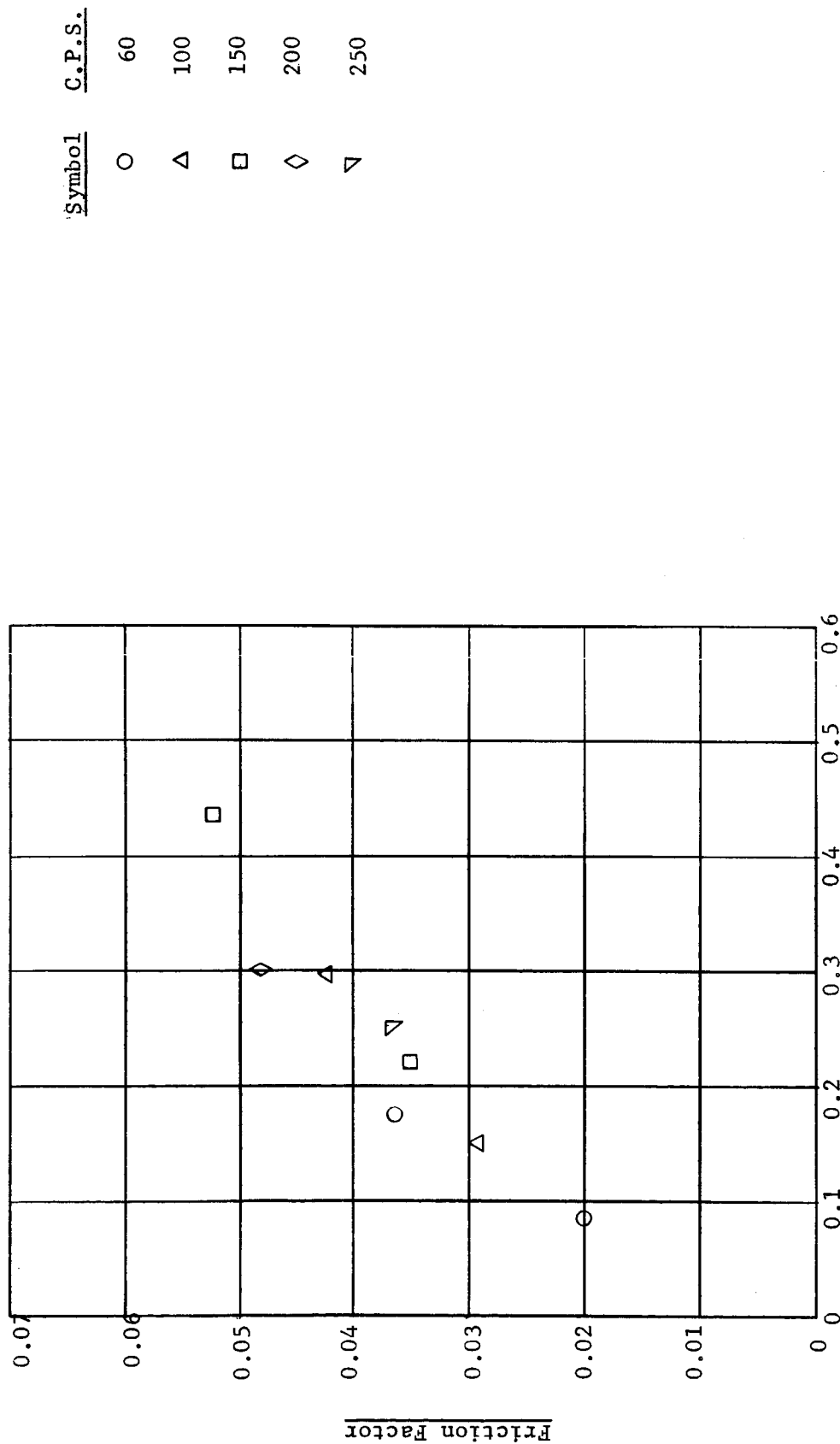


FIGURE 57 - SOMMERFELD NUMBER VS. FRICTION FACTOR

Test No. 13

2 Axial Groove L/D = 1
2 Mil Nom. Diam. Clearance
120°F Nom. Lube Temperature

Symbol C.P.S.

○ 60

△ 100

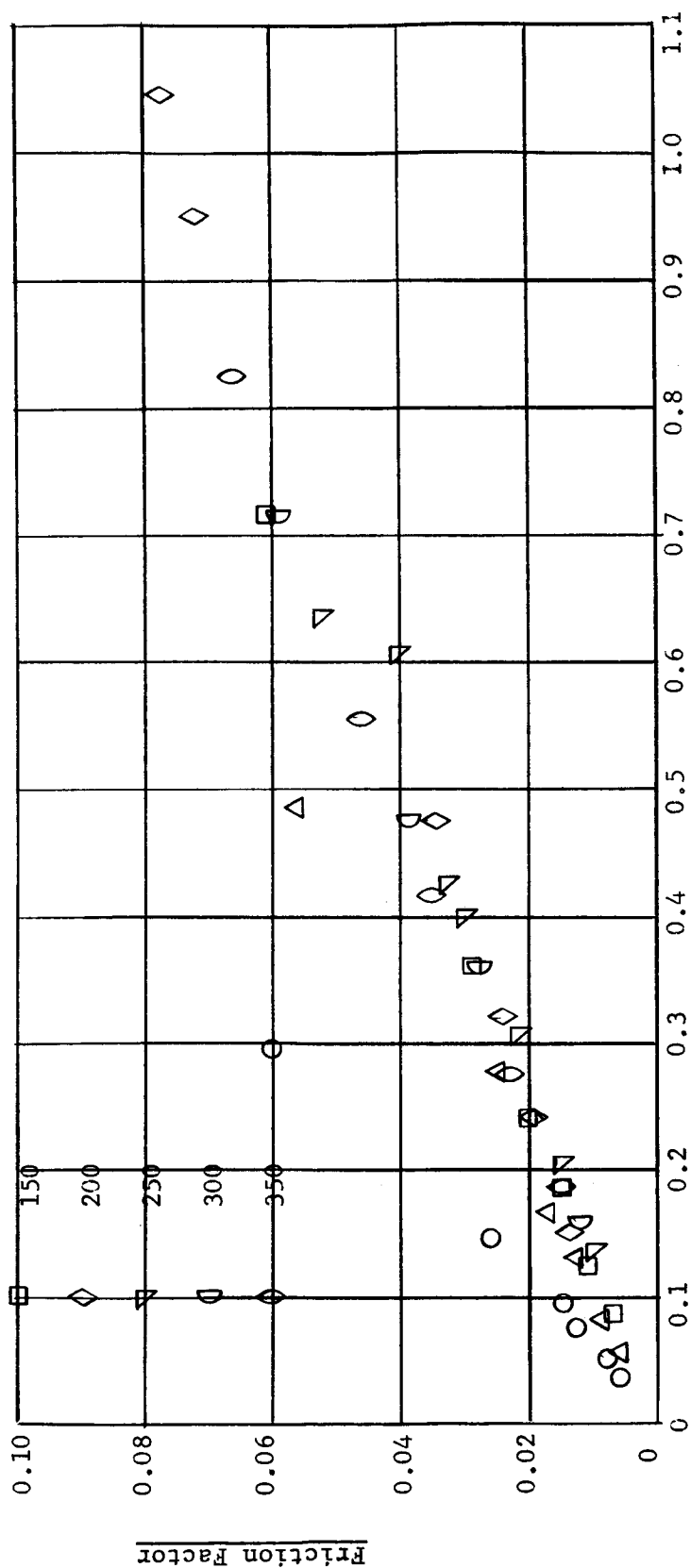


FIGURE 58 - SOMMERFELD NUMBER VS. FRICTION FACTOR

Test No. 18

2 Axial Groove L/D = 1.5
 2 Mil Nom. Diam. Clearance
 120°F Nom. Lube Temperature

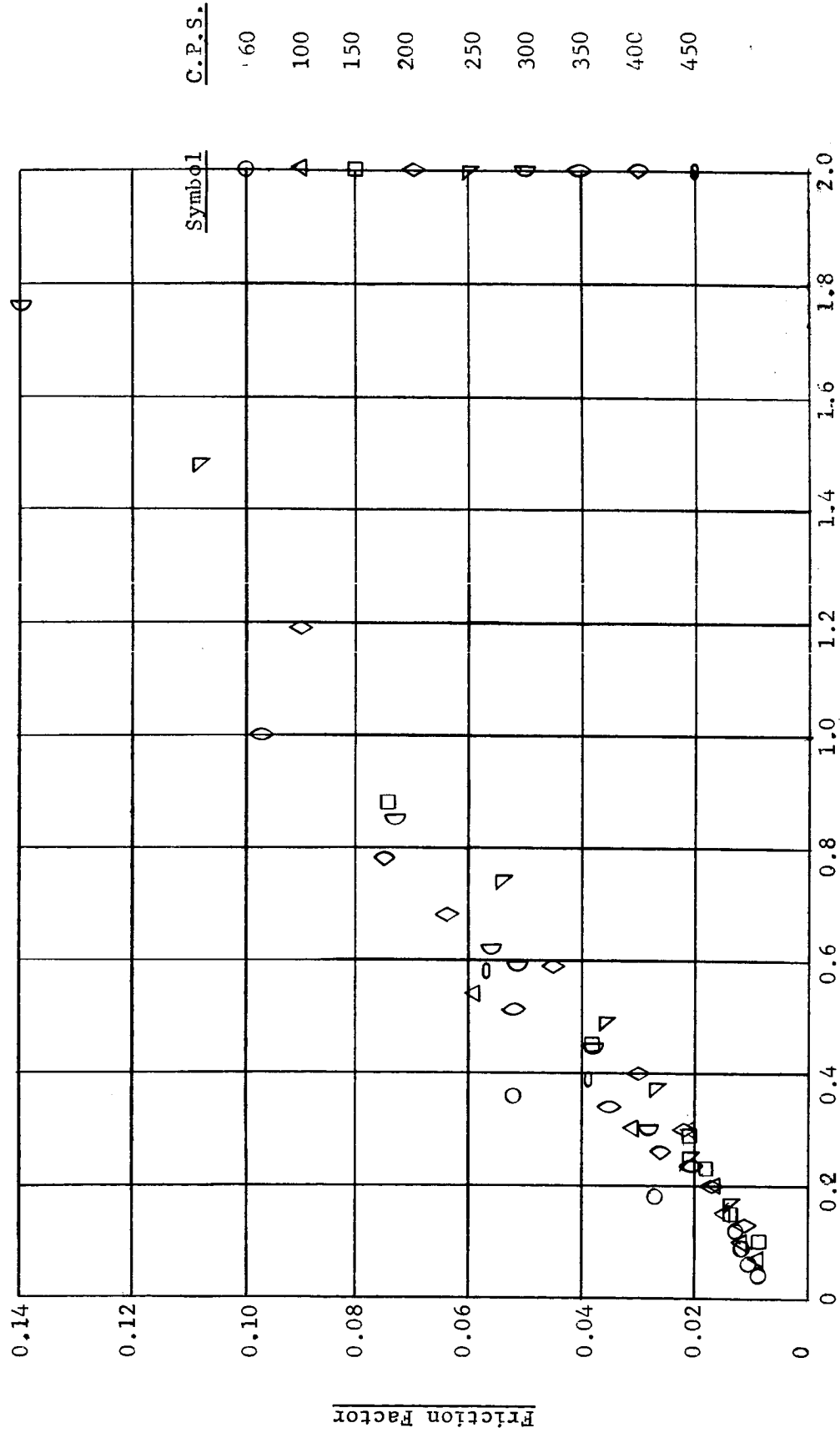
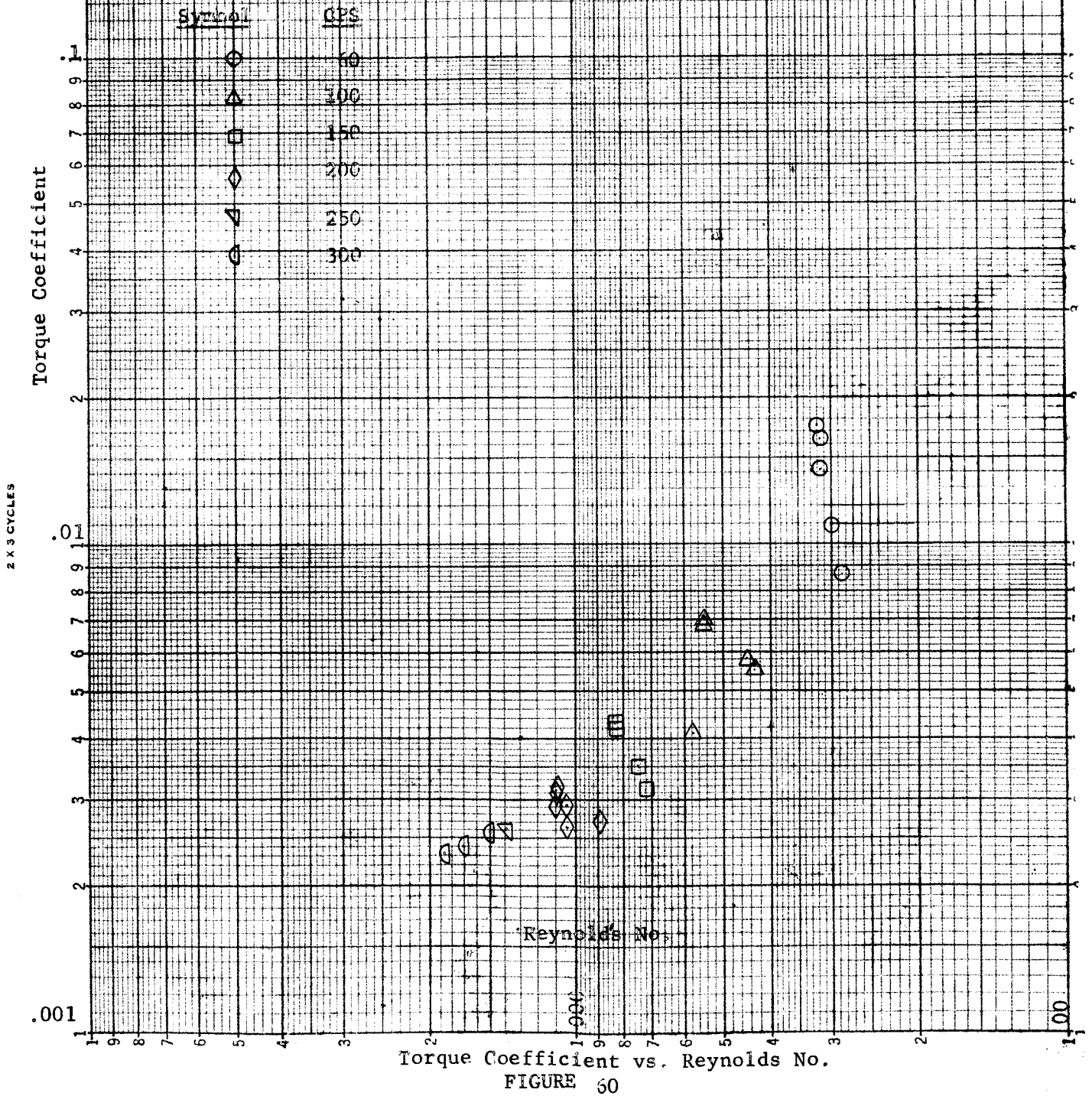


FIGURE 59 - SOMMERFELD NUMBER VS. FRICTION FACTOR

TEST NO. 1

2 Axial Groove L/D = 1
3 Mil Nom. Dia. Clearance
90°F Nom. Lube Temperature
Zero Unbalance

Figure 60



TEST NO. 2

2 Axial Groove L/D = 1
3 Mil Nom. Dia. Clearance
150°F Nom. Lube Temperature
Zero Unbalance

Figure 61

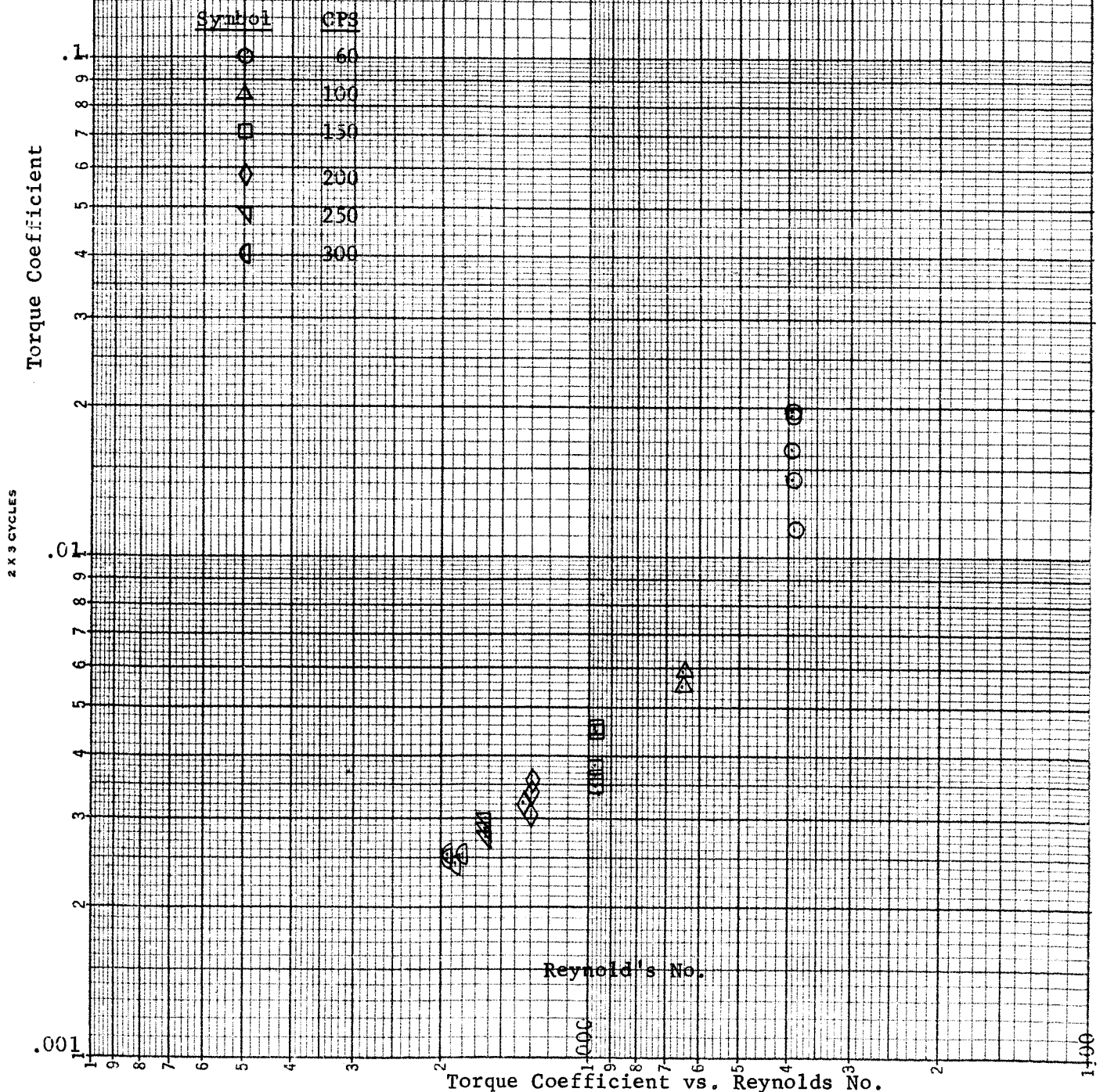


FIGURE 61

2 X 3 CYCLES

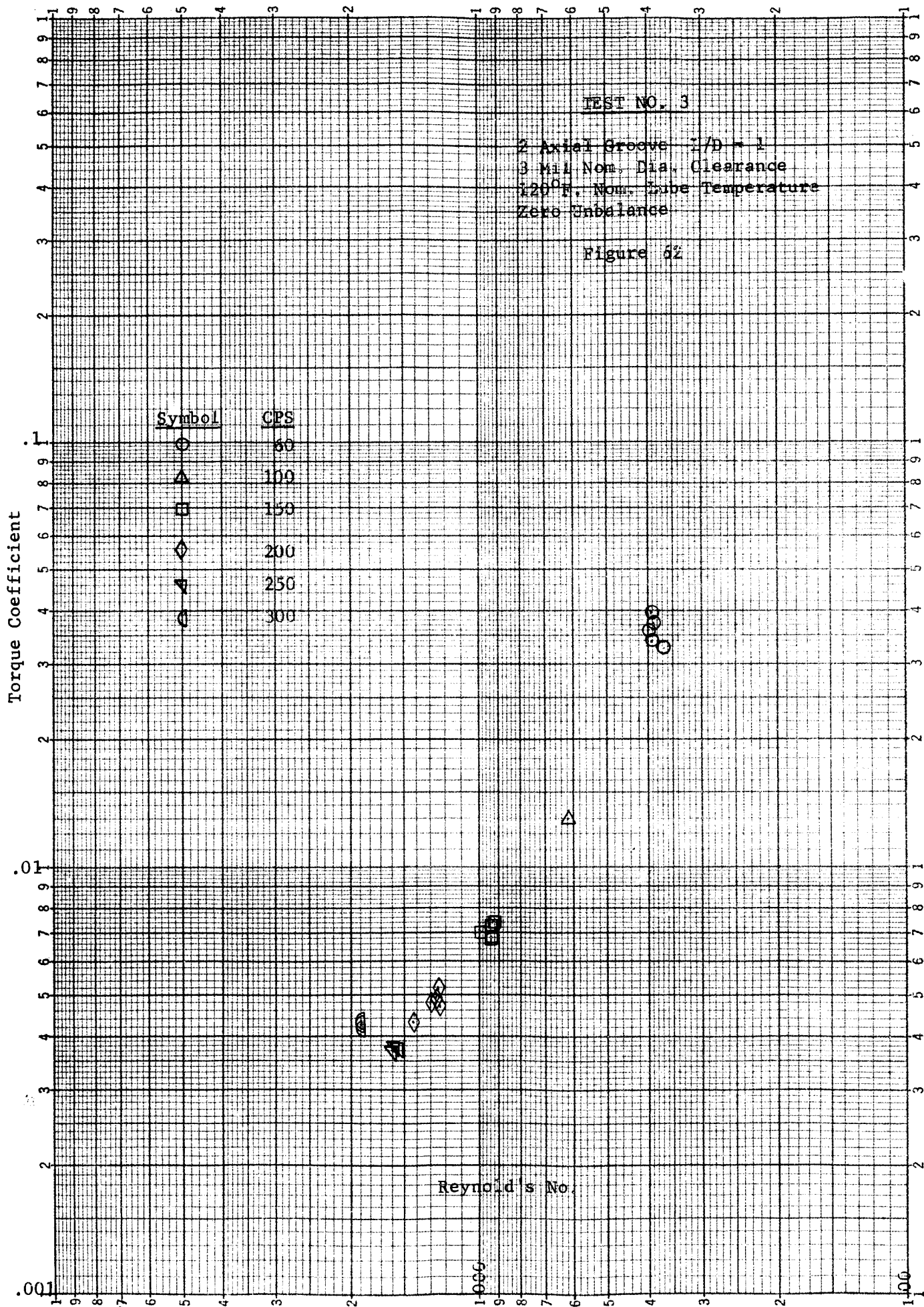


FIGURE 62

2 X 3 CYCLES

Torque Coefficient

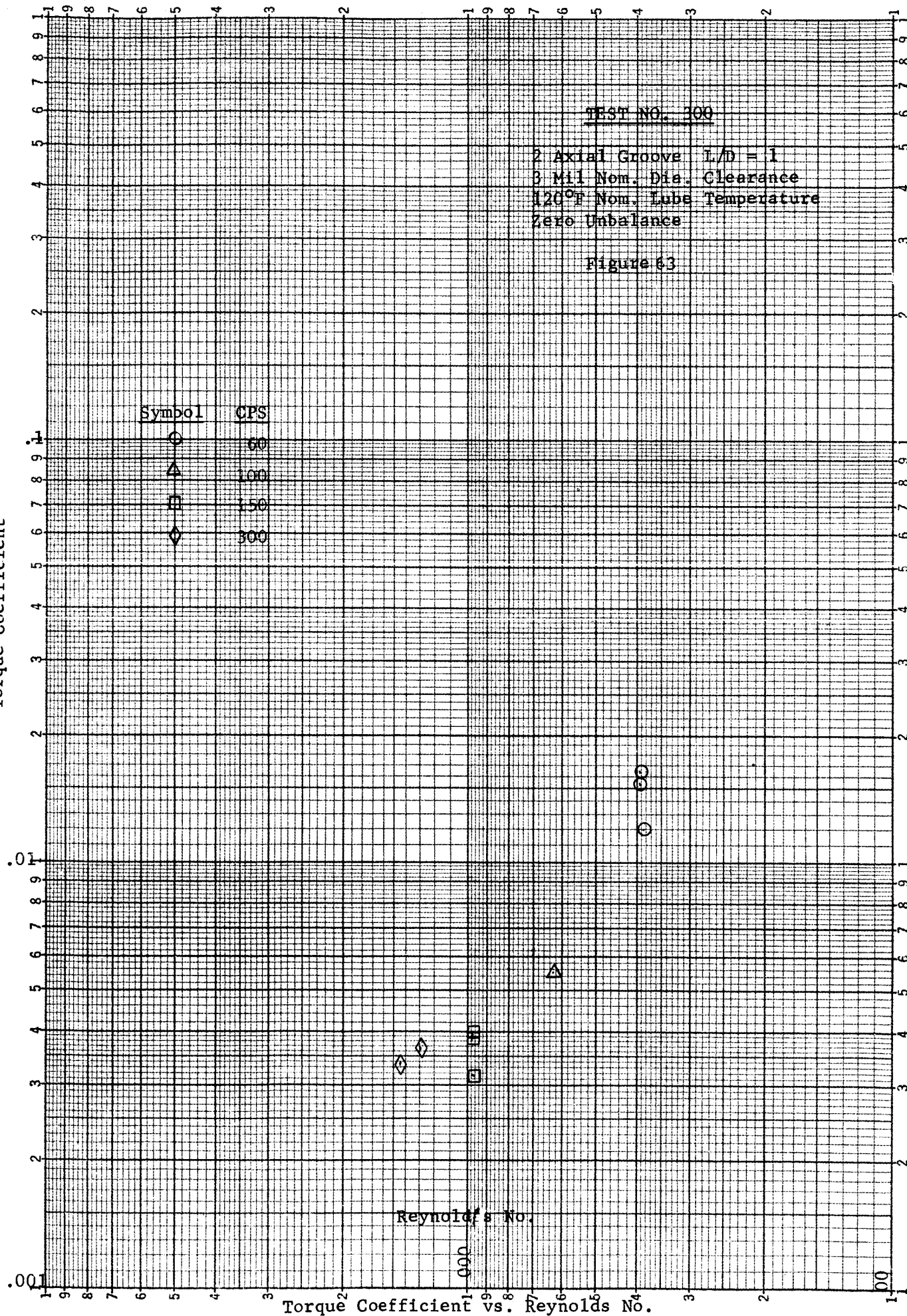


FIGURE 63

2 X 3 CYCLES

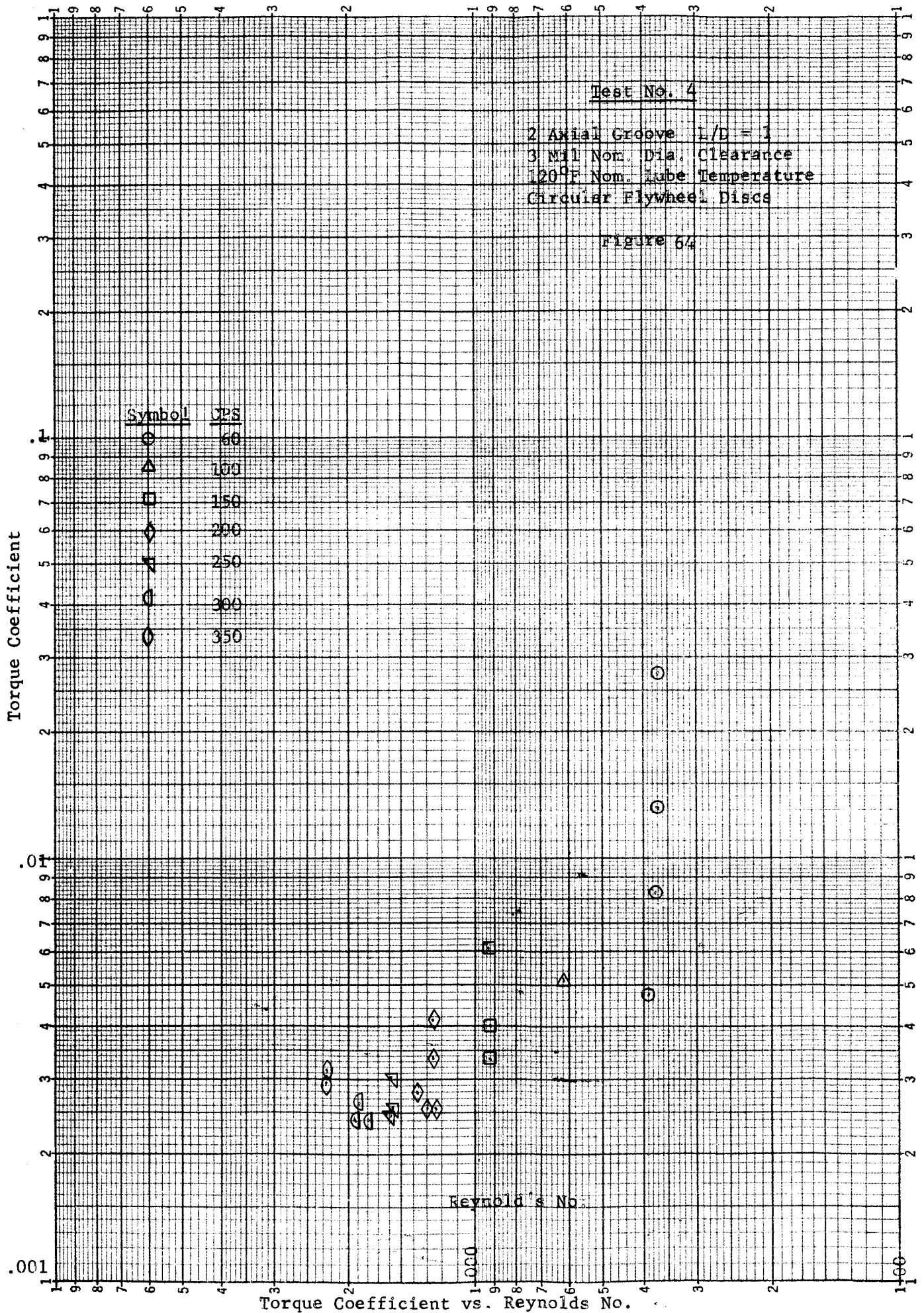


FIGURE 64

2 X 3 CYCLES

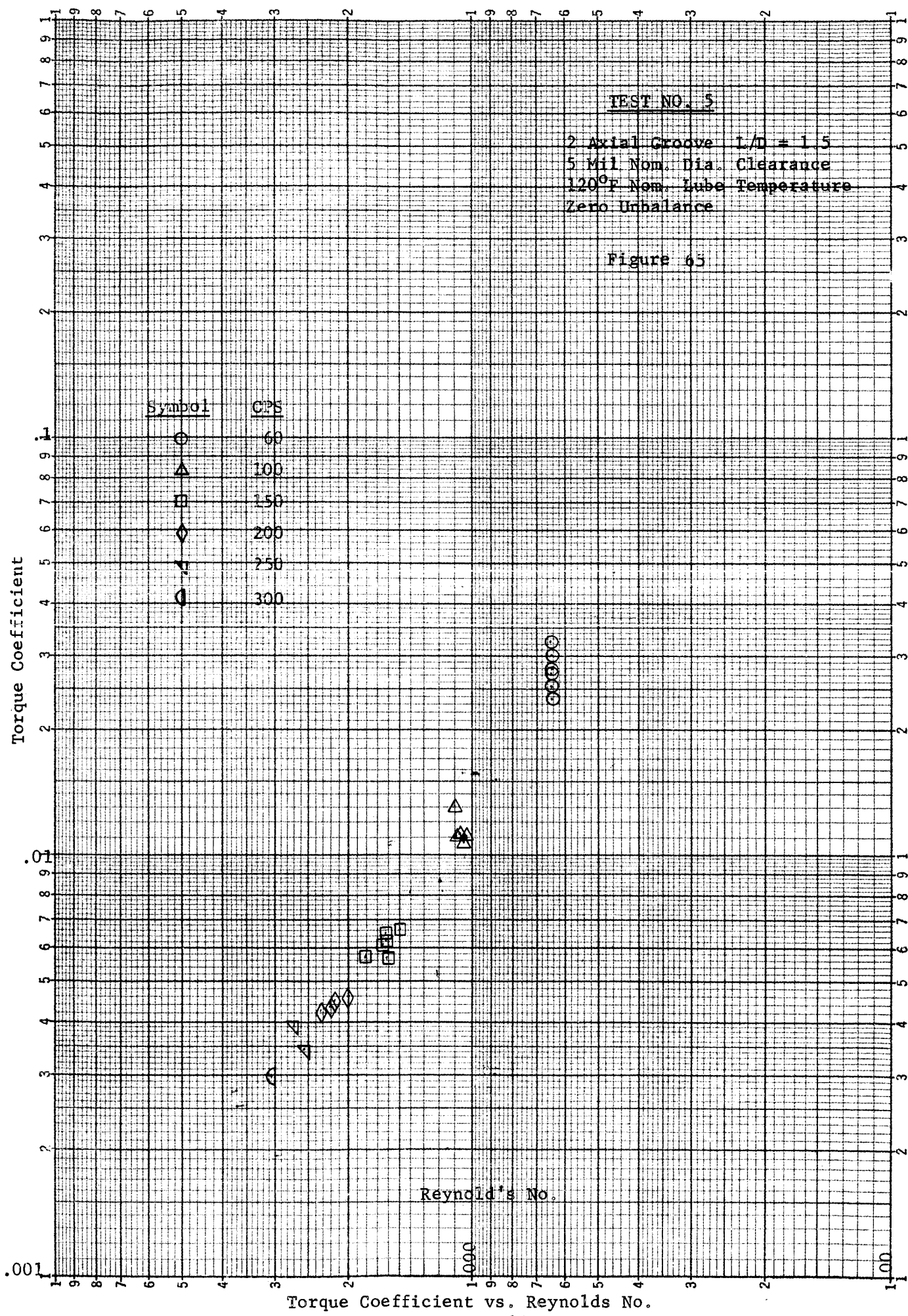


FIGURE 65

TEST NO. 501

2 Axial Groove L/D = 1.5
 5 Mil Nom. Dia. Clearance
 120°F Nom. Lube Temperature
 5° Unbalance

Figure 66

Torque Coefficient

2 X 3 CYCLES

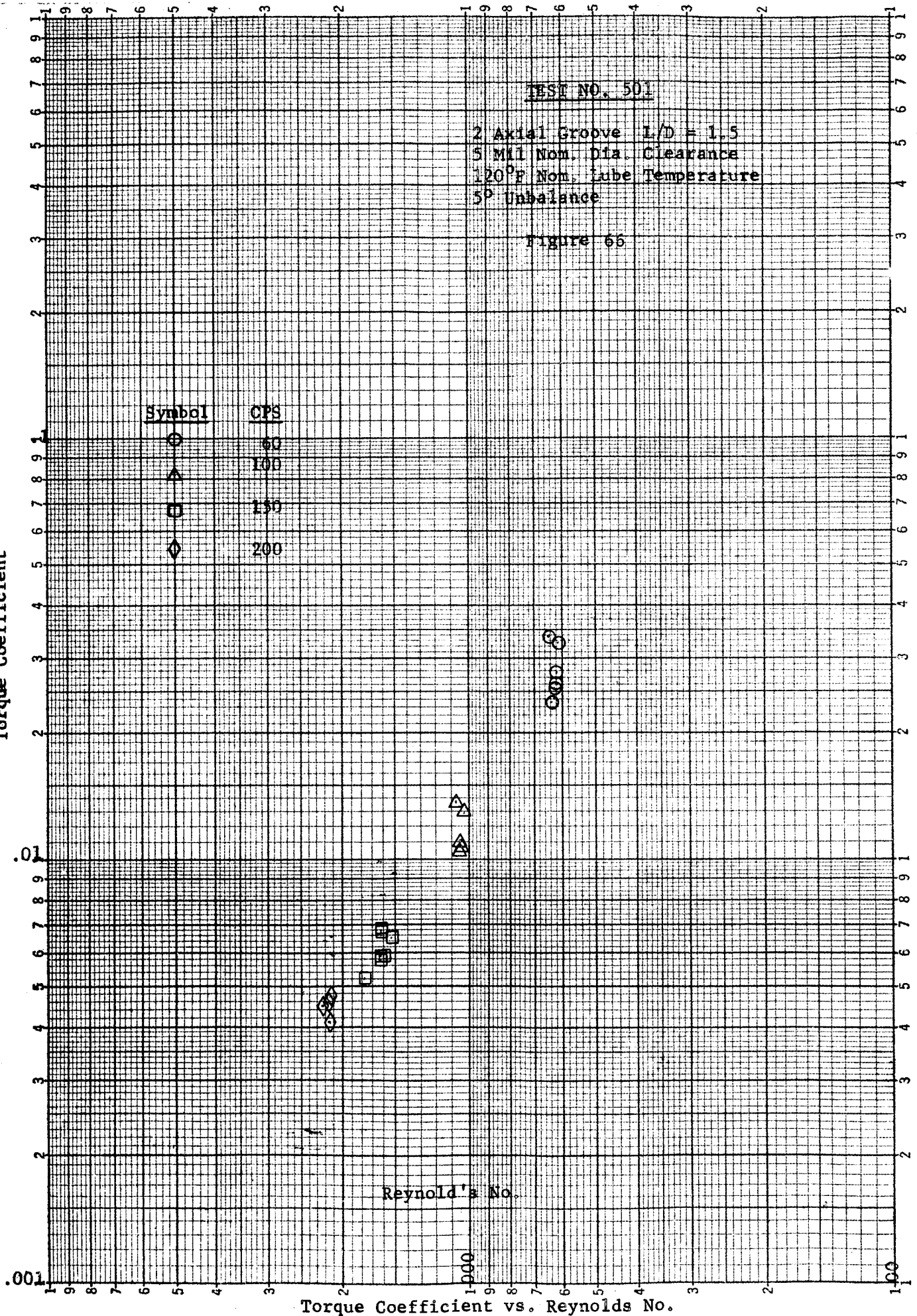
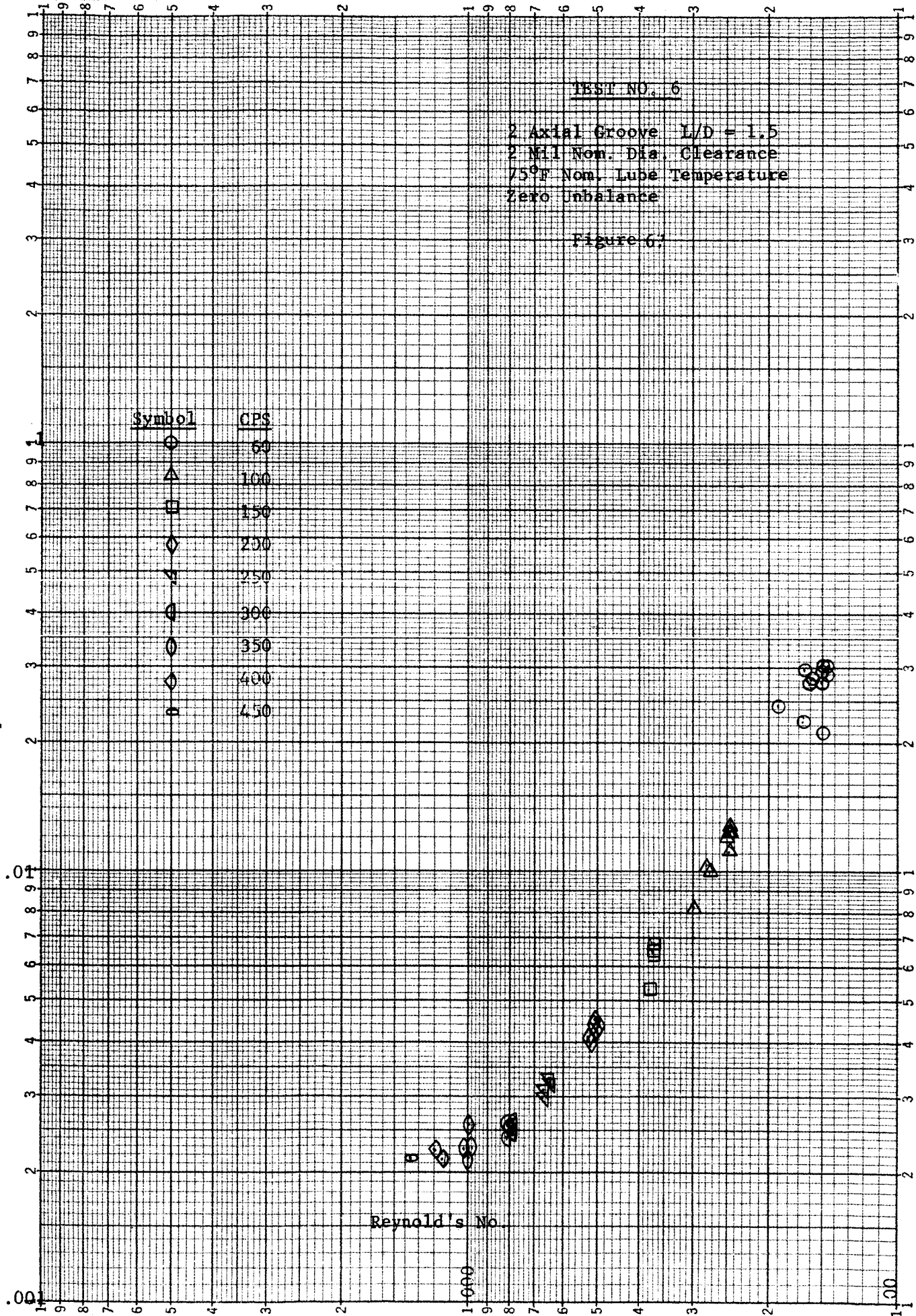


FIGURE 66

2 X 3 CYCLES

Torque Coefficient



Torque Coefficient vs. Reynolds No.

FIGURE 67

TEST NO. 600

2 Axial Groove L/D = 1.5
 2 Mil Nom. Dia. Clearance
 75°F Nom. Lube Temperature
 Zero Unbalance
 70 PSIG Lube Inlet Pressure

Figure 68

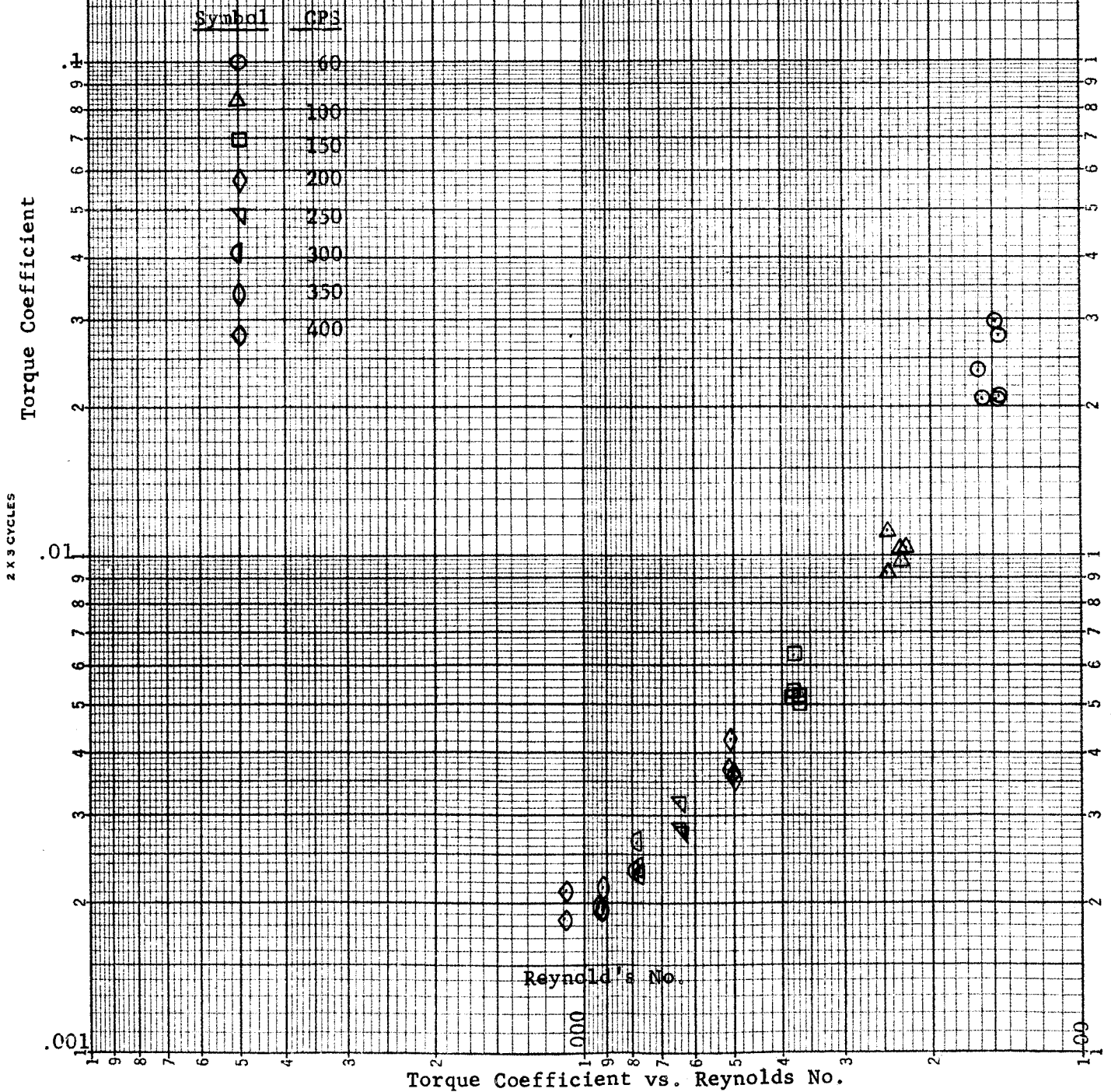


FIGURE 68

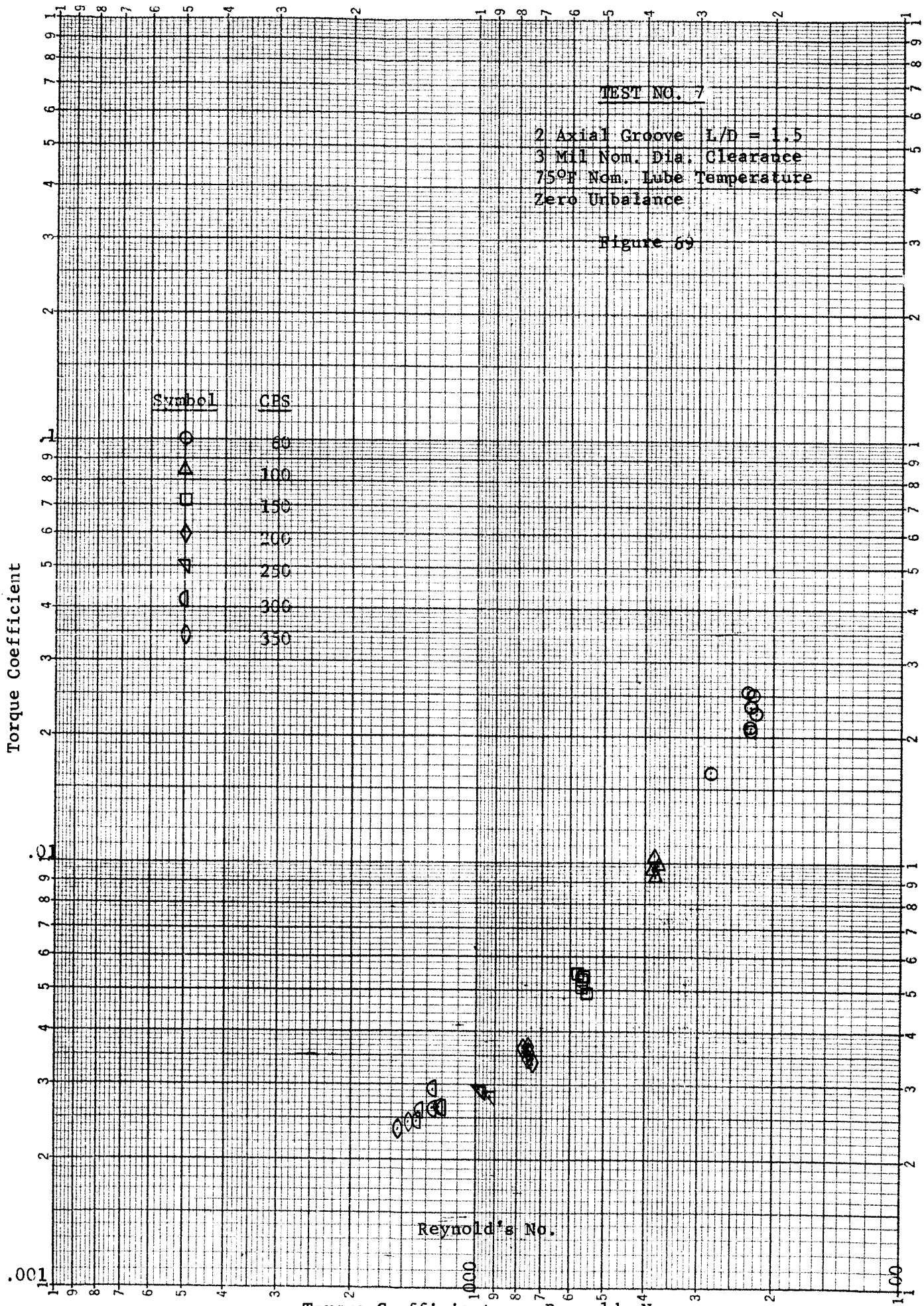
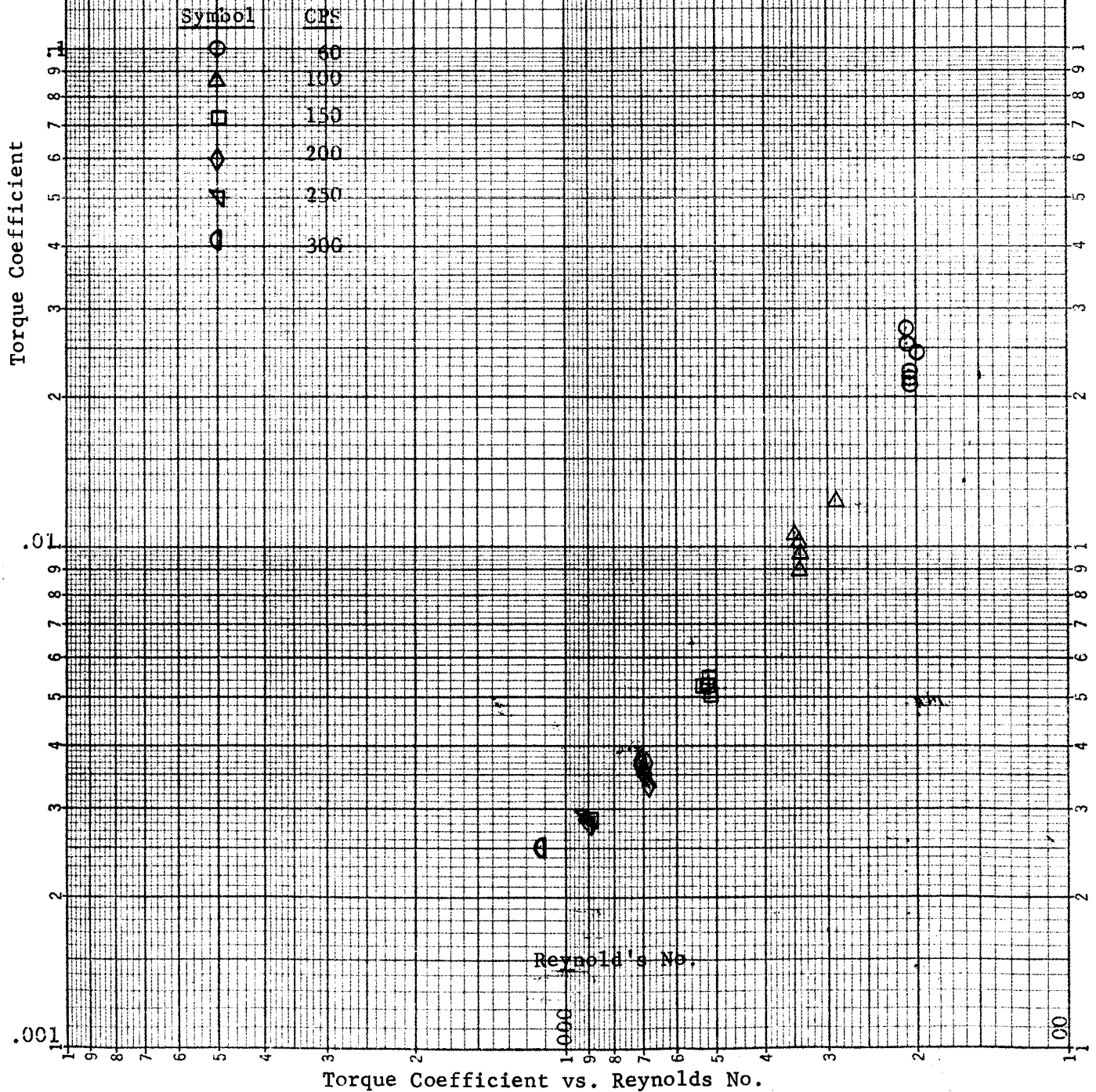


FIGURE 69

TEST NO. 701

2 Axial Groove L/D = 1.5
 3 Mil Nom. Dia. Clearance
 75° Nom. Lube Temperature
 10° Unbalance

Figure 70



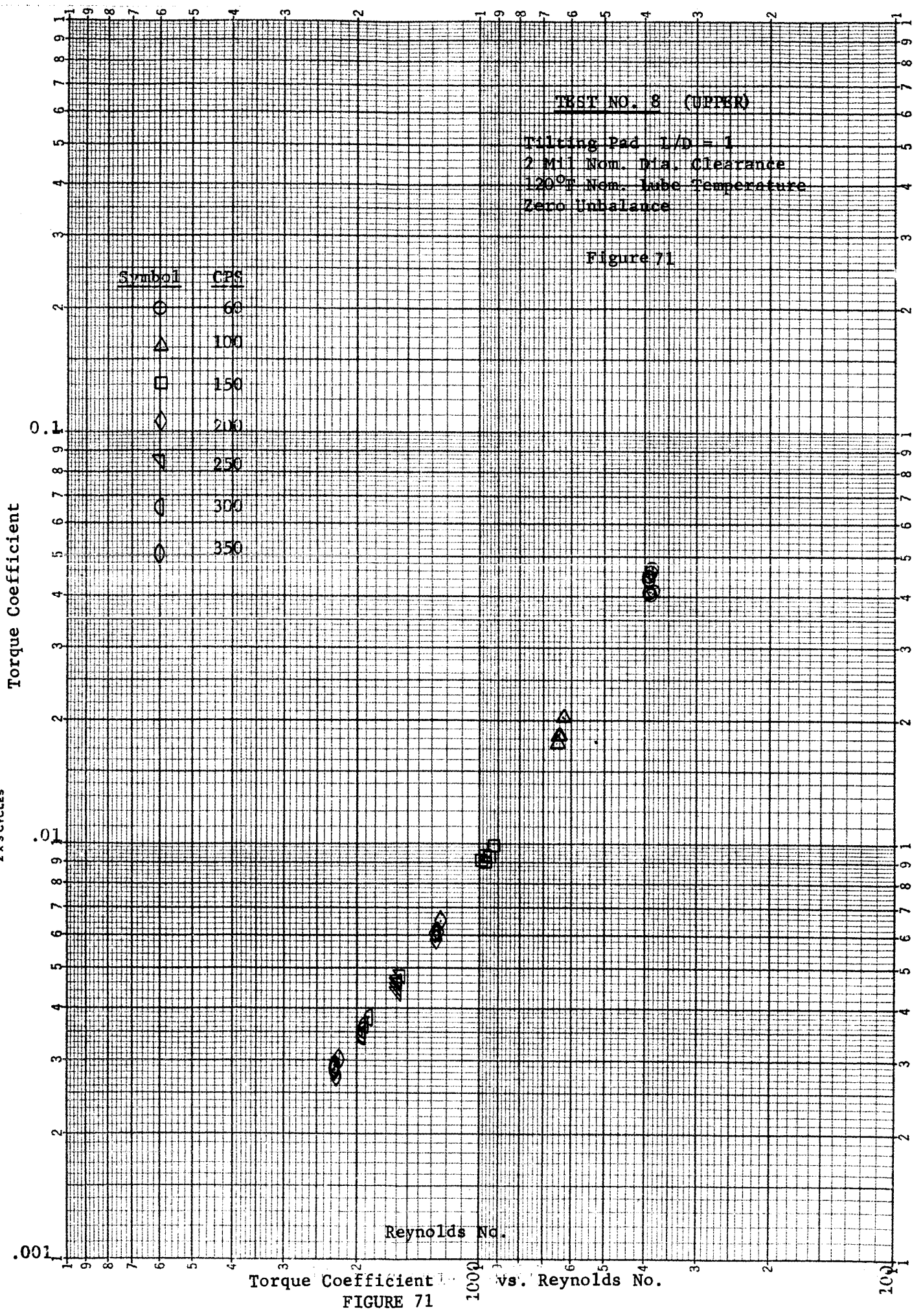
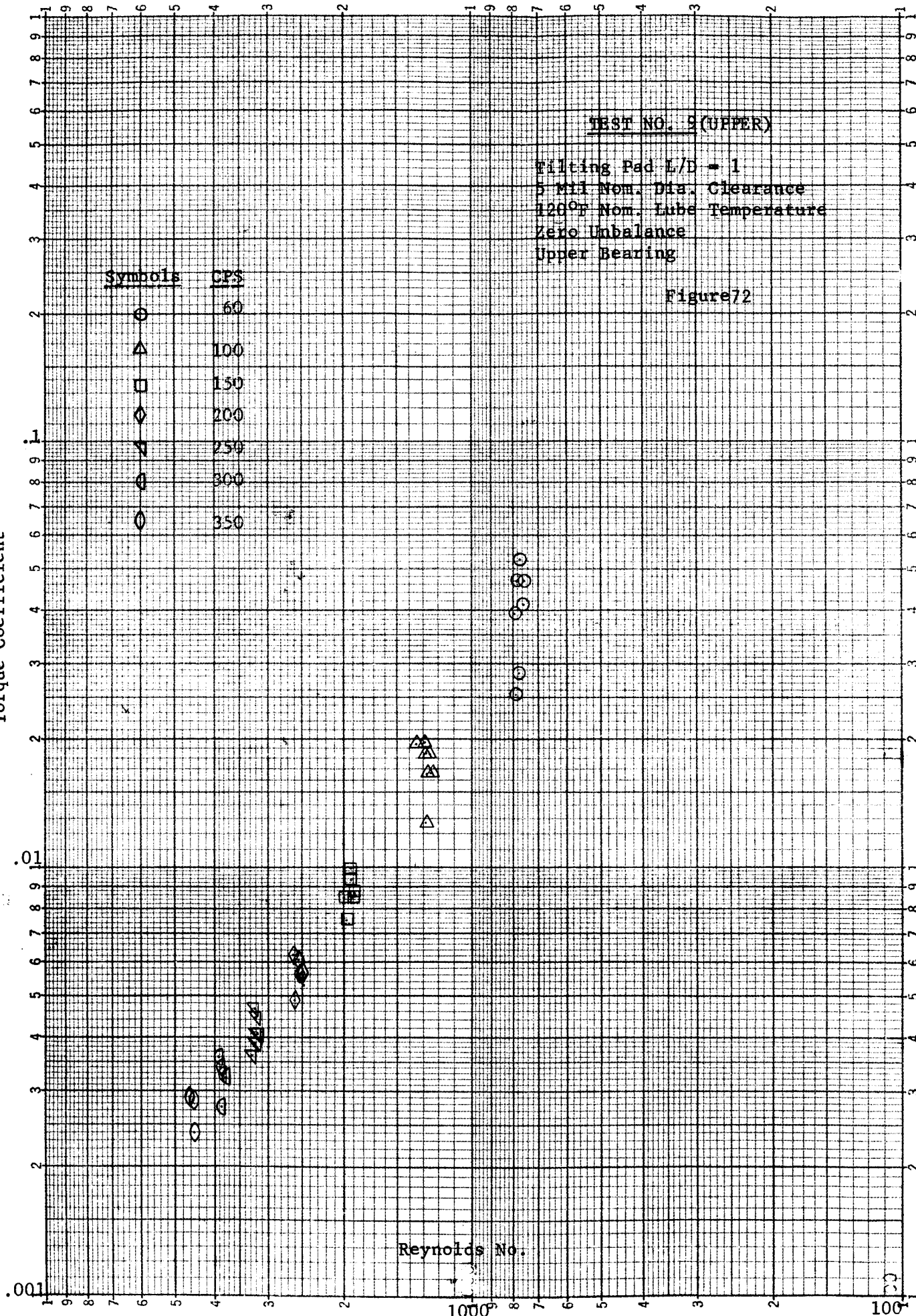


FIGURE 71

2 X 3 CYCLES

Torque Coefficient



Torque Coefficient vs. Reynolds No.

FIGURE 72

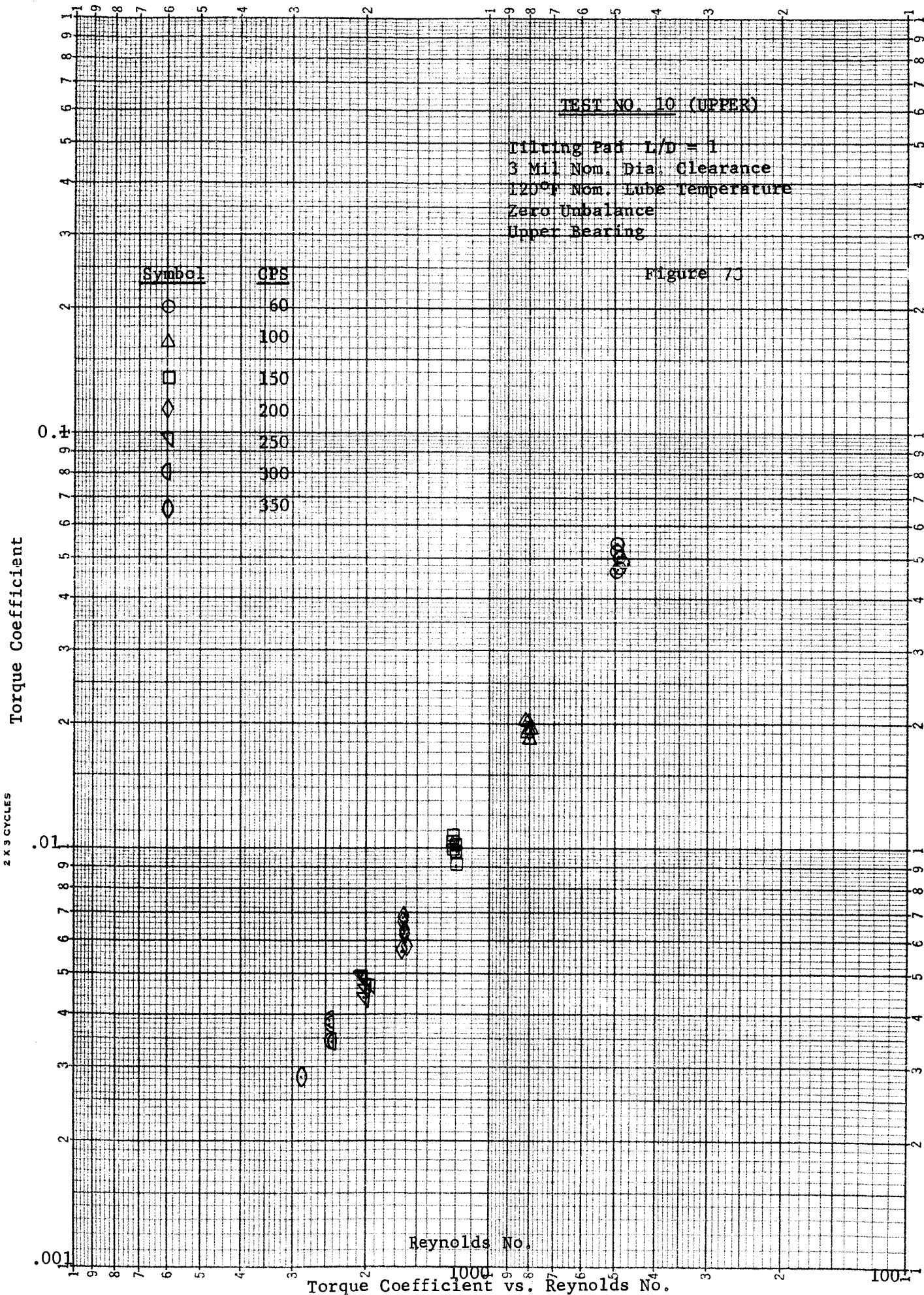
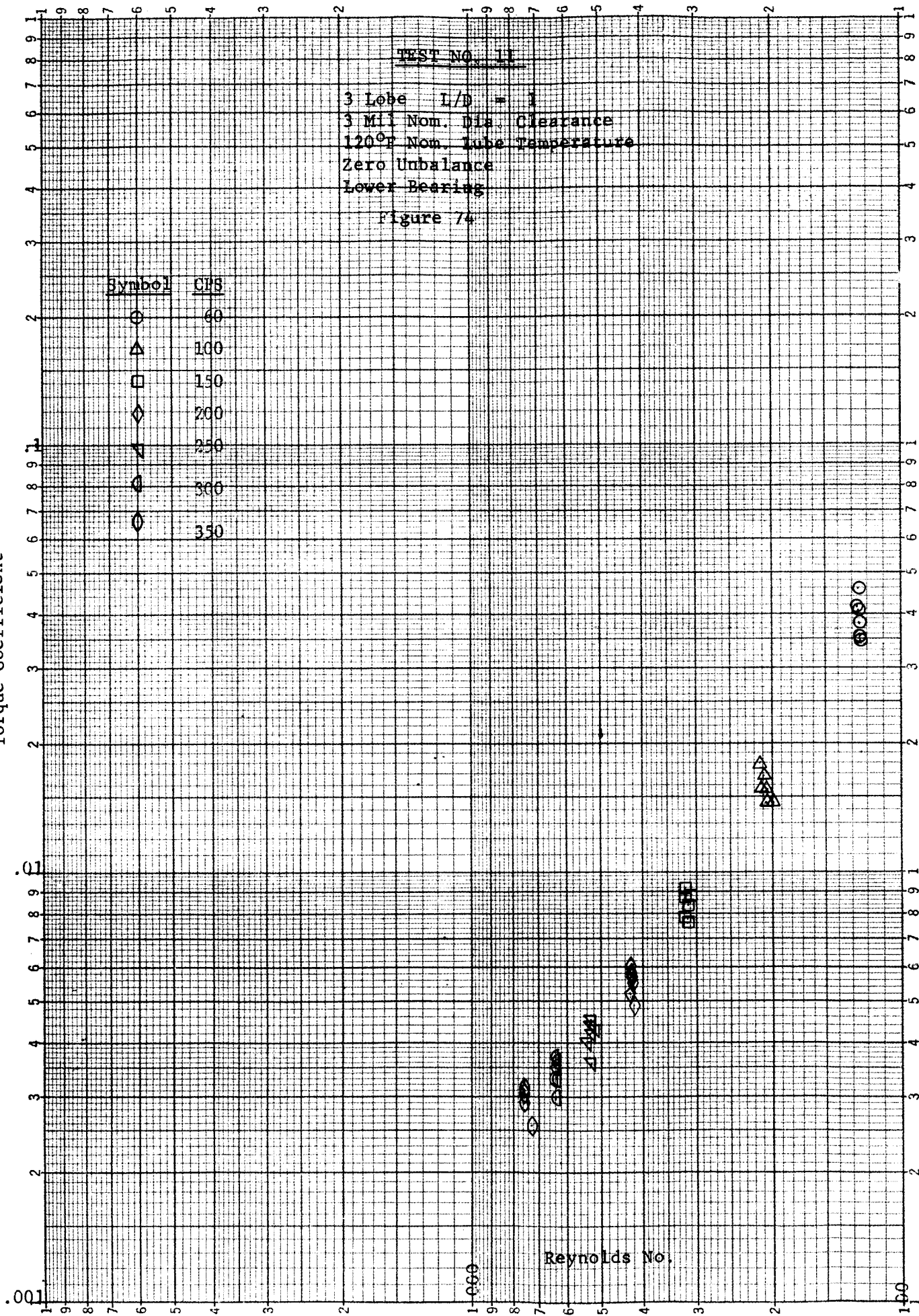


FIGURE 73

2 X 3 CYCLES

Torque Coefficient

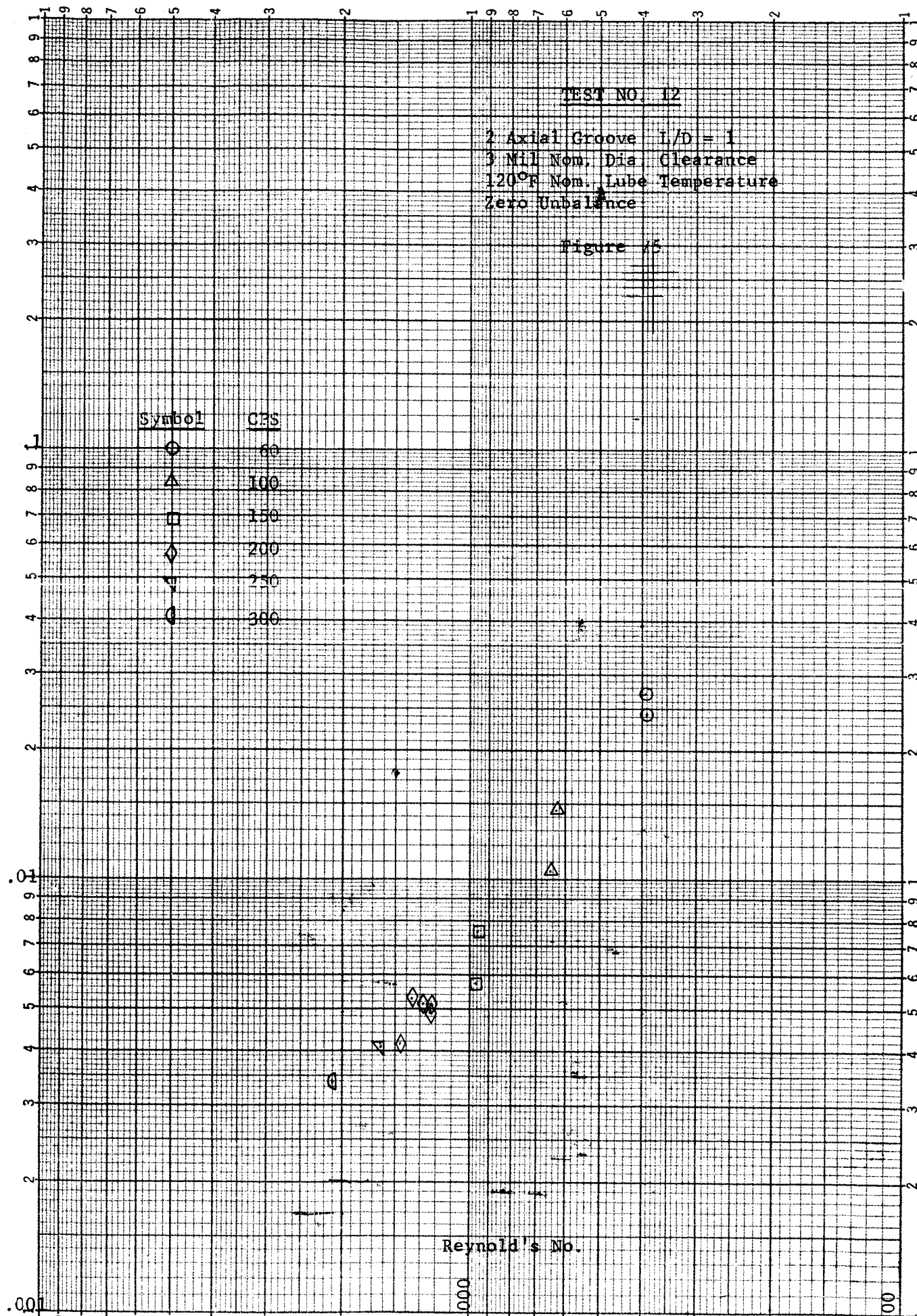


Torque Coefficient vs. Reynolds No.

FIGURE 74

2 X 3 CYCLES

Torque Coefficient



Torque Coefficient vs. Reynolds No.

FIGURE 75

Torque Coefficient

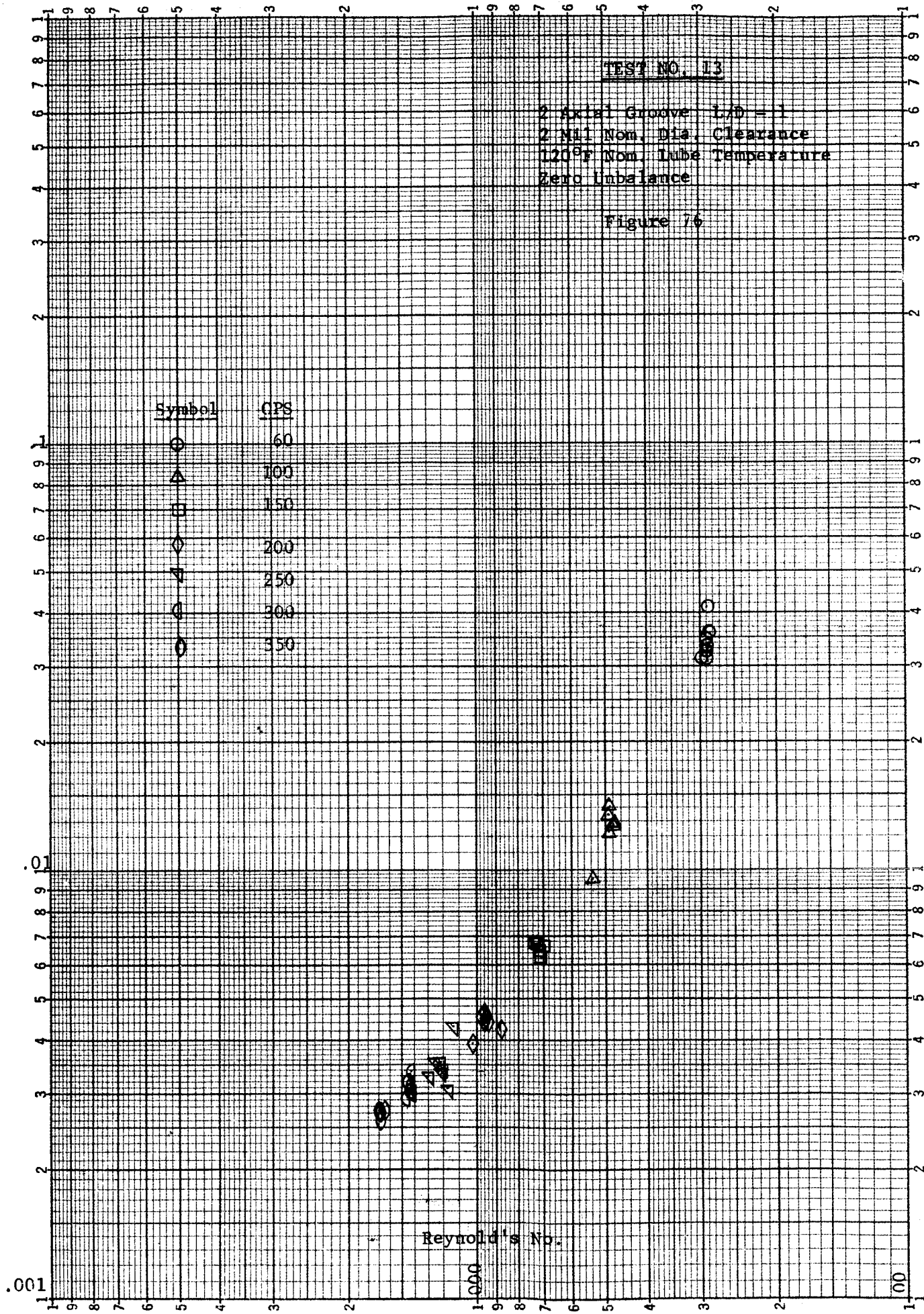
2 X 3 CYCLES

TEST NO. 13

2 Sided Groove L/D = 1
2 MIL Nom. Dia. Clearance
120°F Nom. Lube Temperature
Zero Unbalance

Figure 76

Symbol	CPS
⊕	60
△	100
⊞	150
◇	200
◊	250
○	300
○	350



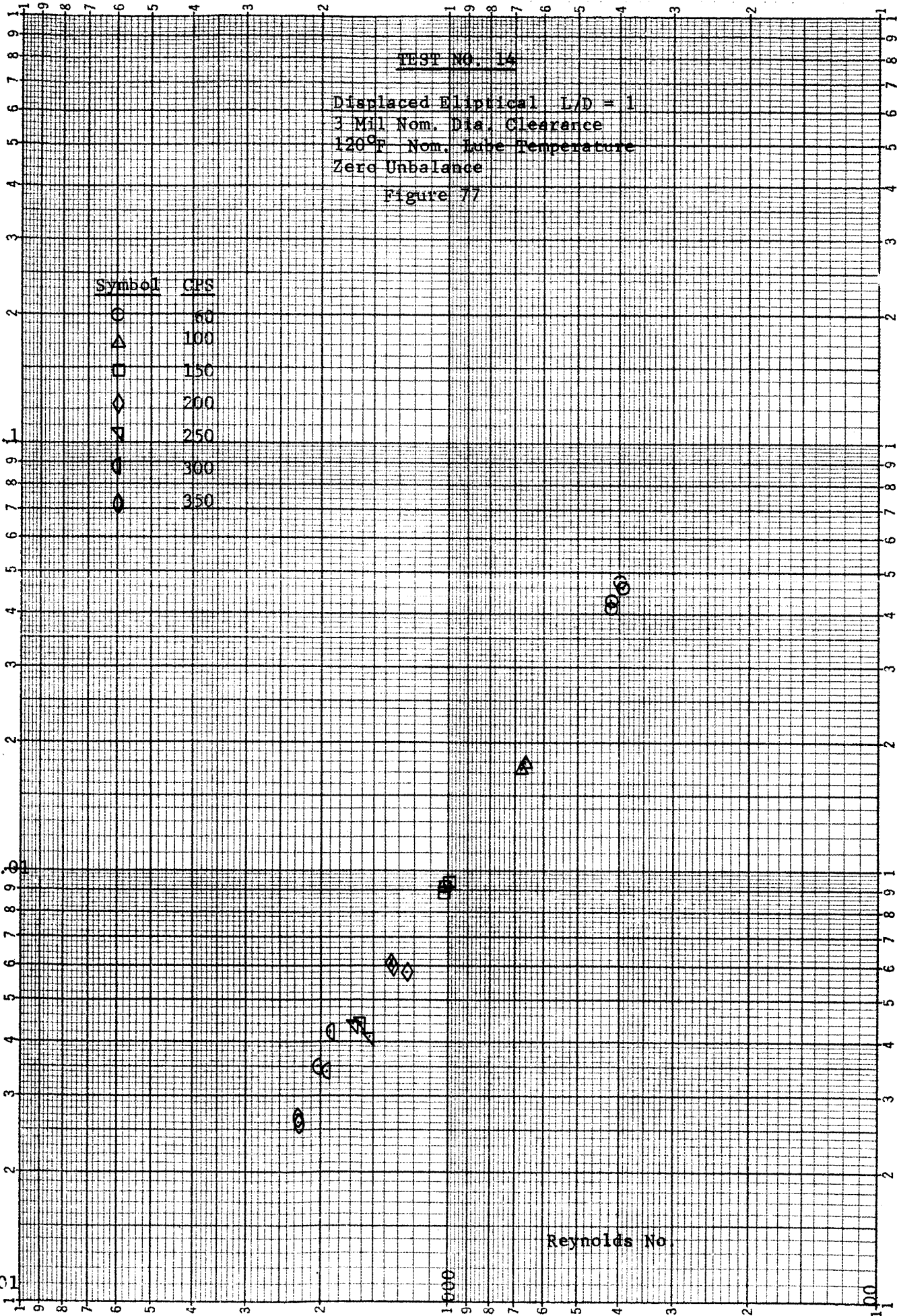
Torque Coefficient vs. Reynolds No.

FIGURE 76

2 X 3 CYCLES

Torque Coefficient

.001



Torque Coefficient vs. Reynolds No.

FIGURE 77

TEST NO. 15

Displaced Elliptical $L/D = 1$
 3 Mil Nom. Dia. Clearance
 120°F Nom. Lube Temperature
 Zero Unbalance
 Upper Bearing
 Figure 78

Symbol	CPS
○	50
△	100
□	150
◇	200
▽	250
⊙	300
⊕	350
⊗	400

Torque Coefficient

2 X 3 CYCLES

.001

Torque Coefficient vs. Reynolds No.

FIGURE 78

Reynolds No.

100

1000

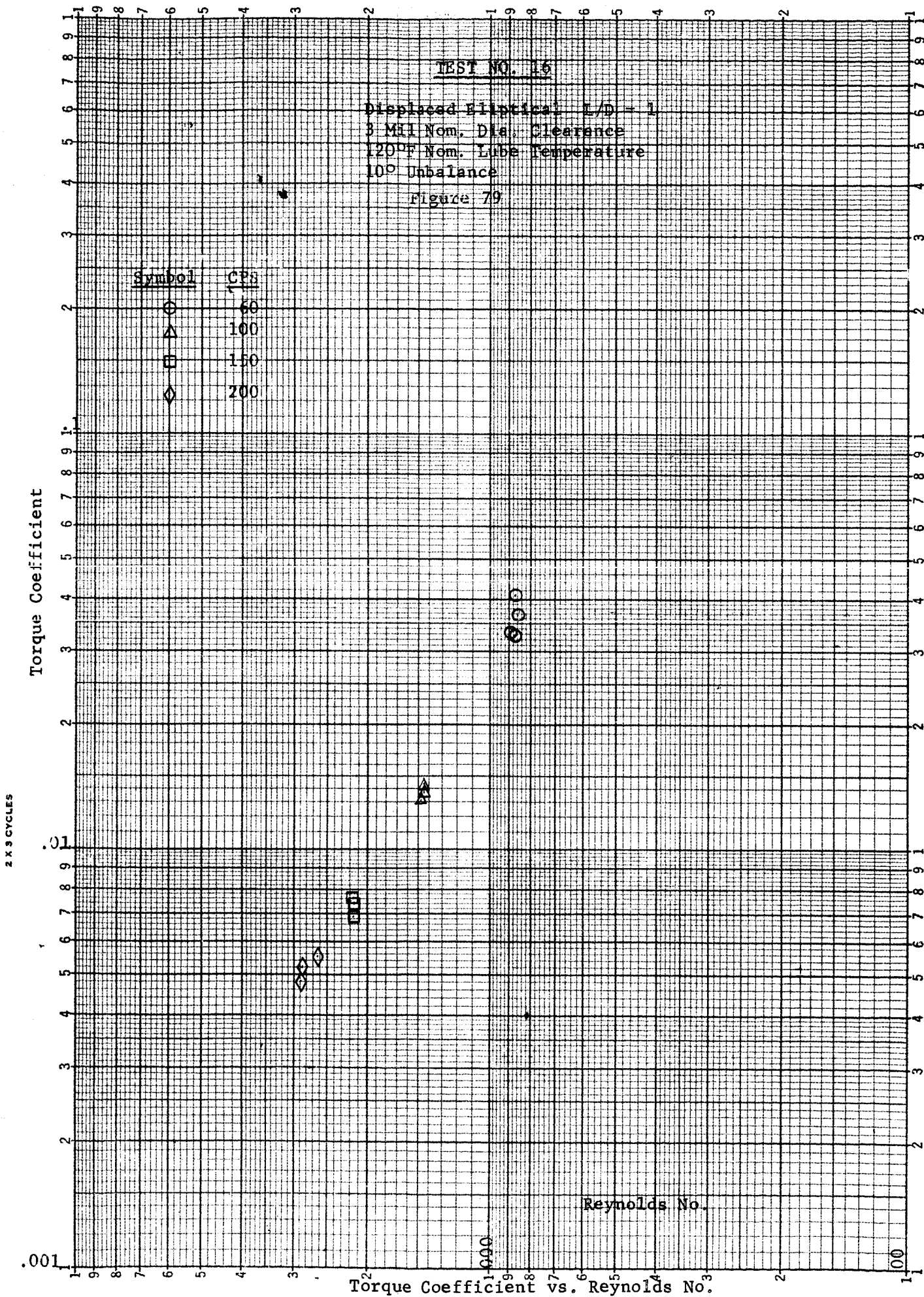


FIGURE 79

TEST NO. 17

Displaced Elliptical $L/D = 1$
 5 Mil. Nom. Dia. Clearance
 120°F Nom. Tube Temperature
 Zero Unbalance

Figure 80

2 X 3 CYCLES

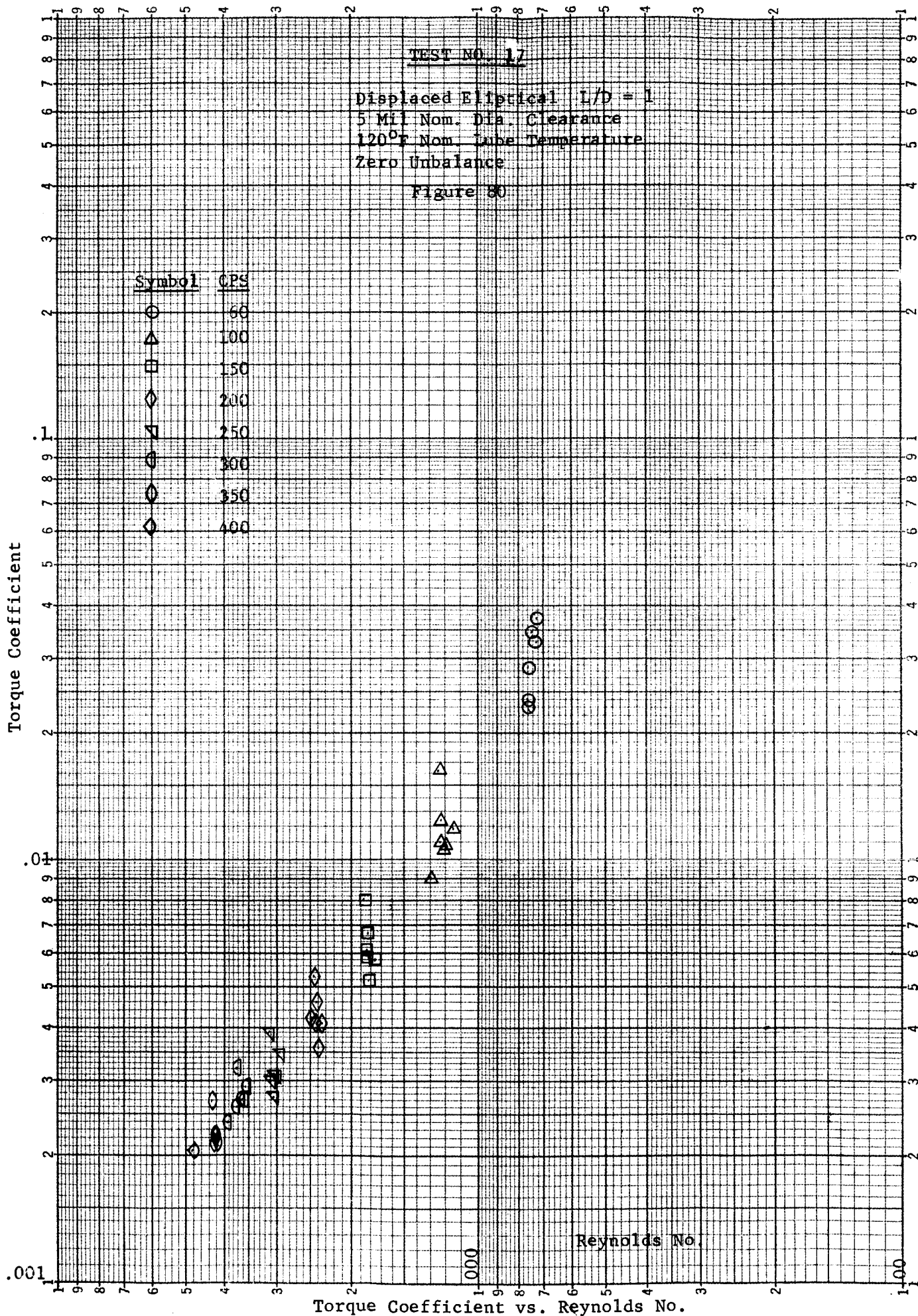


FIGURE 80

2 X 3 CYCLES

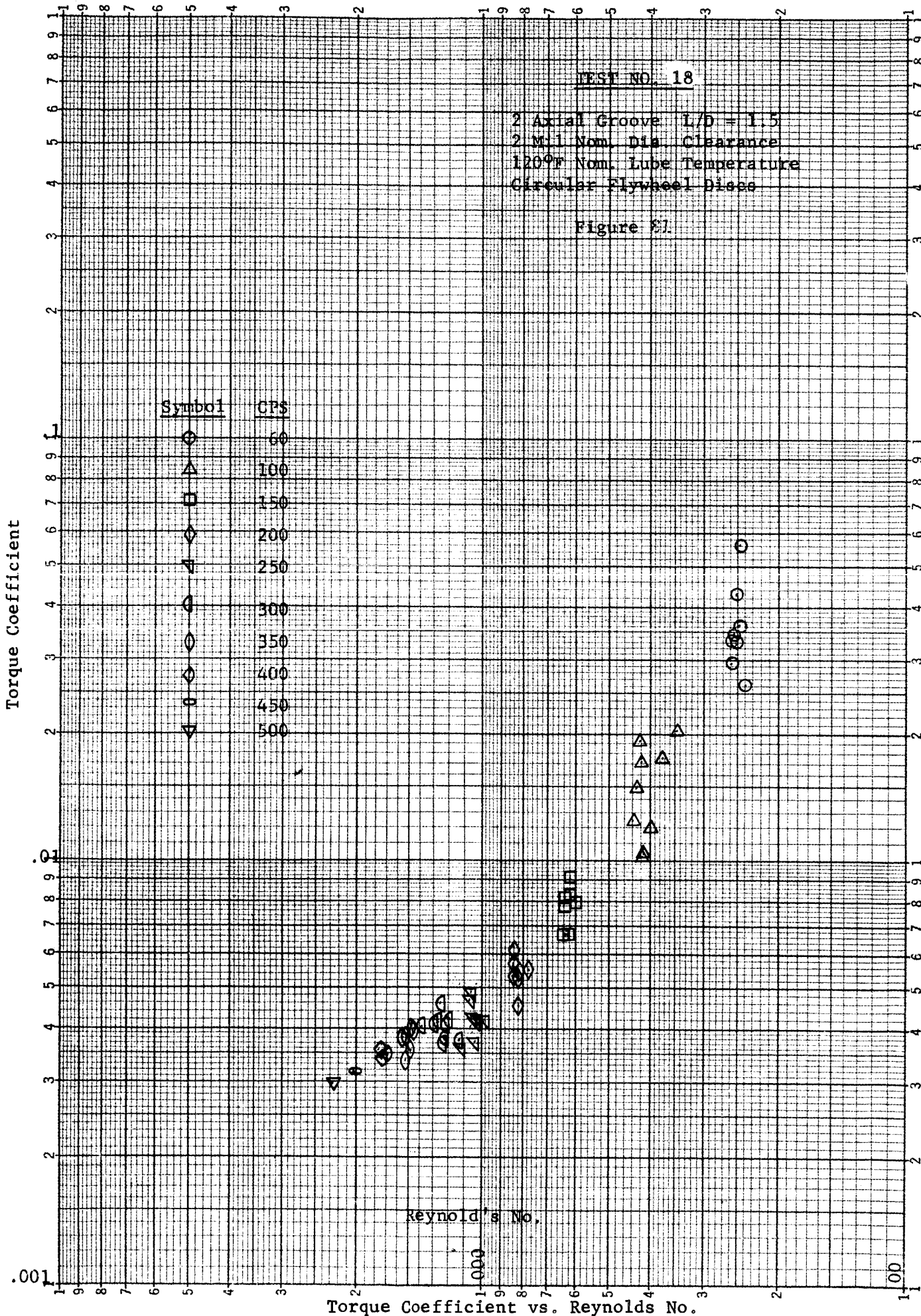


FIGURE 81

Torque Coefficient

2 X 3 CYCLES

TEST NO. 19

2 Axial Groove $L/D = 1.5$
 2 Mil Non. Dia. Clearance
 120°F Non. Lube Temperature
 Zero Unbalance
 Heavy Central Mass Shaft

Figure 82

Symbol	CPS
○	60
△	100
□	150
◇	200
▽	250
○	300
◇	350
◇	400

Reynold's No.

Torque Coefficient vs. Reynolds No.

FIGURE 82

Test No. 3

2 Axial Groove L/D =1
 3 Mil Nom. Diam. Clearance
 120°F Nom. Lube Temperature

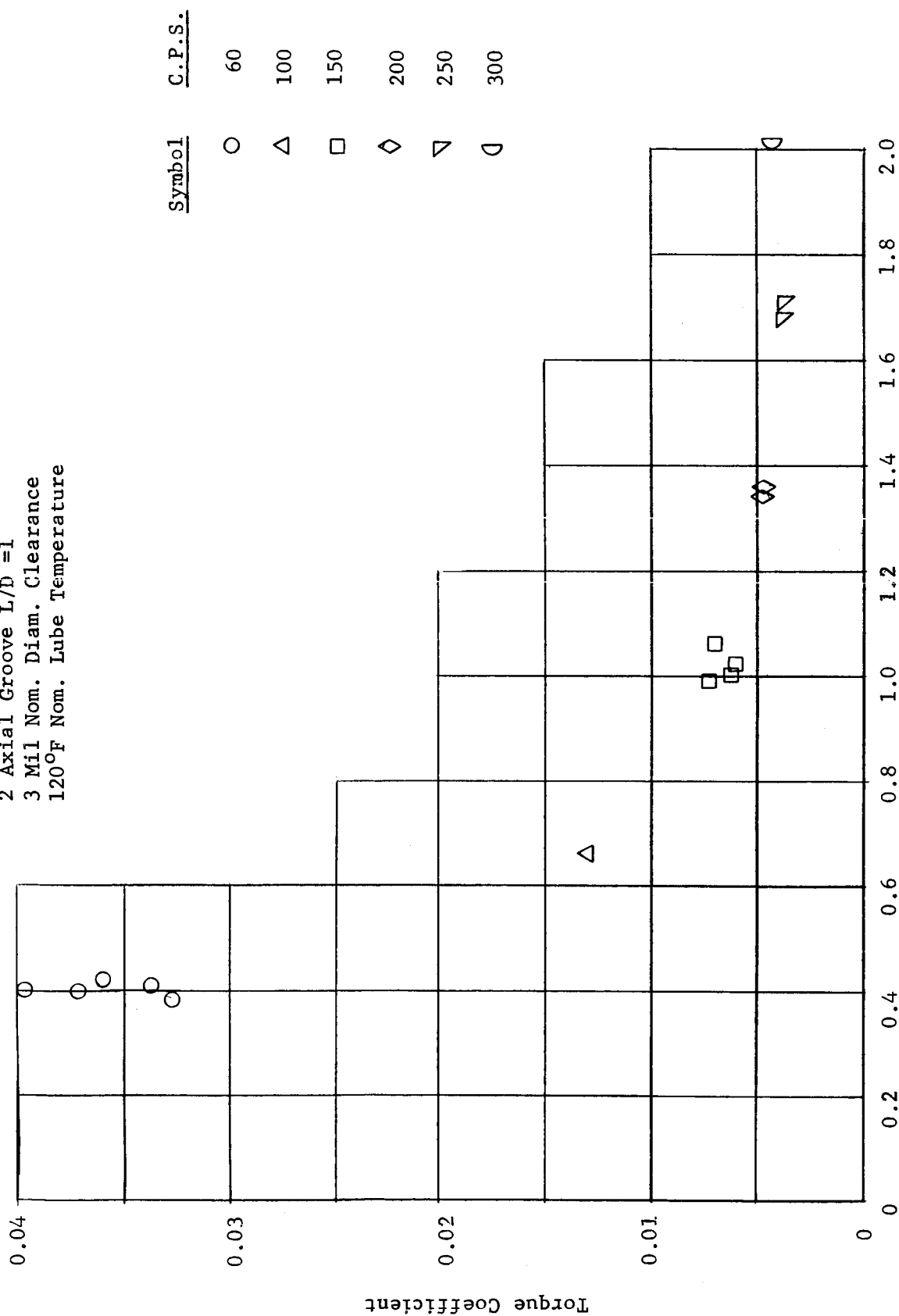


FIGURE 83 - REYNOLDS NO. RATIO VS. TORQUE COEFFICIENT

Test No. 300

2 Axial Groove L/D = 1
 3 Mil Nom. Diam. Clearance
 120°F Nom. Lube Temperature

○

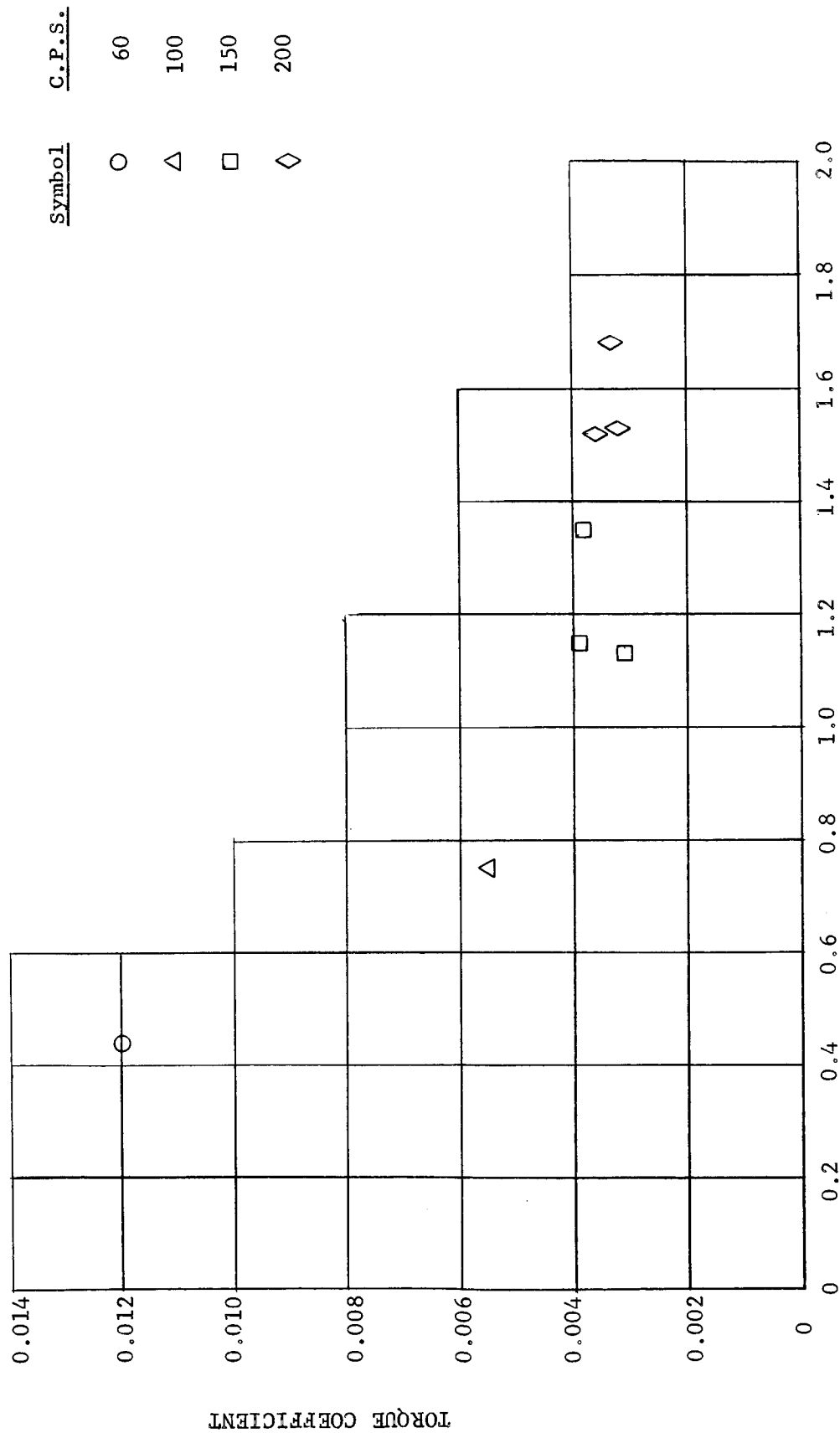


FIGURE 84 - REYNOLDS NO. RATIO VS. TORQUE COEFFICIENT

Test No. 301

2 Axial Groove L/D = 1
 3 Mil Nom. Diam. Clearance
 120°F Nom. Lube Temperature

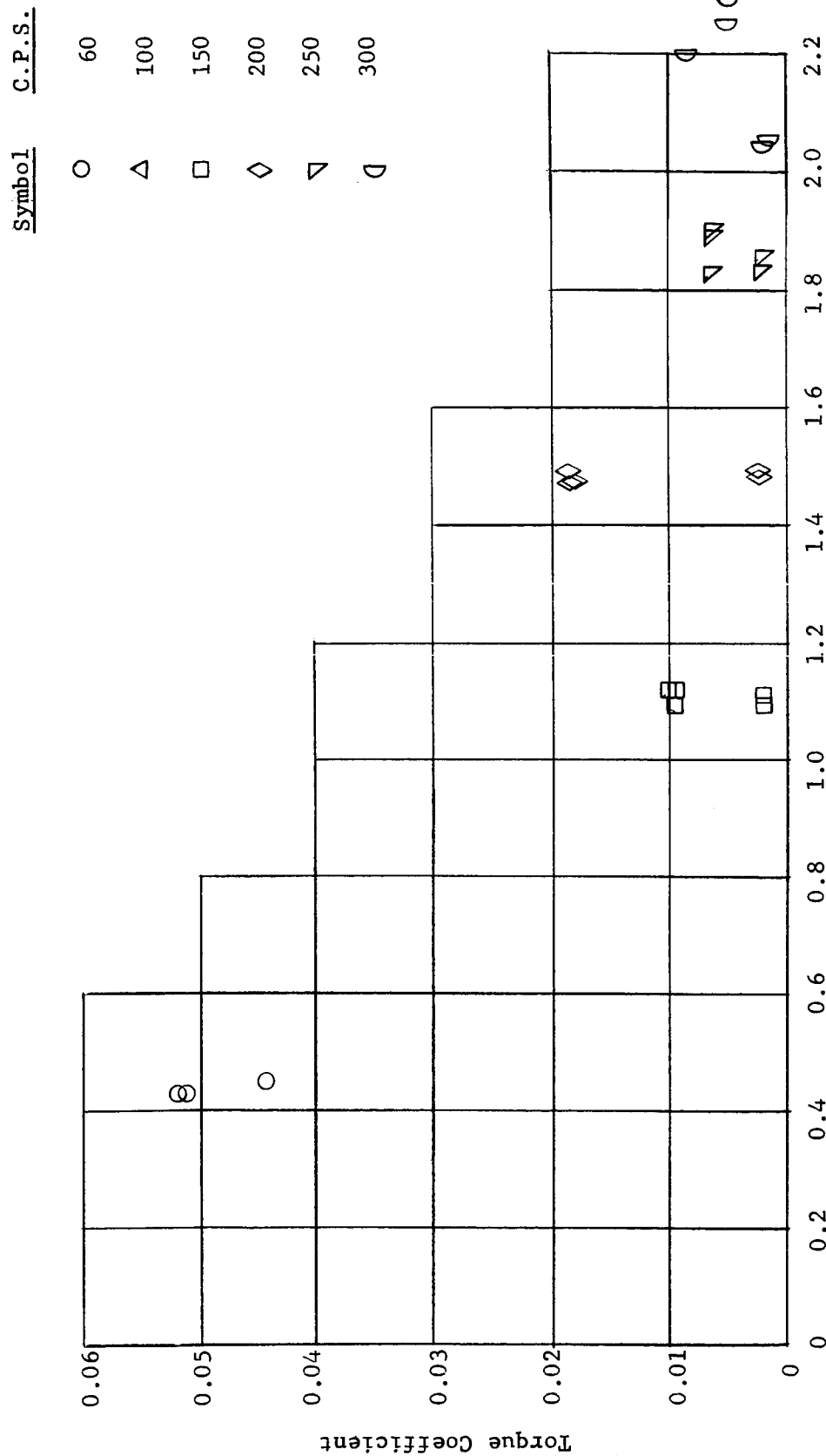


FIGURE 85 - REYNOLDS NO. RATIO VS. TORQUE COEFFICIENT

Test No. 302

2 Axial Groove $L/D = 1$
 3 Mil Nom. Diam. Clearance
 120°F Nom. Lube Temperature

Symbol	C.P.S.
○	60
△	100
□	150
◇	200

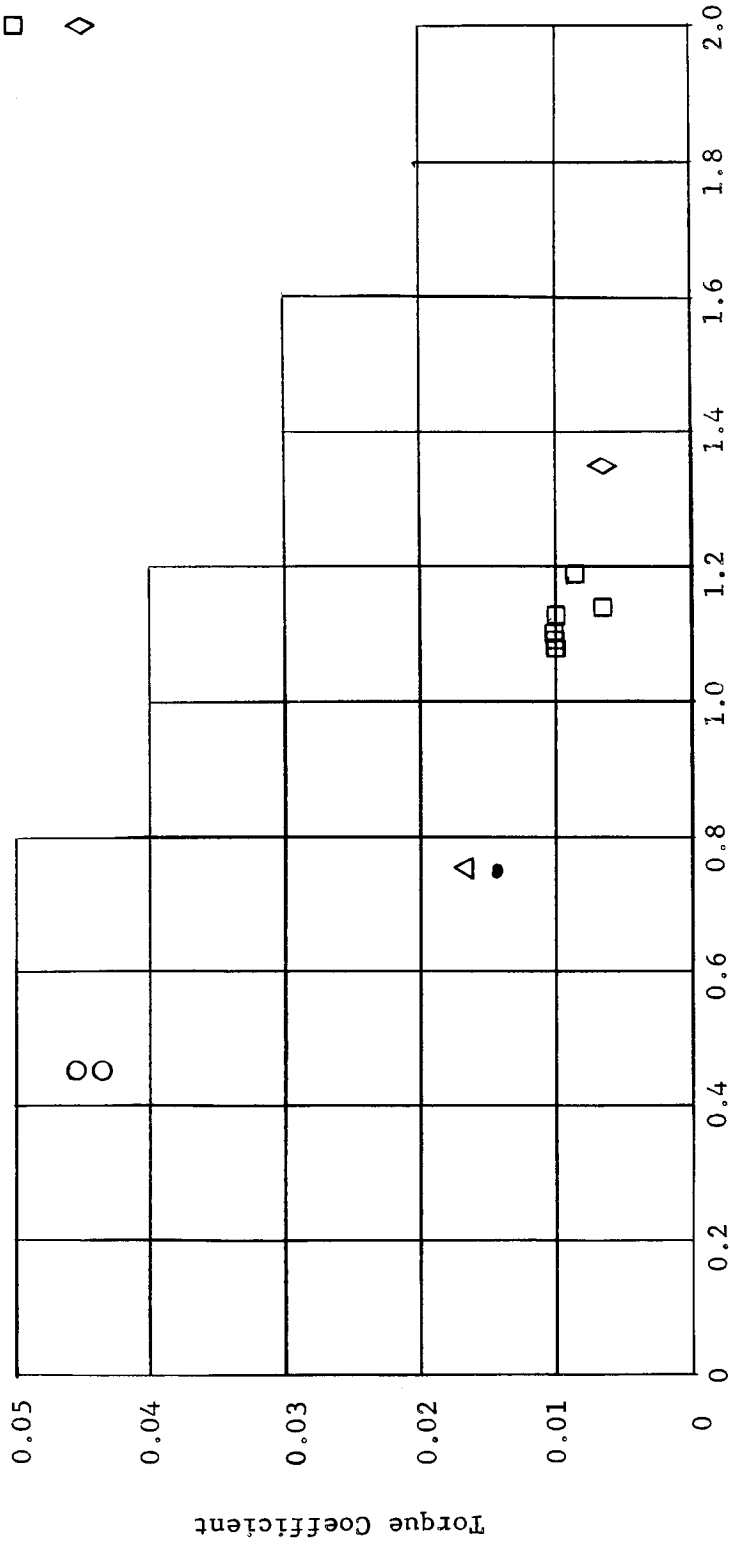


FIGURE 86 - REYNOLDS NO. RATIO VS. TORQUE COEFFICIENT

Test No. 4

2 Axial Groove $L/D = 1$
 3 Mil Nom. Diam. Clearance
 120° Nom. Lube Temperature

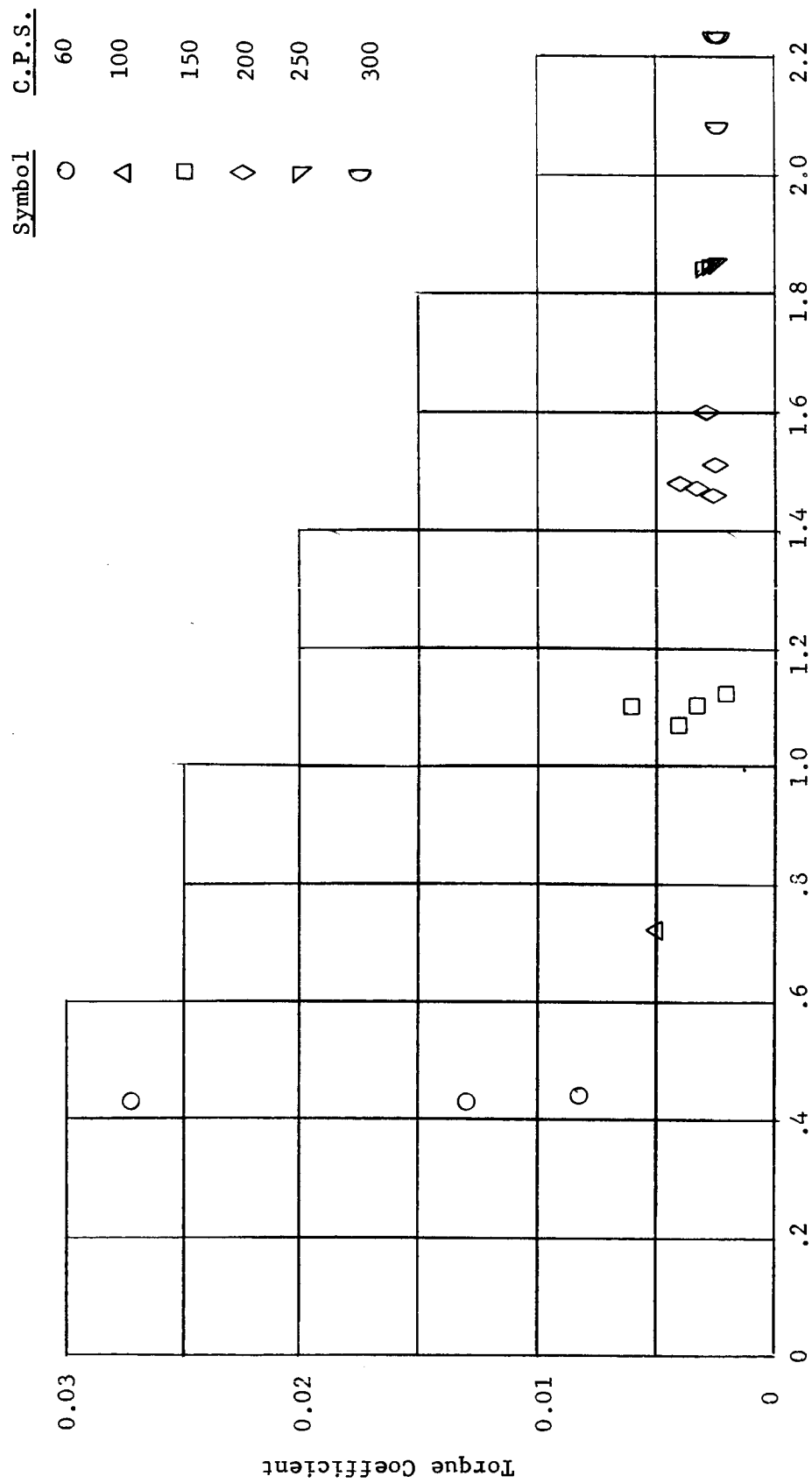


FIGURE 87 - REYNOLDS NO. RATIO VS. TORQUE COEFFICIENT

Test No. 5

2 Axial Groove L/D = 1.5
 5 Mil Nom. Diam. Clearance
 120°F Nom. Lube Temperature

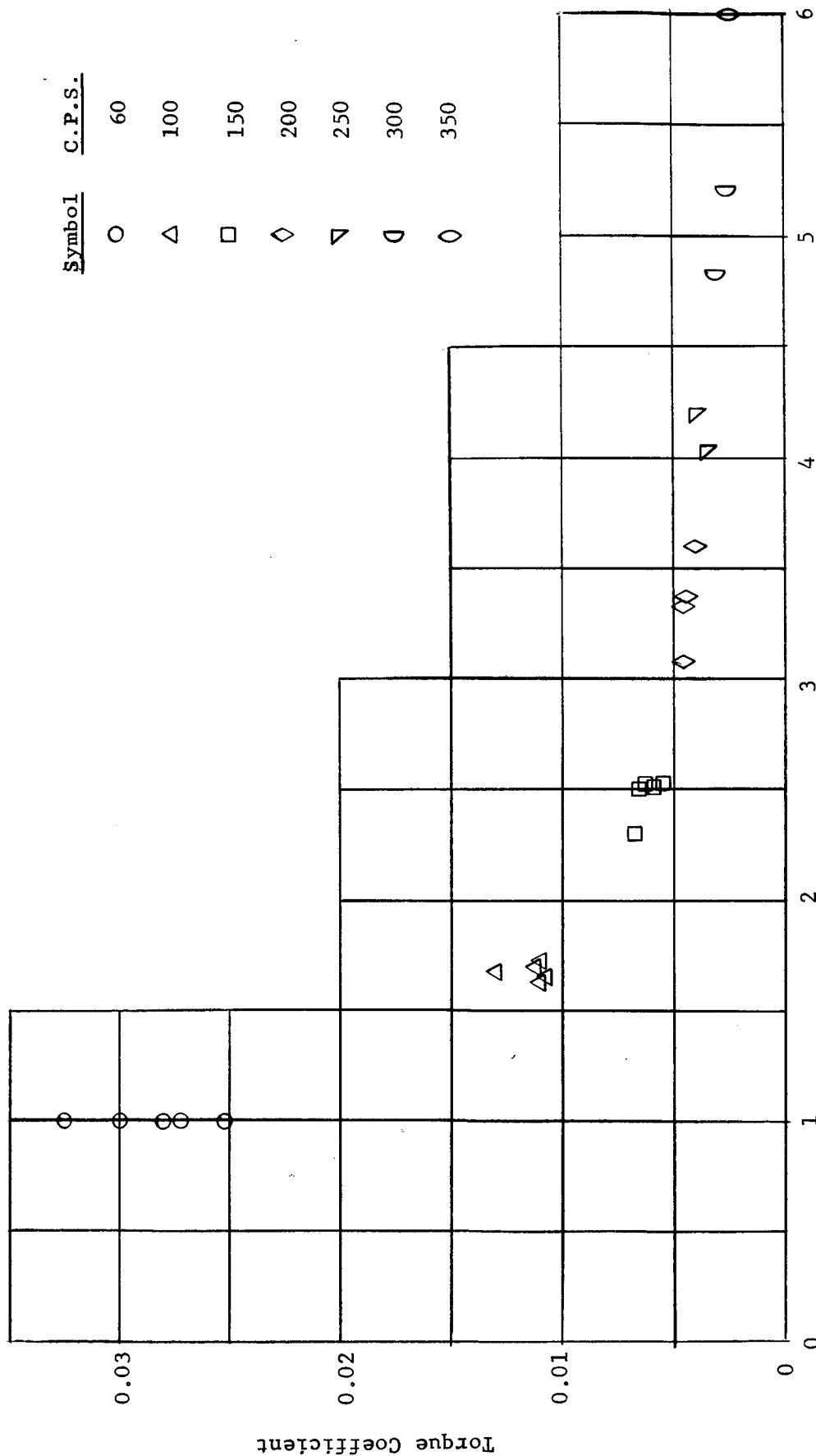


FIGURE 88 - REYNOLDS NO. RATIO VS. TORQUE COEFFICIENT

Test No. 501

2 Axial Groove L/D = 1.5
 5 Mil Nom. Diam. Clearance
 120°F Nom. Lube Temperature

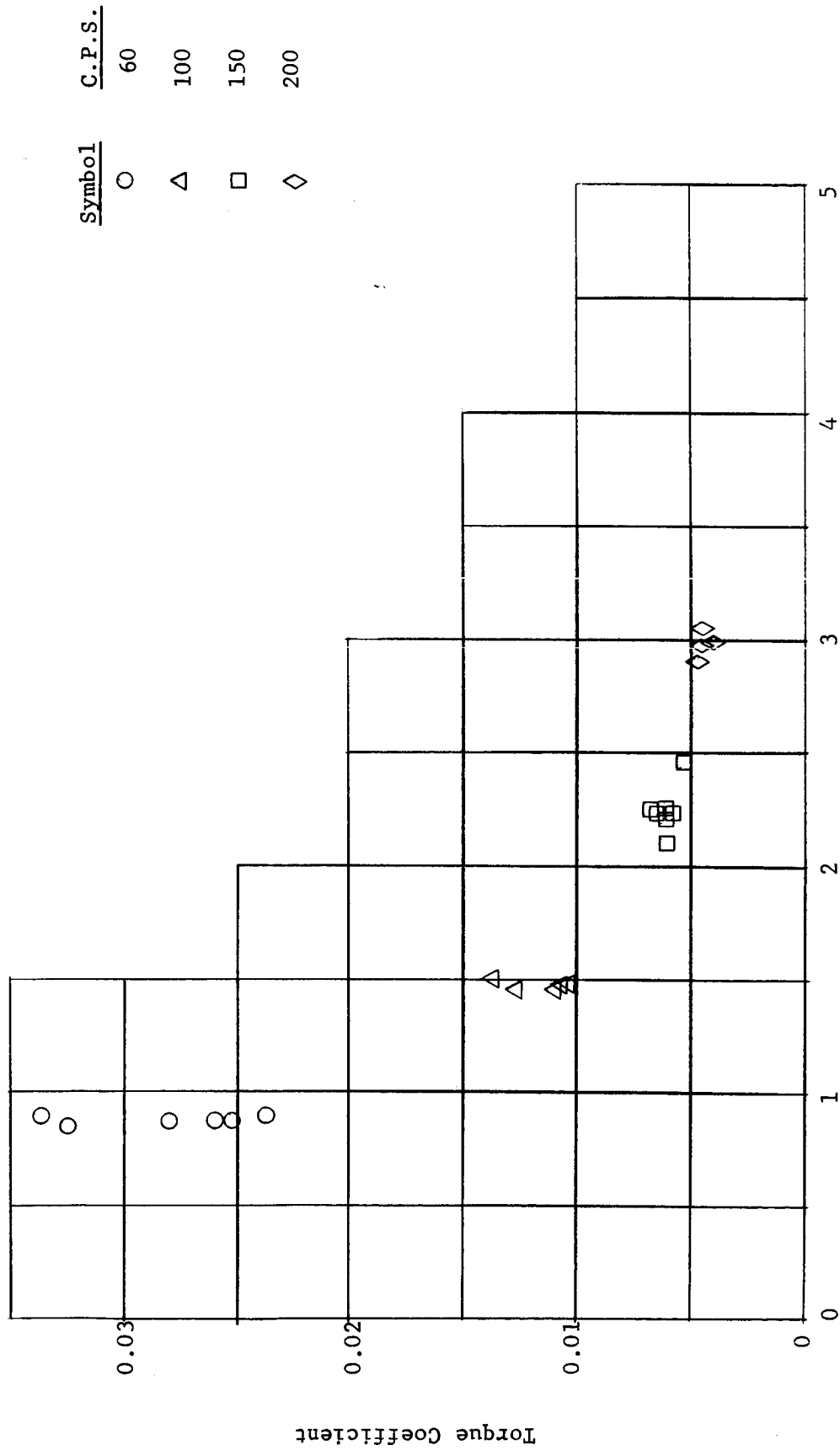


FIGURE 89 - REYNOLDS NO. RATIO VS. TORQUE COEFFICIENT

Test No. 6

2 Axial Groove $L/D = 1.5$
 2 Mil Nom. Diam. Clearance
 75°F Nom. Lube Temperature

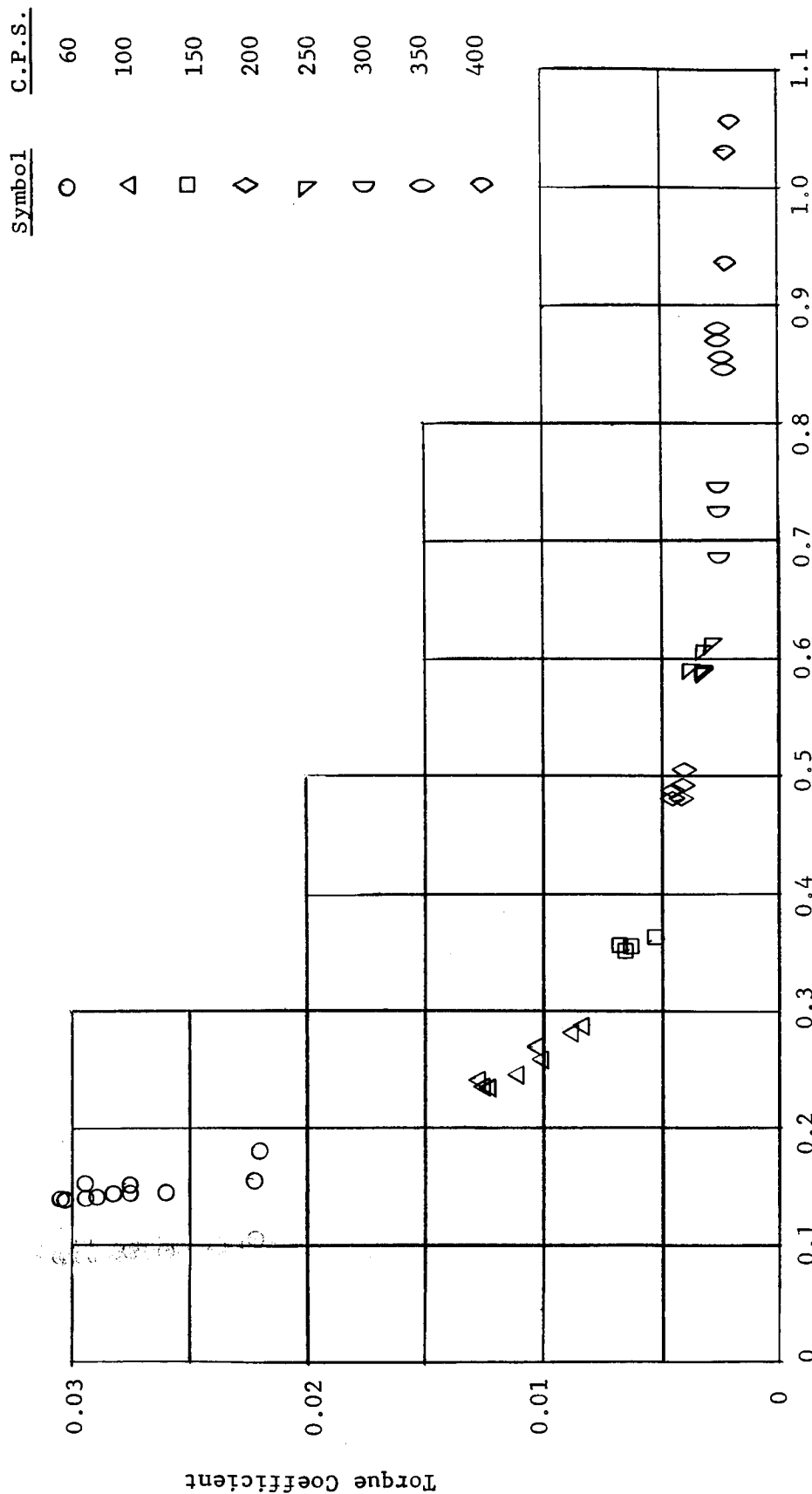


FIGURE 90 - REYNOLDS NO. RATIO VS. TORQUE COEFFICIENT

Test No. 600

2 Axial Groove $L/D = 1.5$
 2 Mil Nom. Diam. Clearance
 75°F Nom. Lube Temperature

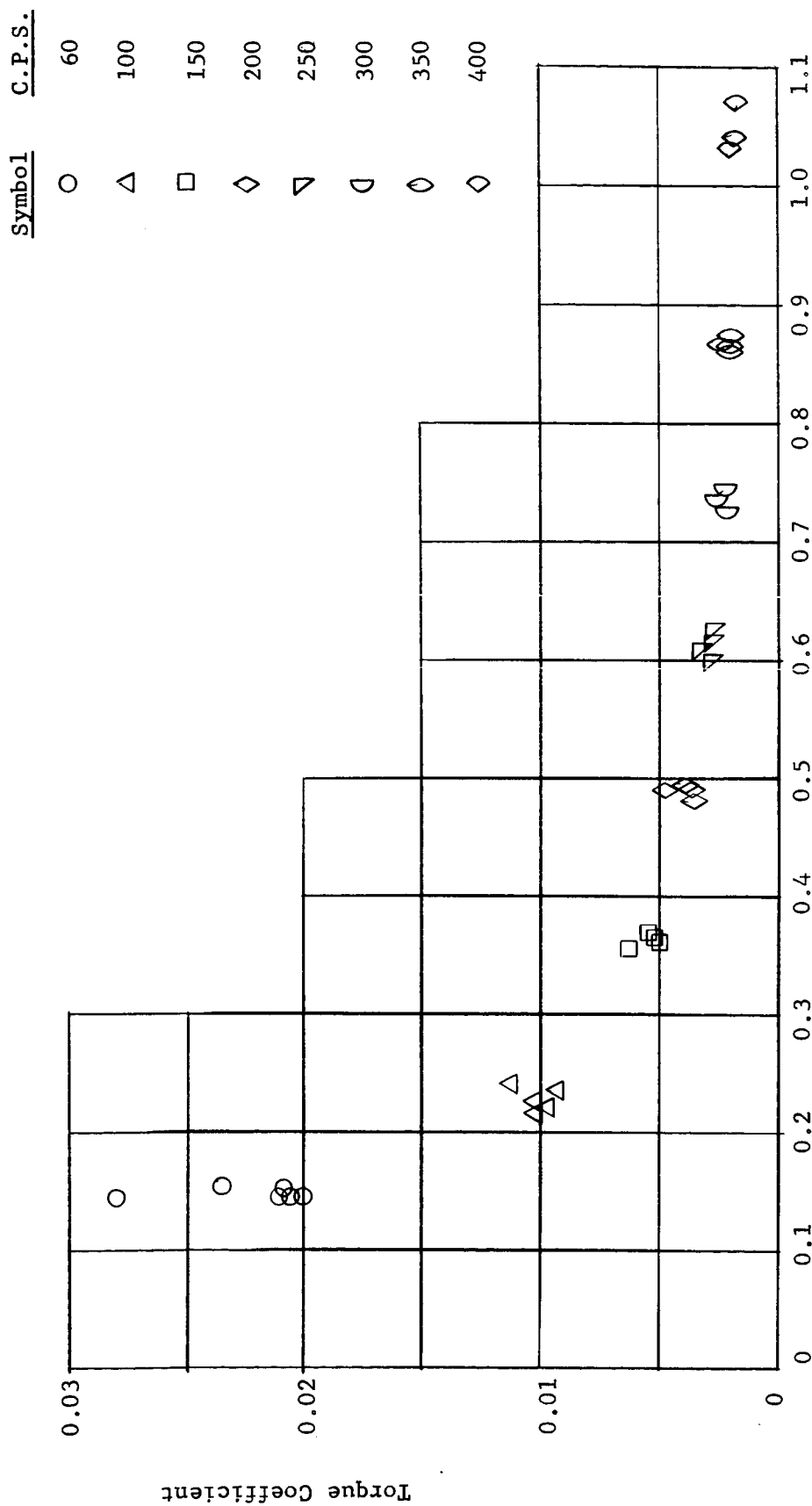


FIGURE 91 - REYNOLDS NO. RATIO VS. TORQUE COEFFICIENT

Test No. 7

2 Axial Groove L/D = 1.5
 3 Mil Nom. Clearance
 750F Nom. Lube Temperature

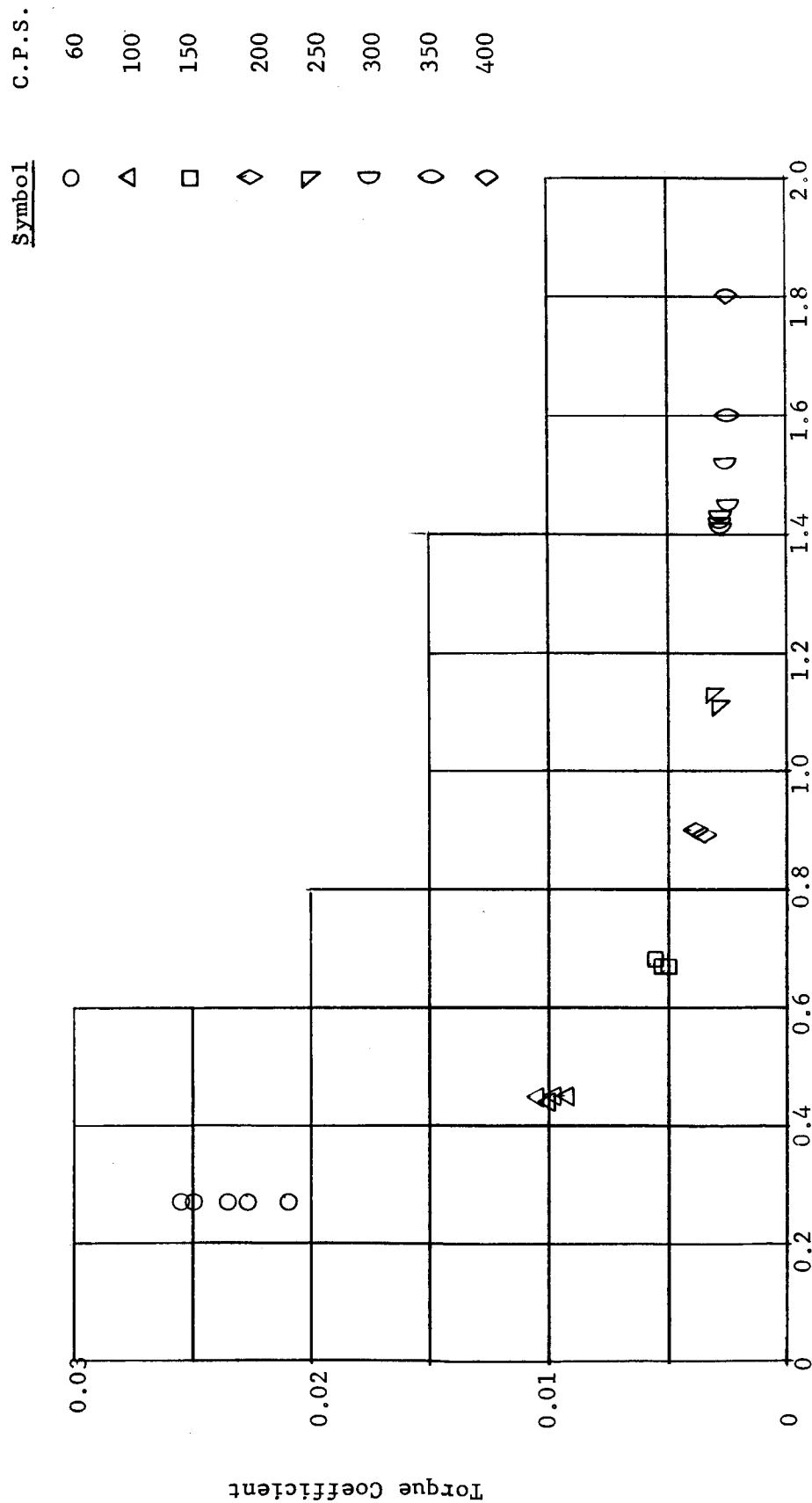


FIGURE 92 - REYNOLDS NO. RATIO VS. TORQUE COEFFICIENT

Test No. 701

2 Axial Groove L/D = 1.5
 3 Mil Nom. Diam. Clearance
 75°F Nom. Lube Temperature

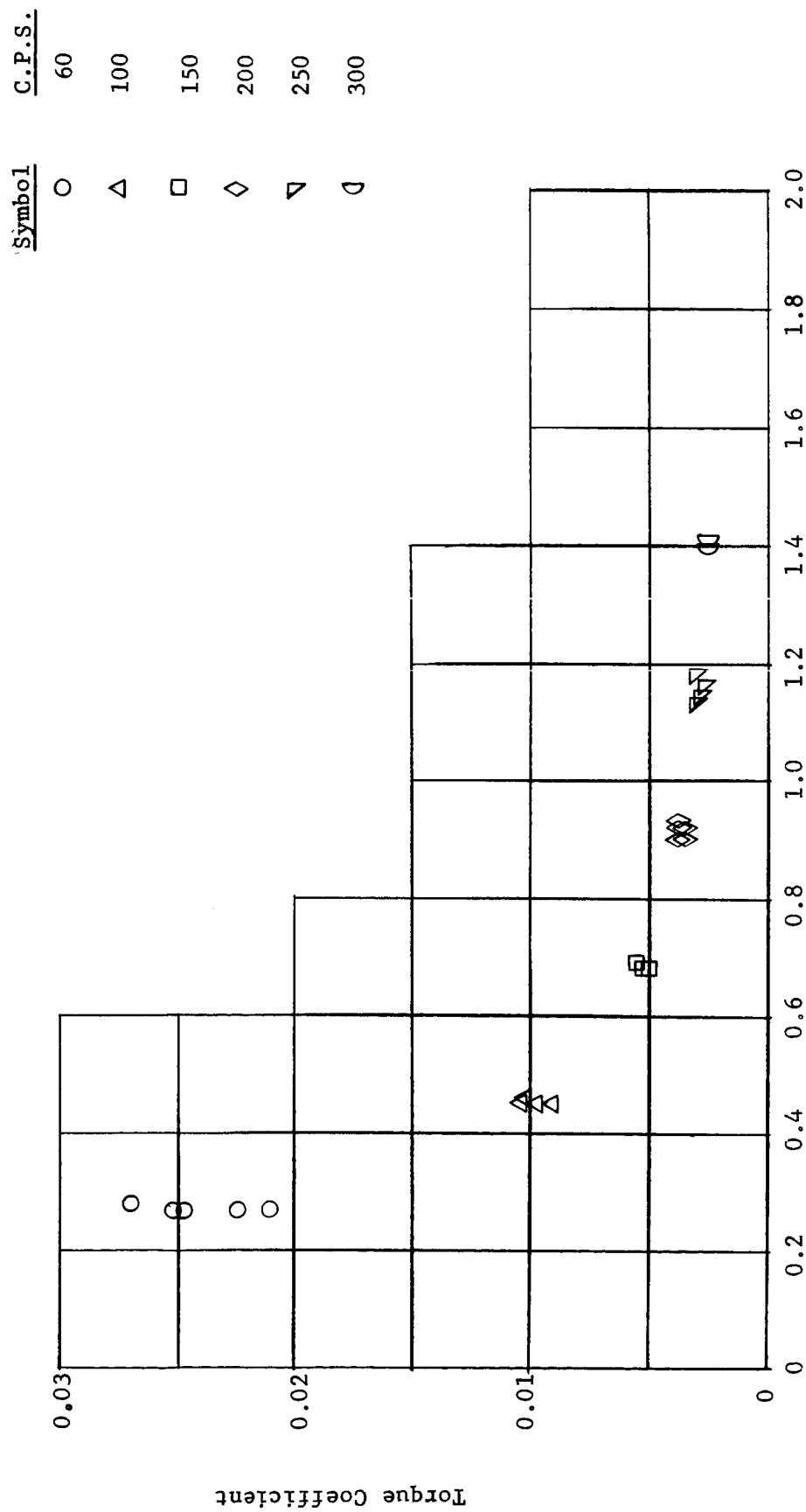


FIGURE 93 - REYNOLDS NO. RATIO VS. TORQUE COEFFICIENT

Test No. 12

2 Axial Groove L/D = 1
 3 Mil Nom. Diam. Clearance
 120°F Nom. Lube Temperature

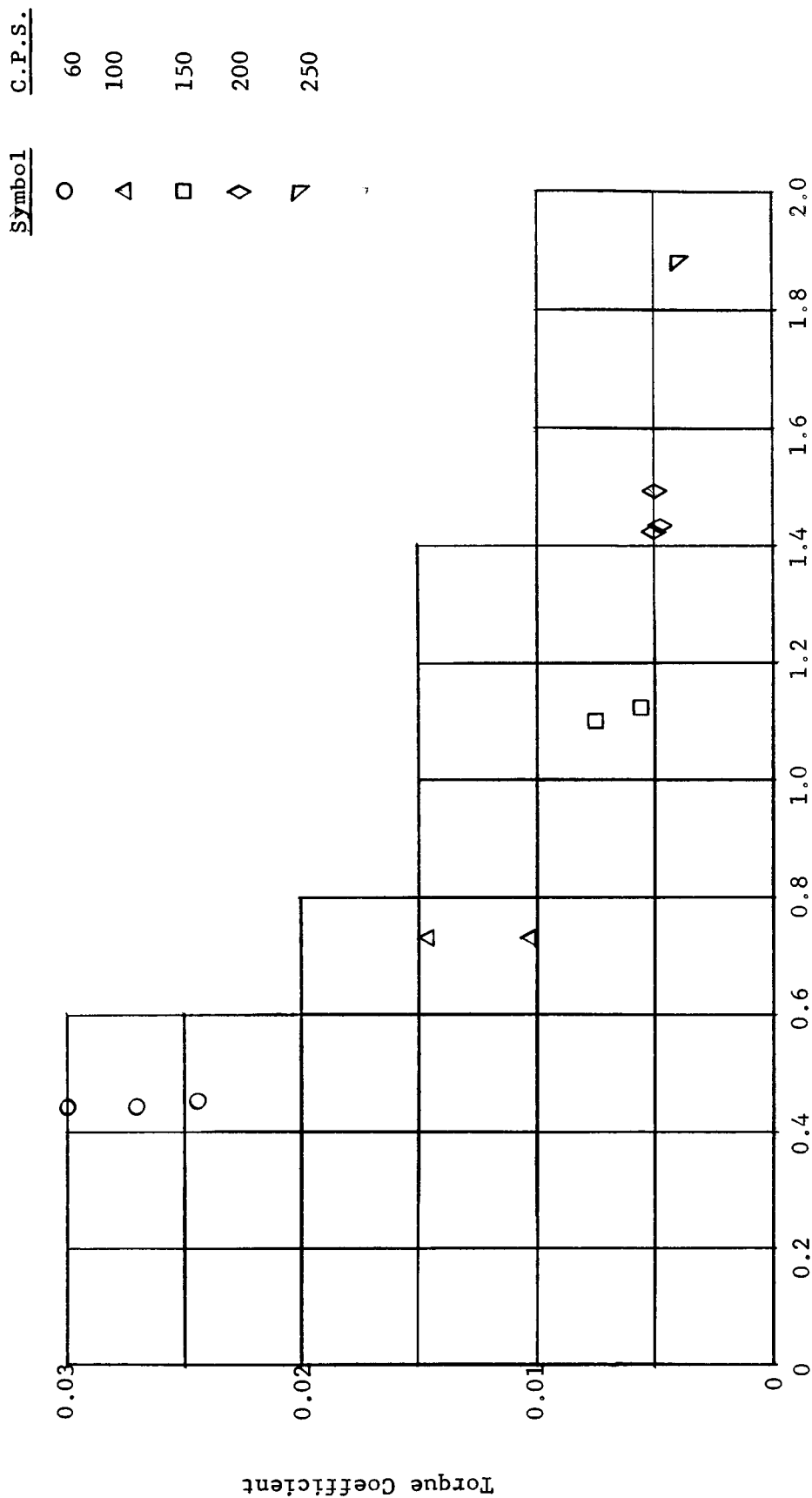


FIGURE 94 - REYNOLDS NO. RATIO VS. TORQUE COEFFICIENT

Test No. 13

2 Axial Groove L/D = 1
 2 Mil Nom. Diam. Clearance
 120°F Nom. Lube Temperature

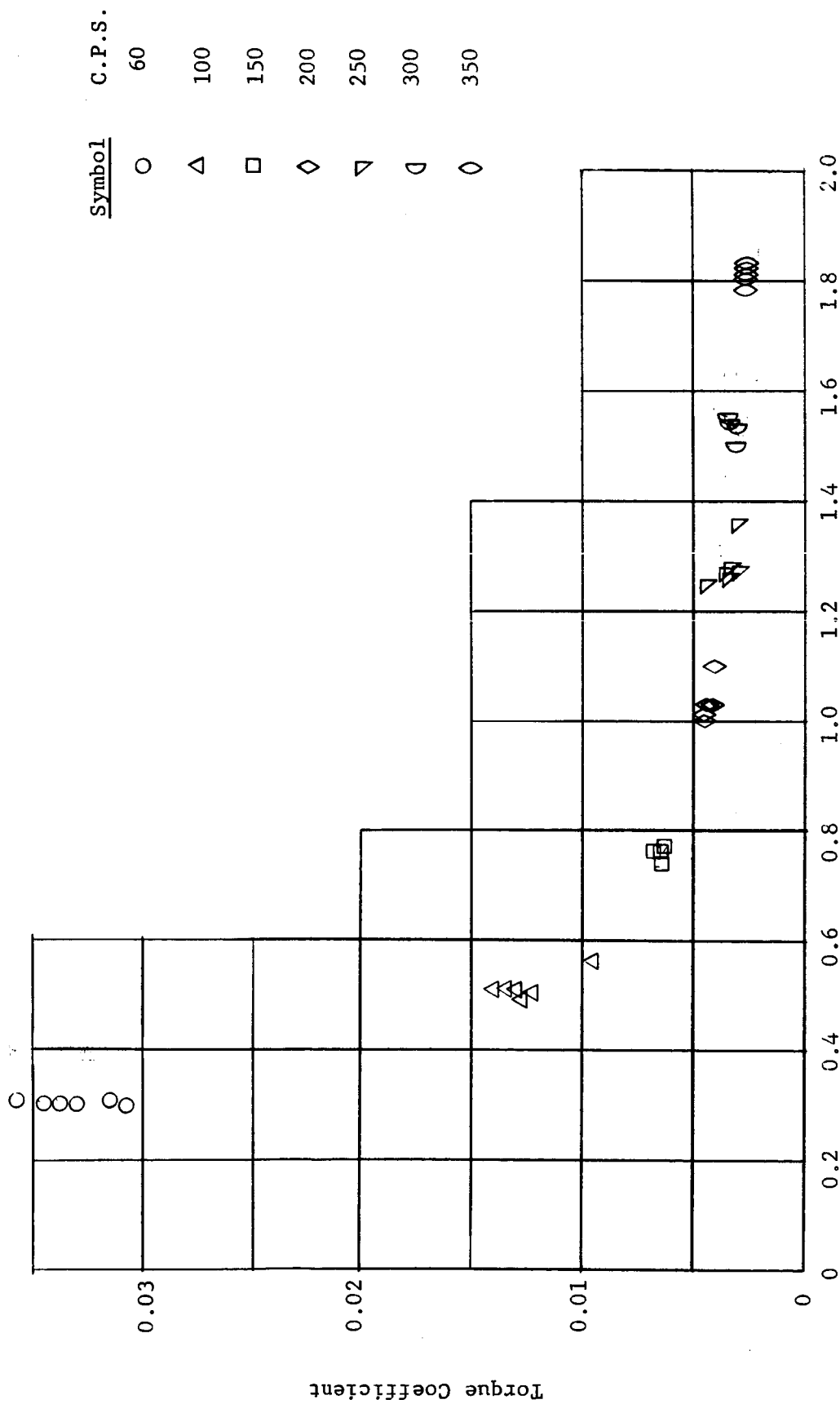


FIGURE 95 - REYNOLDS NO. RATIO VS. TORQUE COEFFICIENT

Test No. 18

2 Axial Groove $L/D = 1.5$
 2 Mil Nom. Diam. Clearance
 120° F Nom. Lube Temperature

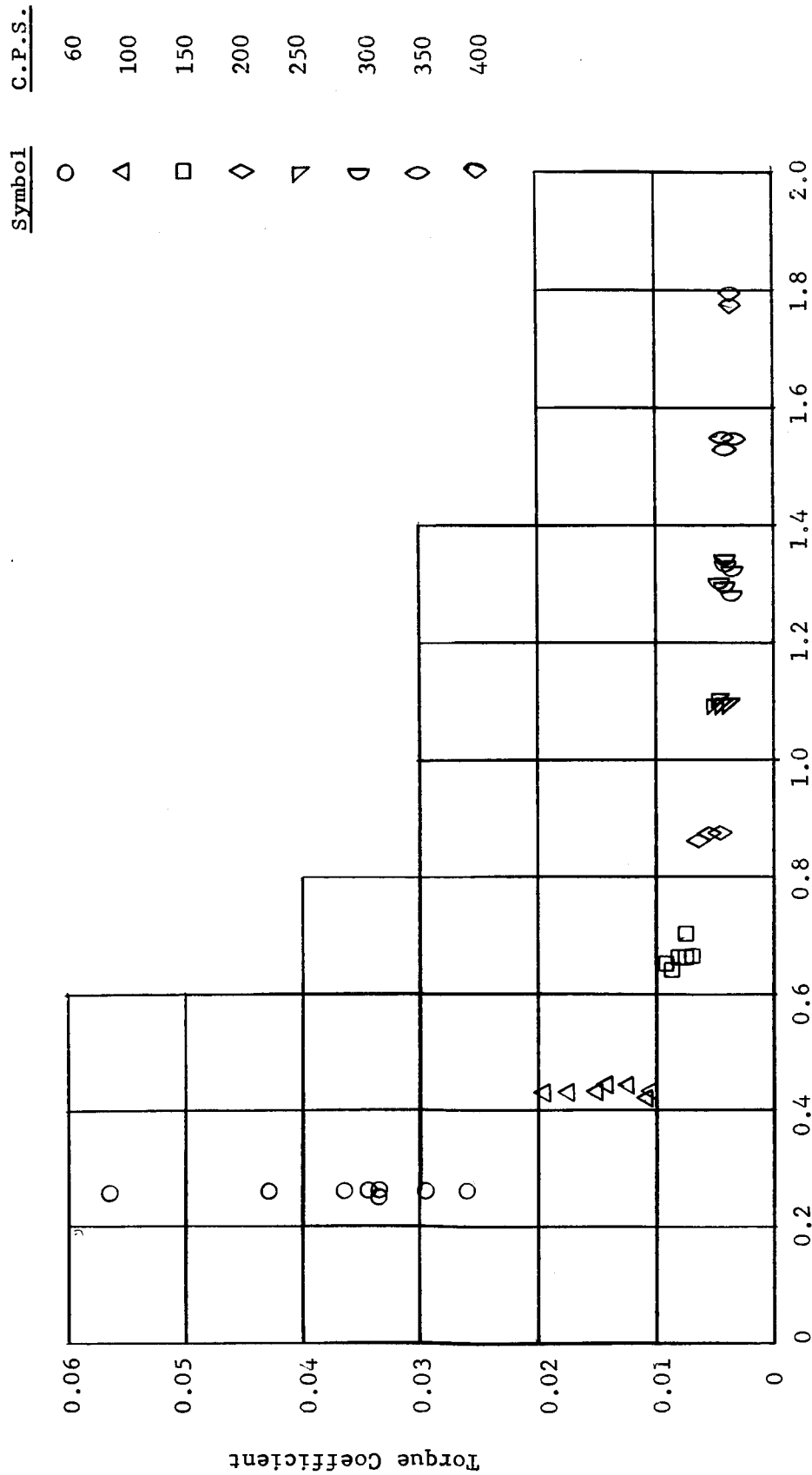


FIGURE 96 - REYNOLDS NO. RATIO VS. TORQUE COEFFICIENT

Distribution List - Contract NAS3-2111
August 9, 1963

Advanced Research Project Agency
The Pentagon, Washington 25, D. C.
Attn: Mr. John Huth

Air University Library
Maxwell Air Force Base, Alabama
Attn: Director

ASTIA
Fort Myer, Virginia

Armour Research Foundation of Illinois
Institute of Technology
Technology Center
Chicago 16, Illinois
Attn: Dr. W. H. Baier

Aerojet-General Corporation
Power/Equipment Division
Azusa, California
Attn: Mr. A. M. Taylor

Allison Division
General Motors Corporation
Indianapolis, Indiana
Attn: Mr. D. T. Lawrence

Atomics International
P. O. Box 309
Canoga Park, California
Attn: Mr. Carl E. Johnson

Battelle Memorial Institute
505 King Avenue
Columbus 1, Ohio
Attn: Dr. R. W. Dayton

The Garrett Corporation
AirResearch Manufacturing Division
Phoenix, Arizona
Attn: Mr. J. Castor

General Electric Company
Missile & Space Vehicle Department
3198 Chestnut Street
Philadelphia 4, Pennsylvania
Attn: Mr. Edward Ray
Space Power Project

General Atomic Division
P. O. Box 8, Oldtown Station
San Diego 10, California
Attn: Mr. R. W. Pidd

Materials Central
Fluids & Lubricants Branch
Wright Patterson Air Force Base, Ohio
Attn: Mr. R. J. Benzing
Fluids & Films Section

MSA Research Corporation
Callery, Pennsylvania
Attn: Mr. G. E. Kennedy

NASA
1520 H Street, Northwest
Washington 25, D. C.
Attn: J. Lynch
Code: RNP-NASA Headquarters

NASA
Lewis Research Center
21,000 Brookpark Road
Cleveland 35, Ohio 44135
Attn: Mr. Henry O. Slone

NASA
Lewis Research Center
21,000 Brookpark Road
Cleveland 35, Ohio
Attn: Mr. Robert E. English
Nuclear Systems Division

NASA
Lewis Research Center
21,000 Brookpark Road
Cleveland 35, Ohio
Attn: Mr. Warner L. Stewart
Fluid System Components Division

NASA
Lewis Research Center
21,000 Brookpark Road
Cleveland 35, Ohio
Attn: Mr. James H. Dunn

NASA
Jet Propulsion Laboratories
California Institute of Technology
4800 Oak Grove Drive
Pasadena, California
Attn: Mr. John Paulson

NASA
Lewis Research Center
21,000 Brookpark Road
Cleveland 35, Ohio
Attn: Mr. William J. Anderson
Fluid Systems Components Division

NASA
Lewis Research Center
21,000 Brookpark Road
Cleveland 35, Ohio
Attn: Mr. Thomas P. Moffitt
Fluid Systems Components Division

NASA
Lewis Research Center
21,000 Brookpark Road
Cleveland 35, Ohio 44135
Attn: Mr. Joseph P. Joyce (2)

NASA
Lewis Research Center
21,000 Brookpark Road
Cleveland 35, Ohio
Attn: Mr. Robert L. Johnson
Fluid Systems Components Division

NASA
Lewis Research Center
21,000 Brookpark Road
Cleveland 35, Ohio
Attn: Mr. George Mandel
Library

NASA
Goddard Space Flight Center
Greenbelt, Maryland
Attn: Office of Technical Information
Code 250

NASA
Western Operations Office
150 Pico Boulevard
Santa Monica, California
Attn: Mr. John Keeler

NASA
Lewis Research Center
21,000 Brookpark Road
Cleveland 35, Ohio
Attn: Mr. John R. Biggs
Procurement & Supply Division

Pratt & Whitney Aircraft
Division of United Aircraft Corp.
East Hartford, Connecticut
Attn: Mr. R. P. Shevchenko

The RAND Corporation
1700 Main Street
Santa Monica, California
Attn: Mr. F. R. Collbohm

Rocketdyne
Nucleonics Subdivision
Rocketdyne Engineering
Canoga Park, California
Attn: Mr. R. B. Dillaway

Sundstrand Aviation-Denver
A Division of Sundstrand Corporation
Denver 21, Colorado
Attn: Mr. P. H. Stahlhuth

Southwest Research Institute
8500 Culebra Road
San Antonio 6, Texas
Attn: Dr. R. A. Burton

U. S. Atomic Energy Commission
Technical Information Service Extension
P. O. Box 62
Oak Ridge, Tennessee

Westinghouse Electric Corporation
Research Laboratories
Pittsburgh, Pennsylvania
Attn: Mr. J. Boyd

Air Force Systems Command
Aeronautical Systems Division
Wright-Patterson Air Force Base, Ohio
Attn: Mr. Bernard Chasman
ASRCE

Air Force Systems Command
Aeronautical Systems Division
Wright-Patterson Air Force Base, Ohio
Attn: Mr. J. L. Morris
ASRCNL-2

Mechanical Technology, Inc.
968 Albany - Shaker Road
Latham, New York
Attn: Dr. Beno Sternlicht

Scientific and Technical
Information Facility
P. O. Box 5700
Bethesda, Maryland
Attn: NASA Representative
(S-AK/RKT)

U. S. Atomic Energy Commission
Germantown, Maryland
Attn: Col. William A. Tesch
Asst. Director for Experimental Concepts
Division of Reactor Development

Aeronautical Systems Division
Flight Accessories Laboratory
Wright-Patterson Air Force Base, Ohio
Attn: Mr. Charles Armbruster
ASRMFP-1

Westinghouse Electric Corporation
Lima, Ohio
Attn: R. W. Drake,
Advanced Systems Department

Battelle Memorial Institute
505 King Avenue
Columbus 1, Ohio
Attn: Mr. C. M. Allen

SNAP-8 Project Mechanical Design
Aerojet General Corporation
P. O. Box 298
Azusa, California
Attn: Mr. J. Rogoza

Aeronautical Systems Division
Aeromechanical Branch
Wright-Patterson Air Force Base, Ohio
Attn: Mr. Charles Amburster
ASRMFP-1

Oak Ridge National Laboratory
Post Office Box Y
Oak Ridge, Tennessee
Attn: Mr. H. W. Savage

NASA
Scientific & Technical Information
Agency
Box 5700
Bethesda 14, Maryland
Attn: NASA Representative (2 + Repro.)

TAPCO - A Division of Thompson Ramo
Wooldridge Inc.
Rankine-Cycle Power Systems
7209 Platt Ave.
Cleveland 4, Ohio
Attn: Mr. Otto Decker

NASA

AEC Deputy, SNAP-50, SPUR Office
1512 H Street, Northwest
Washington 25, D. C.
Attn: Col. E. L. Douthett (RN)

Clevite Corporation
Mechanical Research Division
Project Administrator
540 E st 105 Street
Cleveland 8, Ohio
Attn: Mr. N. C. Beerli

United Aircraft Corporation
Pratt & Whitney Aircraft Division
CANEL
P. O. Box 611
Middletown, Connecticut
Attn: Glenn M. Wood

Aerojet-General Corporation
Subsidiary of General Tire & Rubber Co.
Technical Library
Building 2015, Dept. 2410
P. O. Box 1947
Sacramento 9, California

NASA

Lewis Research Center
21000 Brookpark Road
Cleveland, Ohio 44135
Attn: Rober F. Mather